HYDROGEN PRODUCTION FROM CATALYTIC STEAM REFORMING OF BIO-OIL OVER NANO Ni$_x$Mg$_y$O SOLID SOLUTION

Xiang LUO, BEng.

Thesis submitted to the University of Nottingham for the degree of Doctor of Philosophy

SEPTEMBER 2016

Abstract

Hydrogen production from bio-resource is a promising option. In order to economically and practically derive hydrogen from biomass on a sustainable scale, novel catalysts are needed to be developed with properties of effective and inexpensive.

In this study, initial works include the preparation of Ni/MgO catalysts via different methods including co-precipitation, hydrothermal treatment and wet-impregnation. These catalysts formed solid solutions after calcination at 600 ℃. It was found that hydrothermal treatment increased the specific surface area of the catalyst from 49.7 m^2/g to 79.8 m^2/g. In addition, the total pore volume and t-plot micropore volume of the hydrothermally treated Ni/MgO (Ni_xMg_yO-hydro) increased by a great extent. In the 20 h methanol steam reforming tests, Ni_xMg_yO solid solutions prepared via different methods were examined for their catalytic performance, stability and resistance to carbon deposition. Amongst all the catalysts tested, the Ni_xMg_yO-hydro catalyst exhibited the highest conversion rate of 97.4mol% with no carbon deposition. This was particularly true when the steam-to-carbon ratio (S/C) was 3. When S/C was 1, similarly, the Ni_xMg_yO-hydro showed the highest performance and the lowest amount of carbon deposition. Characterizations of the spent Ni_xMg_yO-hydro revealed that it had very low portion of highly ordered carbon on its surface. It is

attributed to the rapid removal of atomic carbon, which led to the prevention of carbon accumulation and subsequent transformation into highly ordered structure. The carbon removal mechanism was confirmed by CO_2-TPD analysis. The strong basic sites on the Ni_xMg_yO-hydro surface enhanced the reaction between deposited carbon and adsorbed CO_2. In addition, the catalytic activity of Ni_xMg_yO-hydro catalyst was compared with the Ni/γ-Al_2O_3 catalyst and several other commercial catalysts. Its outstanding performance in steam reforming of methanol was further verified.

Although the Ni_xMg_yO-hydro catalyst showed good performance in the steam reforming of methanol, it was not the case for ethanol reforming. The Ni_xMg_yO-hydro catalyst showed low hydrogen yield and serious carbon deposition during ethanol steam reforming. The low hydrogen yield was caused by the suppression of water-gas shift reaction (WGSR) at high temperatures, whilst the carbon fouling was due to the existence of C-C bonds in ethanol and high selective conversion towards ethylene. Therefore, the modification of the Ni_xMg_yO-hydro catalyst was carried out to overcome these drawbacks. Various elements, i.e., Ce, La and Co, were as catalytic promoters and individually added to the Ni_xMg_yO-hydro catalyst. Most of the modified catalysts exhibited much higher hydrogen yield at 700 ℃ due to the enhancement of WGSR. Some catalysts, such as Ce- and Co-modified catalysts, showed significant increase in

hydrogen yields, which were higher than 80mol% after 30 h of reaction. It is worth mentioning that the La-modified catalysts promoted the hydrogen yield to 53mol% even at low temperature condition (500 ℃), whilst it was only 12.5mol% with the unmodified catalyst at the same temperature. The reason for this was due to the lack of suitable acid sites on La surface, which led to the accelerated formation of acetaldehyde. The advantage of acetaldehyde is it could be decomposed at very low temperature. The formation of carbon on Ce- and La-modified catalysts was also suppressed. The Ce element showed outstanding oxygen storage and release capability to improve the gasification of carbon deposition. Similarly, La_2O_3 would form $La_2O_2CO_3$ species which could achieve carbon removal by offering CO_2.

Subsequently, the modified catalysts were tested with acetic acid (HAc) and phenol as feedstock, both of which are the most common-seen compounds in bio-oil. The results of these tests, such as catalytic performance and anti-carbon abilities, were consistent with the findings in ethanol steam reforming. Most of the modified catalysts showed very high hydrogen yields above 80mol%, which were only 61.9mol% and 73.7mol% for the unmodified NiMgO catalyst in the steam reforming of HAc and phenol, respectively. The better resistant abilities of the modified catalysts over carbon deposition were also confirmed in the steam reforming of HAc and

phenol. In order to determine the performance of the catalysts in steam reforming of actual bio-oil, all of the modified catalysts were evaluated based on their performance in the reforming of major model compounds of bio-oil. Three hydrothermally treated catalysts, i.e., 1%Ce/NiMgO, 2%La/NiMgO and 2%Co/NiMgO, were selected and tested. All three catalysts showed carbon conversions above 90mol% and hydrogen yield in excess of 70mol% after 100 h test. The amounts of carbon deposition on these catalysts were also within an acceptable range. It can therefore be concluded that the Ni_xMg_yO solid solution with proper modification, i.e. addition of suitable promoter, could be developed as a promising catalyst for hydrogen production via the steam reforming of bio-oil.

Disseminations

Journal papers

X. Luo, Y. Hong, F. Wang, S. Hao, C. H. Pang, Ed. Lester, T. Wu*, Development of nano NixMgyO solid solutions with outstanding anti-carbon deposition capability for the steam reforming of methanol. Applied Catalysis B: Environmental, 2016, 194(0): 84-97.

H. Zhang, **X. Luo**, X. Li, G. Z. Chen, F. He*, T. Wu*, Preparation and characterization of a sulfonated carbon-based solid acid microspheric material (SCMs) and its use for the esterification of oleic acid with methanol. Austin Chemical & Engineering, 2016, 3(1):1024-1029.

H. Zhao, **X. Luo**, J. He, C. H. Peng and T. Wu*. Recovery of elemental sulphur via selective catalytic reduction of SO_2 over sulphided CoMo/γ-Al2O3 catalysts. Fuel, 2015, 147(0): p. 67-75.

Journal papers under preparation

X. Luo, Y. Hong, H. Zhang, Ed. Lester, C. H. Pang, T. Wu*, Enhanced steam reforming of ethanolover Ni/MgO catalysts doped with Ce, La or Co. Applied Catalysis B: Environmental, under preparation.

X. Luo, Ed. Lester, C. H. Pang, T. Wu*, Outstanding performance of La-promoted Ni catalysts in Low-temperature steam reforming of ethanol. Under preparation.

Conference papers

X. Luo, Ed. Lester, T. Wu*, Hydrogen production from steam reforming of phenol as a coal pyrolysis product (Abstract). 8th International Freiberg Conference on IGCC & XtL Technologies, 2016, Cologne, Germany.

X. Luo, K. Shi, Ed. Lester, T. Wu*, A novel nano-Ni/MgO catalyst for hydrogen production from steam reforming of bio-oil (Abstract). 10th European Conference on Coal Research and its Applications, 2014, Hull, UK.

X. Luo, Ed. Lester, T. Wu*, Hydrogen production via steam reforming of bio-oil model compounds over Ni_xMg_yO solid solution (Abstract). 11th European Conference on Coal Research and its Applications, 2016, Sheffield, UK.

A. M. Parvez, **X. Luo**, N. Miles, T. Wu*, Simulation of conventional and CO2 enhanced biomass gasification: a comparative assessment using aspen plus (Abstract). 11th European Conference on Coal Research and its Applications, 2016, Sheffield, UK.

Acknowledgements

Finally, and most importantly, I want to deliver my gratitude to my parents for their endless encouragement and trust. I wish to extend my special thanks to my wife Shu Tang, for her understanding and support.

Table of Contents

Chapter 1. Introduction

1.1 Research background

Compared with biomass, bio-oil has much higher bulk density and energy density, which make it more convenient for transportation and utilization. Therefore, hydrogen production from steam reforming of bio-oil has been widely studied (Rioche et al., 2005, Trane et al., 2012). The research mainly focuses on the development of catalysts, which requires the study of the mechanism of steam reforming and catalysts deactivation, and also couple with the application of novel techniques in catalyst synthesis and treatment (Bartholomew, 2001, Mattos et al., 2012, Trane et al., 2012).

Bio-oil steam reforming is normally conducted approximately at 600-900 ℃, within which carbon deposition could be easily mitigated (Lima da Silva et al., 2009). However, high temperatures (> 600 ℃) thermodynamically restrain the formation of H_2 from water-gas shift reaction (WGSR) and lead to excessive CO contents in the production. Thus, the majority of the current research on low temperature ethanol steam reforming involves the use of various noble metals (e.g, Pt, Rh, Ru, and Pd) (Mattos et al., 2012, Rioche et al., 2005, Palma et al., 2014, Chen et al., 2010). However, the high costs coupled with low accessibility limit the commercial

application of such noble catalysts. Therefore, it is of great significance to alternate the catalyst and enhance WGSR without the use of noble metals. In the past few decades, Ni-based catalysts are the most widely studied catalysts. It is because of its low price, as well as its high ability in selectively breaking the C-C bonds. It is believed (Rioche et al., 2005) that a reliable supporting material plus a suitable promoter could make an outstanding Ni-based catalyst for steam reforming of bio-oil.

1.2 Aim and objectives

This study aims to develop a novel nano-scale Ni-based catalyst for hydrogen production from steam reforming of bio-oil. Apart from the catalytic efficiency, the anti-carbon deposition and anti-sintering abilities of catalyst are the main focuses of this work. The specific objectives of this thesis are:

- To establish a Ni_xMg_yO solid solution as a promising catalyst for steam reforming. Several trivial methods for the preparation of Ni_xMg_yO solid solutions are to be developed and applied.
- To understand the morphology and chemical properties of the Ni_xMg_yO solid solution. A matrix of characterization methods will be applied throughout this work. Transmission electron microscopy (TEM), N_2 physisorption and X-ray diffraction (XRD) will be used for the study of physical properties of the

catalysts, whilst H_2-temperature programmed reduction (H_2-TPR), H_2-temperature programmed desorption (H_2-TPD), CO_2-temperature programmed desorption (CO_2-TPD) and X-ray photoelectron spectroscopy (XPS) will be applied for the study of chemical properties. The carbon deposition will be characterised using thermogravimetric analysis (TGA), Raman spectra, and temperature programmed hydrogenation (TPH).

- To further improve the durability and integrity of the NiMgO catalyst. The modification of catalysts will be carried out via the addition of promoters, i.e., Ce, La and Co. To investigate the catalytic performance of these catalysts, more representative bio-oil model compounds, such as ethanol, acetic acid (HAc) and phenol, are to be employed to explore the possibility of the adhibition of the modified NiMgO in bio-oil steam reforming.

- To test effectiveness of the screened catalysts using a model bio-oil. The tests are to be carried out for 100 h to examine the performance of the catalysts and their stability.

1.3 Thesis structure

There are seven chapters in this thesis:

Chapter 1 introduces research background and research objectives. It also details the structure of this thesis.

Chapter 2 contains a comprehensive literature review. It reviews the current technologies of bioenergy conversion and hydrogen production. The catalytic steam reforming of bio-oil was critically reviewed, which included various aspects, such as the development of catalysts, deactivation of catalysts and promotion methods.

Chapter 3 describes the preparation methods employed for catalyst preparation. The characterization techniques for the catalysts are also detailed in this chapter including the setups and experimental procedures for each test.

Chapter 4 establishes the Ni_xMg_yO solid solution as a promising catalyst for catalytic steam reforming of bio-oil. Several techniques were used for the characterization of both fresh and used catalysts are detailed. The carbon deposition and sintering issues remained the primary considerations.

Chapter 5 is focused on the modification of the Ni_xMg_yO solid solution developed in the previous work in Chapter 4. The catalysts, doped with Ce, La and Co as promoters, were tested in the steam reforming of ethanol.

Chapter 6 covers performance of the modified catalysts in the steam reforming of phenol and HAc. A mixture of ethanol, phenol and HAc was prepared as a model bio-oil, which had similar C/H/O ratio with bio-oil derived from rice husk. The model bio-oil was then

tested using three catalysts (selected based on previous study in this thesis) at 800 ℃ for 100 h.

Chapter 7 provides a general conclusion of the thesis and also includes several directions for future studies.

Chapter 2. Literature review

2.1 Biomass and its conversion technologies

2.1.1 Characteristics of biomass

Biomass is derived from solar energy via photosynthesis. It includes all the living or recently living organisms, like land plants, grasses, water-based vegetation and manures (McKendry, 2002a) and these organisms consist of a number of major elements such as C, H, O, N, P and S. The classification of biomass into different categories could be in different systems. One feasible way is based on the appearances and the growth environment of biomass: woody plants, herbaceous plants/grasses, aquatic plants, manures and wastes (McKendry, 2002a). Biomass could also be divided into two types: low moisture content and high moisture content. The low moisture content biomass can be used in thermo-chemical processes (i.e., gasification, combustion and pyrolysis), whilst the high moisture content plants are more suitable to be used in some wet processing technologies (i.e., fermentation, anaerobic digestion) (McKendry, 2002b). Such high moisture contents would consume a large amount of energy for the drying process if employed as resources for thermo-chemical processing. The characteristics of biomass are detailed in the following sections.

Sustainability

Biomass is produced via photosynthesis without geographical restrictions. Under a good illumination condition, carbon dioxide in the atmosphere can be converted into organic materials or, in another way, the solar energy is stored as chemical energy existed as chemical bonds of the organisms (Fallot et al., 2009). The said chemical energy is released when these bonds are broken either via thermo-chemical or wet processing. This is an ongoing energy transfer from the sun and hence the sustainability of biomass resource could be ensured.

Clean

Biomass is carbon-neutral. On a view of carbon network, the net emission of carbon dioxide into the environment during the harvesting of energy from biomass is zero. The final products of conversion of biomass (CO_2 and H_2O) are originally taken into the plants from the atmosphere during photosynthesis. The conversion of biomass also has less harmful releases such as NO_x and SO_x compared with fossil fuels (Gan et al., 2012).

Low calorific value and high moisture content

Compared with other energy carriers, biomass has much lower heating values. Taking wood and wheat straw as examples, their lower heating values are only 18.6 and 17.3 MJ/kg, respectively, while the lower heating value of coal is as high as 23-28 MJ/kg

(McKendry, 2002a, Demirbas, 2004). The reason of this disparity is that the oxygen content of biomass carbohydrates is very high whilst the combustible elements such as C and H are low. In addition, the intrinsic moisture content in biomass is also very high, which require more energy for drying before further processes take place (McKendry, 2002b).

Availability and diversity

Biomass is highly dispersed in both regional distribution and species distribution. Total energy captured annually in biomass is more than that of the annual energy consumption globally (Field et al., 1998). The low volumetric of biomass would also make it uneconomical for the collection and transportation. On the aspect of species diversity, the varieties of biomass resource also lead to different heating values and moisture contents, both of which increase the complexity in material handling, pre-treatment and the design of processing facilities (McKendry, 2002b).

2.1.2 Conversion technologies of biomass

It is unlike any other renewable resources (solar, wind, hydropower) where it is able to be stored directly and transported to somewhere else. However, the energy conversion technologies employed for biomass are more complex and diverse if compared with technologies used in the conversion of fossil fuels (Demirbaş, 2001). This could be attributed to the diversity of biomass species with

different characteristics including heating value, moisture content, and handleability. Illustrated in Fig. 2.1, the common conversion technologies could be classified in three categories: mechanical extraction; thermo-chemical conversion; biological conversion (Demirbaş, 2001, McKendry, 2002b). Direct combustion, gasification and pyrolysis are considered as the thermo-chemical processes.
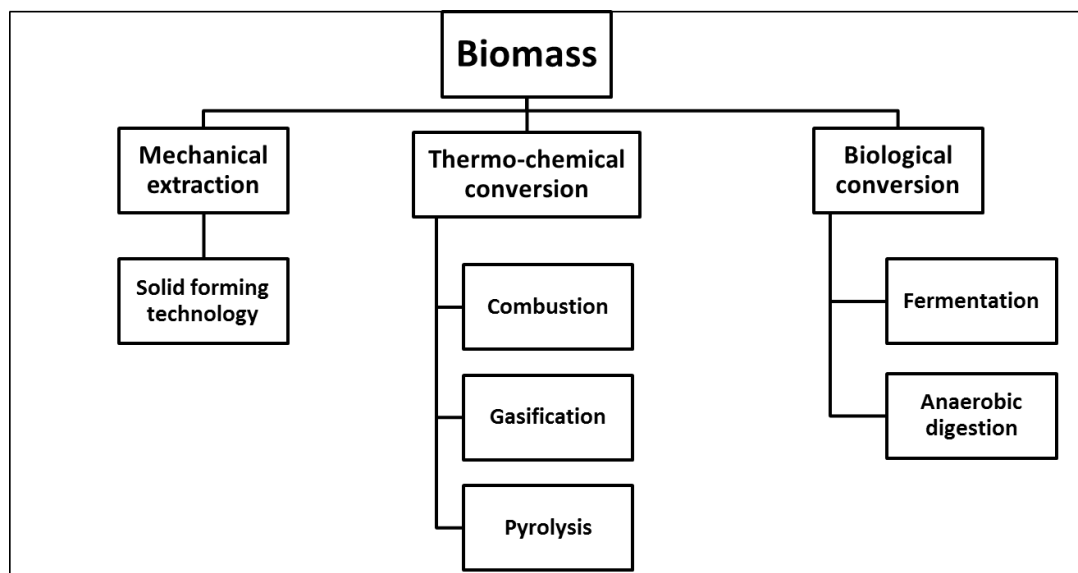
Fig. 2.1 The main processes for the biomass conversion technologies (McKendry, 2002b).

Direct combustion

The direct combustion of biomass is widely applied in small scale cooking and domestic heating by converting chemical energy stored in biomass into heat (Faaij, 2006). In modern industrial technology, combustion is also employed in large scale application to produce mechanical power and electricity with the aid of boilers, steam

turbines and turbo-generators. The temperature range of biomass combustion is within 800-1000 ℃. Materials with the moisture content higher than 50wt% are not suitable for combustion processes (McKendry, 2002b). The net efficiency of electricity generation from biomass combustion varies between 20% and 40% (Demirbaş, 2001). The efficiency could be improved either by scaling up the system to over 100 MWe or co-firing with coal (< 10wt% by weight) (van den Broek et al., 1996).

Gasification

Gasification process converts biomass, a low energy density material, into a gaseous product (LHV at 4-11 MJ/N/m^3), which is a mixture of CO, H$_2$, CH$_4$ and CO$_2$ (LRZ, 1993). Gasification is a partial oxidation process and it is commonly operated at 800-900 ℃ for biomass gasification (McKendry, 2002b). In some cases, steam would also be used as the gasifying agents. The gaseous products from the gasifier can be utilized in gas engines or gas turbines for the generation of electricity. In terms of economics, it has also been proven that the performance of a biomass gasification plant with a combined cycle gas turbine (CCGT) is comparable to that of a conventional coal power plant (Demirbaş, 2001), if not better.

Pyrolysis

Pyrolysis is a thermos-chemical process, in which biomass decomposes into fuel gas, bio-oil and solid char in the absence of

oxygen. The selectivity leading to different types of product could be controlled by manipulating the operating conditions (temperature and residence time). Low temperatures (< 500 ℃) and long residence time favour the production of solid char (up to 35wt% yield), whilst high temperatures (700-1100 ℃) and short reaction time favour the production of gases (up to 80wt% yield) (Lan, 2011). Bio-oil production is normally favoured at 500 ℃, with a very short retention time (< 1 s) (Bridgwater et al., 1999). The comprehensive review of the fast pyrolysis process is detailed in Section 2.3.1.

Fermentation

Fermentation is a bio-chemical process which is used for the production of about 80% of world's ethanol (Lin and Tanaka, 2006). The main process of fermentation involves using microorganisms to convert sugars into ethanol under a warm and wet environment. The sugar is typically obtained from the mechanical handling (crushing and mixing with water) of sugar rich crops, such as sugar cane and sugar beet. However, the high cost of sugar rich crops has diminished its proportion of utilization in fermentation. The starch based biomass is also commonly used for ethanol production. However, it requires an extra step to convert starch into sugar by enzymatic reactions.

Anaerobic digestion

Anaerobic digestion involves using anaerobic microorganisms to convert biomass into bio-gas (CH_4 and CO_2 as the main gaseous products) by means of decomposition. Under the anaerobic environment, the organic material in biomass would be decomposed into usable-sized molecules, such as sugar, as the first step. The sugar molecules would then be converted into organic acids and further decomposed to CH_4 gas. This process has been proven as a commercially feasible technology and is widely applied in the rural areas of China.

2.2 Biomass based hydrogen production

2.2.1 Hydrogen energy carrier

The world energy timeline can be divided into three eras from the past to the future: fossil-fuel era, transition era and hydrogen era (Rosen and Koohi-Fayegh, 2016). Due to the depletion of fossil energy and the associated environmental concerns, hydrogen and electricity will be the major energy carriers within the hydrogen era in the future. The virtue of hydrogen includes non-polluting, inexhaustible, high efficiency and cost-effective, thus making it a very versatile energy carrier (Navarro et al., 2007, Ma et al., 2016). At the beginning of this century, the International Energy Agency (IEA) published the IEA Hydrogen Program and acknowledged the significant role of hydrogen energy in future energy mix (Elam et al.,

2003). The main advantageous and disadvantageous aspects of hydrogen as an energy carrier are summarized (Rosen and Koohi-Fayegh, 2016):

- Producible: Hydrogen is a widely available element on the earth. It could be produced from carbohydrates (i.e., biomass and fossil fuels) and water, which covers more than 70% of the earth surface and is the most available hydrogen mine.

- Utilizable: Hydrogen gas can be used in a variety of areas on a massive scale: production of ammonium, upgrading of heavy oil, desulfurization of petroleum and chemicals, portable power generation and transportation (Levin and Chahine, 2010).

- Transportable: Hydrogen can be transported to the energy consumers over long distances by many ways. The technology of conventional pipelines is one of the feasible ways. It is reported that its energy loss is lower than that of electricity transportation involving high-voltage electrical lines (Balat, 2008, Ball and Wietschel, 2009).

- Environmental friendly: The hydrogen energy could be derived from oxidation reactions, such as direct burning. During its conversion, it only produces water as product. A trace amount of nitrogen oxide would be released only when burning

hydrogen in air. However, a careful design of burner could help solve this problem (Wallace and Ward, 1983).

- Low energy density: Albeit having the highest heat value on mass basis (excluding the nuclear energy), the energy density of hydrogen is lower than other common fossil fuels on volume basis due to its lowest molecular weight. Calculations show that the liquid hydrogen only has ca. 80% of the energy storage density of gasoline whilst the solid storage with metal hydride has an even lower density with only 35% that of gasoline storage (Wallace and Ward, 1983). Low energy density restricts the development of hydrogen energy.

- High cost: The utilization of hydrogen as an energy carrier incurs higher costs compared with traditional fossil fuels based on current technologies and reserves of fossil fuels at the moment. However, such a prediction will be changed in the near future.

- Lack of public awareness: The public's fear of safety associated with hydrogen utilization also affects the hydrogen energy development negatively (Rosen and Koohi-Fayegh, 2016). In fact, many studies have reported that hydrogen energy is safer than that of gasoline and methane when comparing the density, flame temperature and explosion energy (Cipriani et al., 2014, Sharma and Ghoshal, 2015). Considering that hydrogen is non-toxic, any leakage of

hydrogen would have lower risk of human health and environmental damages. Efforts to raise public awareness should be emphasized.

2.2.2 Current status of the hydrogen production

The global hydrogen output was ca. 38 Mt in 2004, and reached 53 Mt in 2011 (Levin and Chahine, 2010). The rapid increase is attributed to the increasing demand in oil refining industry as well as sulphur removal in gasoline and diesel sectors. The common raw materials for H_2 production include natural gas, naphtha, heavy oil, coal, water, biomass, carbonaceous wastes (Navarro et al., 2007). According to an earlier statistics, fossil fuels accounted for more than 96% of the hydrogen production, among which 48% of the total production was contributed by natural gas, whilst oil and coal were responsible for 30% and 18% of the production, respectively (Balat, 2008).

Current technologies for hydrogen production are summarized in Table A-1 detailing their characteristics and relative costs. The main processes for hydrogen production include steam reforming of methane (SMR) and partial oxidation of coal and heavy oil (Armor, 1999). However, the production of hydrogen from fossil fuel is highly associated with the formation of large quantity of CO_2 as a by-product. At current stage, the carbon capture and storage (CCS) has no economic benefits for the production of H_2 (Lindsay et al.,

2009). Thus, hydrogen production from clean energy resources, such as biomass, is important and has the potential to be the hotspot of future research (Chen et al., 2016, Chen et al., 2015).

2.3 Steam reforming of bio-oil

Hydrogen production from fossil fuels, such as natural gas, coal and naphtha, is considered as mature and has been commercialized for many decades (Gaudernack, 1998, Navarro et al., 2007). However, the growing consensus of fossil fuel shortages and global warming concern impel the transformation of energy resources from fossil fuel to more sustainable energy resources such as biomass. Bio-oil is derived from biomass by fast pyrolysis. The superiority of bio-oil is in its higher volumetric energy density, which is approximately 10 times of that of conventional biomass (Raffelt et al., 2006). Consequently, bio-oil is associated with a much lower transportation cost. Due to this superiority, pyrolysis unit could be separated from the reforming unit and employed at the place where feedstock is readily available. The Catalytic steam reforming of bio-oil has already been studied by many researchers (Trane et al., 2012). However, its development and up-scaling are still limited by many factors, most of which are limited to the inherent characteristics of bio-oil, such as strong oxidation, strong corrosivity, volatility and complex components. Therefore, in actual operation, bio-oil needs to be pre-processed for upgrading via thermal cracking,

hydrodeoxygenation and/or esterification (Mortensen et al., 2011, Zhao et al., 2009).

2.3.1 Components and production of bio-oil

Previous works have already confirmed that there are over 200 types of oxygenated compounds formed during the pyrolysis of biomass (Mohan et al., 2006, Zhang et al., 2007b). The main components of bio-oil could be summarized as a liquid mixture of water, aldehydes, alcohols, acids and oligomers, which were obtained from the depolymerization and fragmentation of cellulose, hemicellulose and lignin in biomass (Czernik and Bridgwater, 2004). In fact, many of the oligomeric structures are not detectable by gas chromatography-mass spectroscopy (GC-MS) or even high-pressure liquid chromatography (HPLC). In Table 2-1, it shows a typical composition of bio-oil derived from poplar.

Table 2-1 A typical bio-oil composition (Radlein et al., 1991).

Composition of the bio-oil	Mass fraction (wt%)
Acetic Acid	8.2
Formic Acid	4.7
Hydroxyacetaldehyde	15.2
Glyoxal	3.3
Methylglyoxal	1.0
Formaldehyde	1.8
Acetol	2.1
Ethylene Glycol	1.6
Levoglucosan	4.6
1, 6-Anhydroglucofuranose	3.6

Table 2-1 continue

Composition of the bio-oil	Mass fraction (wt%)
Fructose	2.0
Glucose	0.6
Cellobiosan	2.0
Oligosaccharides	1.1
Pyrolytic Lignin	24.6[a]
Unidentified	23.6

[a] material precipitated by addition of water.

Currently, the most effective way to produce bio-oil is via fast pyrolysis of biomass, in which biomass is heated at an extremely high heating rate (>1,000 ℃/s or even at 10,000 ℃/s) and then the resulting products are condensed to form bio-oil (Bridgwater, 1996, Bridgwater et al., 1999). The conventional pyrolysis is operated at a temperature range of 300 to 600 ℃, and the residence time is kept within 3 to 30 min (Maschio et al., 1992). Although the fast pyrolysis is carried out at a similar temperature condition, the residence time used is usually much shorter, i.e., less than 2 S. This difference presents a total different product distribution whereby the fast pyrolysis could boost the liquid fraction to 60-75wt% or even higher compared with originally only 20-45wt% in conventional pyrolysis (Raveendran et al., 1996, Mohan et al., 2006). For example, Mann et al. (Mann et al., 1994) investigated components of biomass-derived oil and emphasized the advantages of fast pyrolysis. The production of bio-oil from biomass could achieve as much as 75-80wt% of production by weight (Bridgwater et al., 1999).

In fast pyrolysis, the organics would decompose into oligomers due to the exposure to high temperatures. Before further decomposition takes place to convert these oligomers into gas products by secondary reactions, the oligomers are condensed into a dark brown liquid due to the short residence time (Bridgwater and Peacocke, 2000). The estimated residence time before condensation occurs is within 2 s, and it can also be extended to 5 s if the temperature could be kept below 400 ℃ (Bridgwater et al., 1999). There are several key features of a fast pyrolysis process listed as follow:

- The biomass feed needs to be maintained in fine particle size in order to achieve high heat transfer rates.

- The biomass should be pre-dried to control moisture under 10wt% by weight.

- The pyrolysis is usually carried out at ca. 500 ℃ with a high heating rate (> 500 ℃/s) (Carlson et al., 2009).

- The residence time of vapour phase should be less than 2 s before condensation.

2.3.2 Steam reforming of methanol

Background

Methanol is the most popular energy carrier for direct generation of electric power due to its high Hydrogen/Carbon ratio and absence of C-C bond (Sá et al., 2010). It is therefore used as a raw material for H_2 production. Furthermore, the additional advantage of steam

reforming of methanol is that it can be operated at low temperatures (200-300 ℃), sometimes even below 200 ℃ (Breen and Ross, 1999), whilst on the other hand, steam reforming of ethanol is usually operated at above 600 ℃ with transition metals based catalysts. The operating temperature of methane reforming is also much higher, which is normally in the range of 400 to 750 ℃ (Ferreira-Aparicio et al., 1998, Mattos et al., 2012). The superiority of methanol includes: firstly, methanol, unlike methane, could be activated easily without applying high heat energy; secondly, the inexistence of C-C bonds avoid the possibility of the formation of other hydrocarbons, rather than CO or CO_2 (Palo et al., 2007).

The catalysts commonly used for steam reforming of methanol can be divided into two categories: Copper-based catalysts and group 8-10 catalysts. Cu-based catalysts, such as the commercialized $Cu/ZnO/Al_2O_3$, are the most widely studied and used catalysts (Peppley et al., 1999, Shishido et al., 2004, Turco et al., 2004). Its excellent activity is embodied in its high selectivity of H_2 whilst disfavouring the production of CO (Trimm and Önsan, 2001). However, Cu-based catalysts are limited by their pyrophoric characteristic and metal sintering issue (Karim et al., 2008, Yao et al., 2006), both of which cause a mitigation of research direction towards to the group 8-10 catalysts. However, these catalysts

showed relatively lower H_2 selectivity compared with Cu-based catalysts.

Mechanism

The reaction pathways of methanol steam reforming over copper-based catalysts have been published in a great number of literatures in the past 30 years (Peppley et al., 1999, Santacesaria and Carrá, 1983). It is found that methanol can decompose into carbon monoxide and hydrogen first before carbon monoxide is converted by WGSR:

$$CH_3OH \rightarrow CO + 2H_2 \qquad (R\ 2.1)$$

$$CO + H_2O \rightarrow CO_2 + H_2 \qquad (R\ 2.2)$$
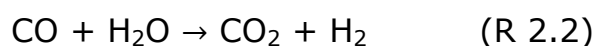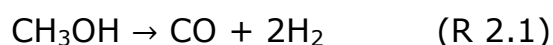
Based on chemical equilibrium, the concentration of CO in the product, which should be higher than the equilibrium level, lower than the equilibrium concentration (Amphlett et al., 1985). Thus, a new mechanism was proposed by Takahashi and Jiang based on the theory of single type active sites (Takahashi et al., 1982, Jiang et al., 1993a, Jiang et al., 1993b). In the proposed mechanism, hydrogen is first generated by dehydrogenation of two methanol molecules to form one methyl formate:

$$2\ CH_3OH \rightarrow HCOOCH_3 + 2H_2 \qquad (R\ 2.3)$$
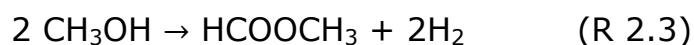
The obtained methyl formate would react with water to produce methanol and formic acid, which would then produce carbon dioxide and hydrogen via decomposition:

$$HCOOCH_3 + H_2O \rightarrow CH_3OH + HCOOH \qquad (R\ 2.4)$$

$$HCOOH \rightarrow CO_2 + H2 \qquad (R\ 2.5)$$
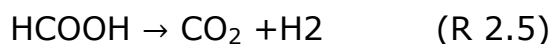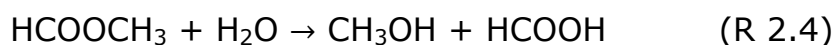
Besides that, Takezawa et al. (Takezawa and Iwasa, 1997) reported a third mechanism involving intermediates such as formaldehyde and formic acid. Methanol dehydrogenates to form formaldehyde, which is then attacked by H_2O to form formic acid followed by the decomposition to CO_2 and H_2:

$$CH_3OH \rightarrow HCHO + H_2 \qquad (R\ 2.6)$$

$$HCHO + H_2O \rightarrow HCOOH + H_2 \qquad (R\ 2.7)$$

In the second and third proposed mechanism, CO is produced via the decomposition of methanol. It suggested that the reverse WGSR is probably the route for CO formation:

$$CO_2 + H_2 \rightarrow CO + H_2O \qquad (R\ 2.8)$$
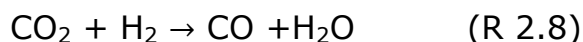
Although there is not a commonly agreed mechanism for methanol steam reforming, it is generally believed that CO is the product of reverse WGS reaction instead of as a product of the direct decomposition of methanol. More recently, a more comprehensive catalytic mechanism cycles was proposed by Frank et al. as shown

in Fig. 2.2 (Frank et al., 2007). The proposed theory assumed that there are two types of active sites on the catalyst surface: H_2 is adsorbed onto S_A whilst all the other intermediates are adsorbed onto S_B. The first cycle, as shown in Fig. 2.2, illustrates how methanol transforms into formaldehyde by dehydrogenation. Subsequently, the combination of formaldehyde and methoxy group leads to the formation of methyl formate, which would further decompose into formate group and methoxy group in the presence of hydroxyl. The second cycle exhibits that the formaldehyde attacked by hydroxyl groups could form dioxomethylene, which would generate CO_2 and H_2 via a two-step dehydrogenation.
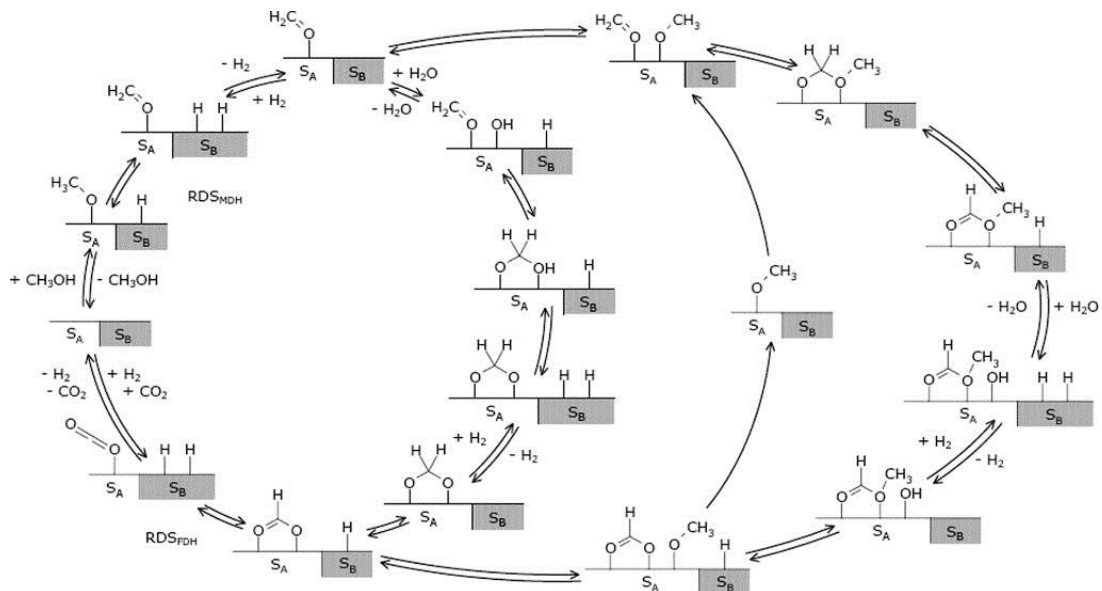
Fig. 2.2 Catalysis cycle of methanol steam reforming including two distinct kinds of active sites: S_A and S_B (Frank et al., 2007).

2.3.3 Steam reforming of ethanol

Background

Recent development in bioethanol production from various types of biomass provides a new opportunity for hydrogen production from biomass. The utilization of lignocellulosic resources, such as wood, corn stover and agricultural waste, boosts the availability of bio-ethanol and weakens the impact on food supply (Huber et al., 2006).

Hydrogen production from steam reforming of bio-ethanol is already widely accepted as a cost-effective and energy-efficient process (Haryanto et al., 2005). Ethanol is also less hazardous to human beings and the environment compared to methanol. However, the drawbacks associated with SRE include the high operating temperature necessary for the scission of C-C bonds as well as carbon deposition that determinates the performance of the catalyst. Much work has been done previously to promote the stability of catalysts. Strategies, such as introducing more stream and co-feeding O_2 or CO_2, are being studied. However, the modification of the catalysts has attracted the most attention (Mattos et al., 2012). The well harnessing of the catalysts requires a good understanding of the reaction mechanisms including reaction pathways and different categories of intermediates.

Mechanism

The reaction pathway of ethanol reforming has been studied extensively, most of which revolve both the analysis of reforming and characterization methods, including the use of spectroscopic technologies and thermal adsorption/desorption technologies. The ultimate aim of catalytic steam reforming of ethanol is to produce only H_2 and CO_2 as products. Compared with other reaction routes such as oxidative steam reforming (OSR) and partial oxidation (POX), the advantage of steam reforming is that hydrogen atoms come from both ethanol and water. The main route of steam reforming is shown in the following reaction:

$$C_2H_5OH + 3\ H_2O \rightarrow 2\ CO_2 + 6\ H_2 \qquad \text{(R 2.9)}$$

However, a number of reaction pathways might exist during ethanol steam reforming. The occurrence of these reaction pathways mostly depends on the nature of the catalysts used and the reaction conditions adopted, which includes operating temperature, pressure, residence time and feed composition. The primary reactions of the ethanol decomposition in steam reforming process can be summarized by following four reactions (Montero et al., 2015, Haryanto et al., 2005):

Ethanol dehydrogenation:

$$C_2H_5OH \rightarrow C_2H_4O + H_2 \qquad \text{(R 2.10)}$$

Ethanol dehydration:

$$C_2H_5OH \rightarrow C_2H_4 + H_2O \qquad \text{(R 2.11)}$$
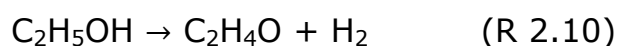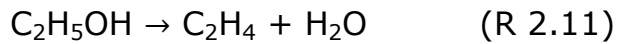
Ethanol decomposition into methane:

$$C_2H_5OH \rightarrow CH_4 + CO + H_2 \qquad \text{(R 2.12)}$$
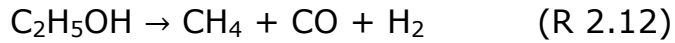
Ethanol decomposition into acetone:

$$2C_2H_5OH \rightarrow CH_3COCH_3 + CO + 3H_2 \qquad \text{(R 2.13)}$$
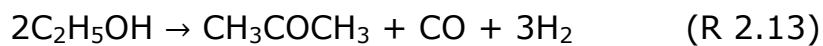
The secondary reaction pathways are represented as follows:

$$C_2H_4O \rightarrow CH_4 + CO \qquad \text{(R 2.14)}$$

$$C_2H_4O + H_2O \rightarrow CO + 3H_2 \qquad \text{(R 2.15)}$$

$$CO + H_2O \rightarrow CO_2 + H_2 \qquad \text{(R 2.16)}$$

$$CH_4 + H_2O \rightarrow CO + 3\ H_2 \qquad \text{(R 2.17)}$$

$$2\ CO \rightarrow CO_2 + C\ (coke) \qquad \text{(R 2.18)}$$

$$CH_4 \rightarrow 2\ H_2 + C\ (coke) \qquad \text{(R 2.19)}$$

$$C_2H_4 \rightarrow polymers \rightarrow coke \qquad \text{(R 2.20)}$$

$$CH_3COCH_3 + H_2O \rightarrow 3CO + 5H_2 \qquad \text{(R 2.21)}$$
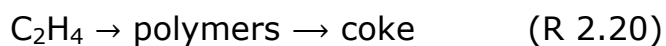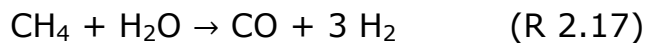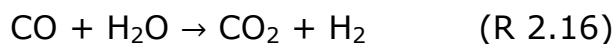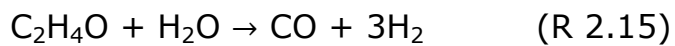
The objective of the ethanol steam reforming is to convert all the hydrogen atoms from ethanol molecules into H_2 and subsequent convert all CO into CO_2 via WGSR (R 2.16). This leads to the formation of H_2 from water. However, the actual steam reforming

involves a very complex reaction pathway and many undesirable intermediate compounds and by-products may form during the reforming process. For example, the dehydration of ethanol could produce ethylene (R 2.11), which is regarded as the precursor of carbon deposition via polymerization (R 2.20) (Vaidya and Rodrigues, 2006, Cai et al., 2013). Therefore, the prohibition of undesirable reaction is based on a good knowledge of mechanism and modification of catalysts.

2.3.4 Steam reforming of bio-oil

Generally, bio-oil has a very complex distribution of components, which include alcohols, acids, hydroxyacetones, furans, phenols and cresols (Zhang et al., 2007b). The steam reforming of bio-oil involves the reforming of various components. The complete chemical reaction could be presented as following (Wang et al., 1996):

$$C_nH_mO_k + (n-k)\ H_2O \rightarrow n\ CO + (n + m/2 - k)\ H_2 \qquad \text{(R 2.22)}$$
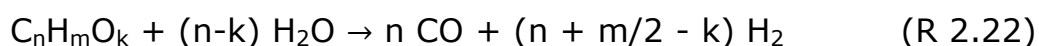
In addition, more H_2 could be produced via WGSR. However, in the actual bio-oil reforming reaction, direct thermal decomposition would occur simultaneously resulting in the formation of coke:

$$C_nH_mO_k \rightarrow C_xH_yO_z + \text{gas products} (H_2, CO, CO_2, CH_4...) + \text{coke}$$
$$\text{(R 2.23)}$$
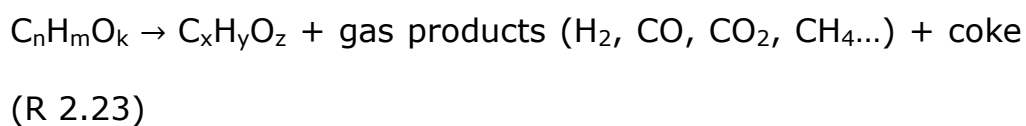
However, the component distribution of bio-oil changes with the biomass precursor as well as pyrolysis conditions. Therefore, it is not possible to develop a universal reaction mechanism or kinetic model for the general bio-oil steam reforming.

Ni-based catalysts remain one of the most popular active components. Chen et al. (Chen et al., 2016) used Ca to modify the chemical properties of Ni/Al_2O_3 surface in the steam reforming of sawdust pyrolytic products. The gas products was found to be of 90vol% syngas (H_2/CO =1.01) when the molar ratio between Ca and Al was 3. The experiment demonstrated a route to control CO concentration in the resulting gas products for different applications by changing the amount of Ca in the supporting material. It was found (Chen et al., 2016) that increasing the Ca content could promote CO yield whilst restraining CO_2 production. However, this experiment was not a continuous reaction and only 5 g of sawdust sample were tested in the fix-bed reactor. Hence the durability of the reforming process was not tested. Most catalysts being studied in steam reforming of bio-oil would lose their initial productivities within 10 h (Trane et al., 2012). The main reason is due to the serious deposition of carbon coupled with sulphur deposition. Sulphur is known to be a poisoning element to a lot of catalysts (it will be detailed again in Section 2.5.3). In addition, there are also many other inorganics in bio-oil, such as alkali salts and phosphor

containing salts, which would also deposit on the catalyst surface and block the active sites (Oasmaa and Czernik, 1999). One of the best performances in terms of catalyst stability was reported by Czernik et al. (Czernik et al., 2002). The commercial nickel-based catalysts utilized remained active for 90 h with a decline of only 10% during the reforming of bio-oil derived from pine sawdust. It is worth mentioning that the reforming bed used in this investigation was a fluidized bed which could have had positive influence on the mitigation of coke.

2.4 Catalysts for steam reforming

Ever since the methodology of hydrogen production from biomass derived oil (bio-oil) was proposed by the US National Renewable Energy Laboratory (NREL) in the 1980s, a number of researches had been carried out on the development of catalysts for steam reforming (Xu and Froment, 1989, Wang et al., 1996, Rostrup-Nielsen, 1984a). The selection of suitable materials for catalyst is crucial, which determines the nature of catalysts, and hence remains the focus of searching for steam reforming catalyst (Rioche et al., 2005, Ni et al., 2007). In previous studies, many novel catalysts with high performance and good durability have been established and tested, however, more work needs to be carried out in order to make the optimal catalysts, which could provide an excellent catalytic performance as well as be of low cost (Hou et al.,

2015). The following section details the development of catalysts in separation parts: transition metal catalyst and noble metal catalyst.

2.4.1 Transition metal catalyst

Transition metals are widely applied in catalytic steam reforming. Among all of the transition metal catalysts, Ni-based catalysts are found to exhibit the highest activity for steam reforming due to its excellent ability to selectively break the C-C bonds and to promote the WGSR. Auprêtre and co-workers (Auprêtre et al., 2002) investigated the natural effects of a suite of active metals (Pt, Rh, Pd, Ni, Cu, Zn, Fe) on SRE reaction and the results showed that Ni and Rh exhibited the highest H_2 yields. Besides, the low costs of nickel make it widely used on commercial scale compared with the expensive noble metal based catalysts (Davda et al., 2005, Nichele et al., 2012). However, the use of Ni-based catalysts in bio-oil steam reforming are usually associated with engineering issues such as deactivation and reactor occlusion which are due to metal poisoning, metal sintering, and its poor coke resistance ability in particular.

At the very early stage, the use of commercial Ni-based catalyst (15wt% Ni by weight in $Al_2O_3/CaAl_2O_4$) in the steam reforming of HAc and hydroxyacetaldehyde showed that the conversion of the two model compounds was almost 100mol% at the temperature above 400 ℃ (Wang et al., 1996). It was also found that the

reforming of HAc resulted in the formation of carbon layer on the surface of the catalyst and the carbon deposit could be converted into carbon monoxide in the presence of hot steam. The adsorbed acetate species, ketene and intermediates CH_x (X = 1-3) acted as the precursors for the carbon deposition. It was later reported that low acidity condition could help suppress carbon formation via the inhibition of direct decomposition of hydrocarbons (Hu, 2009). Therefore, alkali or alkali earth elements, such as B, K, Mg, Ca and La, are often added into alumina catalysts to adjust surface acidity of catalysts (Ni et al., 2012, Vizcaíno et al., 2009). Apart from doping alkali elements into acidic alumina, the usage of basic MgO as the support material to prepare $Ni_xMg_{1-x}O$ solid solution was also tried (Yu et al., 2014). The modified $Ni_xMg_{1-x}O$ showed a very stable performance in CH_4 reforming with a conversion rate of 85mol% for 125 h.

Several other novel support materials have been developed and tested. The sol-gel method was used to prepare the Ni/SiO_2 catalyst for ethanol steam reforming (Wu and Williams, 2010). Compared with general Ni/SiO_2 prepared via impregnation, the sol-gel catalyst showed higher nickel dispersion with smaller nickel particles. The TPO and TEM analysis confirmed that the carbon deposition and metal sintering issue had also been mitigated. The BET test showed that the specific surface area of the sol-gel prepared catalyst was as

high as 300-800 m^2/g, while the surface area of the impregnation catalyst was only 0.6-1 m^2/g. The yield of hydrogen for the sol-gel prepared catalyst was 2-3 times of that of the impregnated catalyst.

Apart from Ni, Co is the second most widely used transition metal in the steam reforming of bio-oil compounds. Co/Al$_2$O$_3$, Co-Ce/Al$_2$O$_3$ and Co-La/Al$_2$O$_3$ catalysts were prepared and used for the steam reforming of HAc (Hu and Lu, 2010). All three catalysts exhibited conversion rates above 90mol% with H$_2$ selectivities above 78mol% even at a very low temperature (450℃). The results showed that cerium restrained the generation of by-products (acetone and ketene) and led to a higher hydrogen production. Some research has explored the blending of Ni and Co as a bimetallic catalyst. Ramos et al. (Ramos et al., 2007) investigated the optimal blending ratio of Ni and Co in a study of acetol steam reforming. The co-precipitation method was employed to prepare catalysts and the results showed that the Ni-Co-Al catalyst at a Ni/Co=0.25 resulted in the highest hydrogen yield. Zhang et al. (Zhang et al., 2007a) had prepared the Ni-Co-Al-Mg catalyst with low Ni and Co content level for the reforming of methane. It was reported in his work that a conversion rate of 83.9mol% was achieved in a 250 hours' test at 750℃ and no carbon deposition was detected on the spent catalyst.

2.4.2 Noble metal catalyst

Compared with transition metals, noble metals are widely known for their higher catalytic activities in steam reforming reactions. Noble metals like Ru, Rh, Pt, Pd and Ir have been tested by various research groups for the steam reforming of bio-oil model compounds specifically (Liguras et al., 2003, Rioche et al., 2005, Vagia and Lemonidou, 2008). Liguras et al. (Liguras et al., 2003) had used Rh, Ru, Pd, and Pt as active compounds instead of Ni. In this work, the catalysts with different metal loadings ranging from 0 to 5wt% were tested in ethanol reforming at 600-850 ℃. The Rh/γ-Al$_2$O$_3$ showed the best catalytic activity on ethanol reforming with the hydrogen selectivity of 95.7mol% at 800 ℃. The γ-Al$_2$O$_3$, MgO, and TiO$_2$ supports have been studied to establish the relationship between high support acidity and the resulting high coke deposition. Similarly, Rioche et al. (Rioche et al., 2005) confirmed that the Rh-based catalyst was the most effective amongst the three selected noble metals as active compounds, i.e., Rh, Pt and Pd. In the steam reforming of several model compounds (HAc, acetone, ethanol and phenol), the performance of various catalysts were found in the following order: 1%Rh-CeZrO$_2$ > 1%Pt-CeZrO$_2$ >1%Rh-Al$_2$O$_3$ > 1%Pd-CeZrO$_2$ > 1%Pt-Al$_2$O$_3$ > 1%Pd-Al$_2$O$_3$. It was reported that Rh-CeZrO$_2$ was the best catalyst yielding approximately 70mol% of hydrogen for each bio-oil model compounds tested. The results also revealed that CeZrO$_2$ support led to a higher H$_2$ yield compared with

alumina counterpart and this could be attributed to the redox of ceria-zirconia. The influence of reforming conditions was also found to be one of the most important factors. Oxygen partial pressure had been introduced as a new parameter along with temperature, GHSV and residence time as the reaction condition. It was shown that excess oxygen would lead to negative effects on reforming reaction.

Moreover, studies of Rh based catalyst were carried out to further improve their activities. Iron was added to $Rh/Ca-Al_2O_3$ to promote the conversion of ethanol at a very low temperature (350 ℃) which was otherwise unachievable by using transition metals (Chen et al., 2010). The selectivity of acetaldehyde was also monitored to prove that the surface of Rh has a high C-C bond breaking ability whilst the hydrogen yield recorded was as high as 68.3mol% at the same temperature. At low temperatures, WGSR favours the production of H_2. In the case of Ni-based catalysts, the operating temperature for the reforming reaction is usually above 600 ℃. However, at such high temperatures, WGSR would be hindered. The $Rh-Fe/Ca-Al_2O_3$ retained a 100mol% ethanol conversion for 300 h. This remarkable stability of the $Rh-Fe/Ca-Al_2O_3$ is attributed to the addition of Fe_xO_y, which alters the Co-Rh bonding force and directs the CO from Rh to Fe and thus reduced the poisoning effects of CO on surface Rh.

Besides Rh, Iridium (Ir) is another promising noble metal based as active component for hydrogen production from steam reforming. More recently, Ir-based catalysts are fast becoming popular due to its great capability in breaking the C-C bond (Siang et al., 2010, Cai et al., 2012b). Ir metal is usually supported on the rare earth metal oxides (CeO_2, La_2O_3) due to its resistance to carbon deposition. Moreover, its excellent anti-sintering ability is attributed to the strong interaction between Ir and support materials (Zhang et al., 2006, Chiou et al., 2012, Yang et al., 2012). Siang et al. (Siang et al., 2010) synthesized Ir/CeO_2 catalyst via combining the reduction-oxidation method with the ultrasonic irradiation. The work demonstrated a 100mol% conversion of ethanol at 450 ℃.

2.5 Deactivation of catalysts

The deactivation of catalysts is inevitable with time-on-stream, particularly in a heterogeneous system. Therefore, a good understanding of deactivation mechanisms is beneficial to the extension of catalysts service life and subsequently billions of dollars could be saved from process shutdown and catalyst replacement. Generally, the intrinsic mechanisms of deactivation into several distinct processes: (I) poisoning, (II) coking, (III) sintering, (IV) solid-state transformation, and (V) attrition/crushing (Forzatti and Lietti, 1999, Bartholomew, 2001). In steam reforming of bio-oil model compounds, such as methanol, ethanol, HAc, and

phenol, (II) and (III) are the primary reasons for catalytic deactivation. For the steam reforming of actual bio-oil, poisoning effects also play a crucial role in deactivation due to the chemisorption of sulphur (Bartholomew et al., 1982). These three deactivation mechanisms are detailed in the following sections.

2.5.1 Coke formation

Coking is the mechanical deposition of carbonaceous species from the decomposition or condensation of hydrocarbons in fluid phase (Rostrup-Nielsen and Trimm, 1977). The coking in initial stage could be observed by activity loss of the catalyst which is due to the encapsulation of active sites and blockage of porous voids. The disintegration of active metals on catalysts and plugging of the reactors are both commonly studied. There are two types of coking occurring during the reforming process: pyrolytic coking and catalyst surface coking (Bartholomew, 2001). The pyrolytic coke originates from thermal decomposition of hydrocarbon as a free radical process in a hot environment (above 600 ℃ for methane). This could be minimized by reducing the length of heated tube in the reactor, which could reduce the space for the formation of pyrolytic coke. On the other hand, the catalyst surface coke refers to the carbon deposition on the surface of catalyst originating from the heterogeneous catalysis reaction.

The chemical properties and physical structure of coke formation depend on the catalyst compositions, reaction types and reaction conditions. For the reaction type, the coking reactions had been classified into coke-sensitive and coke-insensitive reactions (Menon, 1990). The coke-insensitive reactions produce carbon deposits directly onto the catalyst surface as the end product, such as catalytic cracking and hydrogenolysis. The carbon in these reaction systems is not reactive due to the low hydrogen partial pressure. In contrary, the carbon deposited in coke-sensitive reaction system is reactive enough to be mitigated due to a sufficient partial pressure of hydrogen. The coke-insensitive reactions, in which coke is regarded as an intermediate, include steam reforming, Fischer-Tropsch synthesis and hydrocracking. In these systems, the type and location of the coke structure have a much more important influence on the catalytic deactivation compared with the quantity of coke. The possible locations of coke can be summarized as (1) monolayer carbon being chemisorbed or multilayer carbon physically being absorbed on the surface of supported material, (2) carbon being deposited on the active metal particles resulting in encapsulation, and (3) carbon being plugged the micro- or mesopores and cut off the access of the crystallites inside these pores (Bartholomew, 2001). The carbon in location (1) does not contribute to the deactivation, whilst the carbon in locations (2) and (3) reduces the number of accessible active sites and debilitate the

reactant adsorption. The location of the coking is often identified to predict the types of carbon structure and hence prevent the deactivation mechanism from happening. For example, the carbon in location (2) usually involves filamentous structure. Thus, a comprehensive understanding of the carbon formation pathway will benefit the study of deactivation.

Reaction pathways of coking

The reaction pathway of coke formation in steam reforming system is due to the carbon deposition originating from carbon monoxide and hydrocarbon decomposition (Bartholomew, 1982, Trimm, 1999, Bartholomew, 2001, Mattos et al., 2012). For the first step, catalyst surface adsorbs dissociated hydrocarbon and/or carbon monoxide molecules. Their reactions could be written as follow (Bartholomew, 1982):

$$CO \text{ (atom)} \rightarrow C\alpha \text{ (atom)} + O \text{ (atom)} \qquad (R\ 2.24)$$

$$C_nH_m \text{ (atom)} \rightarrow C\alpha \text{ (atom)} + H \text{ (atom)} + CH_x \text{ (atom)} + C_2H_y \text{ (atom)} + \ldots + C_nH_z \qquad (R\ 2.25)$$
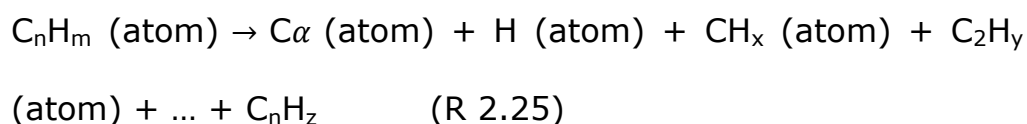
R 2.24 applies throughout the Boudouard reaction and reverse of carbon gasification whilst R 2.25 is the summary of hydrocarbon decomposition. It is believed that the monatomic carbon, denoted as $C\alpha$, is formed after the dissociation of hydrocarbons, which is very reactive and can be easily removed by gasification with steam,

surface atomic oxygen and adsorbed CO_2. It is important to note that steam reforming is a coke-insensitive reaction. The difference between the rate of carbon formation and carbon removal actually dictates both quantity and quality of coking. If the atomic $C\alpha$ is not gasified within a certain period of time, the accumulated $C\alpha$ will then turn into less reactive $C\beta$ via polymerisation. $C\beta$ is a polymeric structure, such as amorphous films and filaments. The gasification rate of $C\beta$ is much lower than that of $C\alpha$. Further accumulation of $C\beta$ will change the carbon structure again where the excess $C\beta$ dissolves into the metallic nickel particles and form nickel carbide (Rostrup-Nielsen and Trimm, 1977). Nickel carbide is regarded as the prerequisite for carbon whiskers growth. The dissolved carbon in nickel would precipitate at the rear side of the nickel particles and lift Ni away from the support surface as the whiskers grow. Thus, growth of whisker carbon will disintegrate the catalyst by loss of active sites. The ultimate growth can also block the catalytic bed and force the reaction system to shut down. As for the evaluation of anti-carbon ability, the existence of carbon whiskers leads to poor performance of catalyst on carbon resistance.

In summary, the pathway of coking in steam reforming involves carbon accumulation and carbon restructuring. It should be pointed out that some forms of carbon do not lead to loss of catalytic activity whilst others do. The contribution to carbon deactivation is

often linked with either encapsulation of Ni with filaments, pores blocking with amorphous films, and/or detachment of Ni with carbon whiskers. However, the amorphous polymeric Cβ and carbon whiskers require much higher temperature for removal compared with Cα. Thus, the mitigation of carbon deposition should be focused on the removal of Cα in the initial stage by increasing its gasification rate.

Carbon characterization methods

The technology of carbon characterization is of great necessities for the investigation and mitigation of carbon deposition. In steam reforming studies, the main propose of characterization is to measure the quantity of carbon deposition and also identify the various carbon species and their weight proportions. Current characterization methods can be divided into two groups: destructive test (or designated as thermal-tech, i.e. TGA, TPO, TPH, etc.) and non-destructive test (or designated as physi-tech, i.e. Raman, XPS, TEM, NMR, etc.).

For the quantification of carbon, thermogravimetric analysis (TGA) is the most commonly used method. In an oxidizing atmosphere (air), TGA measures the weight of the sample as the temperature increases. The burning of coke could be reflected via the loss of the sample weight (shown in Fig. 2.3). However, not all weight losses are linked to the carbon gasification during TGA process. For

example, the evaporation of moisture and volatiles or the gasification of other elements like S and P can also cause a weight loss on the curve. In some cases, the differential scanning calorimetry (DSC) measurement coupled with TG analyser is used to investigate whether the reaction is exothermic or endothermic process. Some works have employed gas chromatography (GC), mass spectrometry (MS) or Fourier transform infrared spectroscopy (FTIR) connected to the TG analyser to monitor the end gaseous products which is useful for identifying the reactions (Fushimi et al., 2003, Sturzenegger et al., 2006).
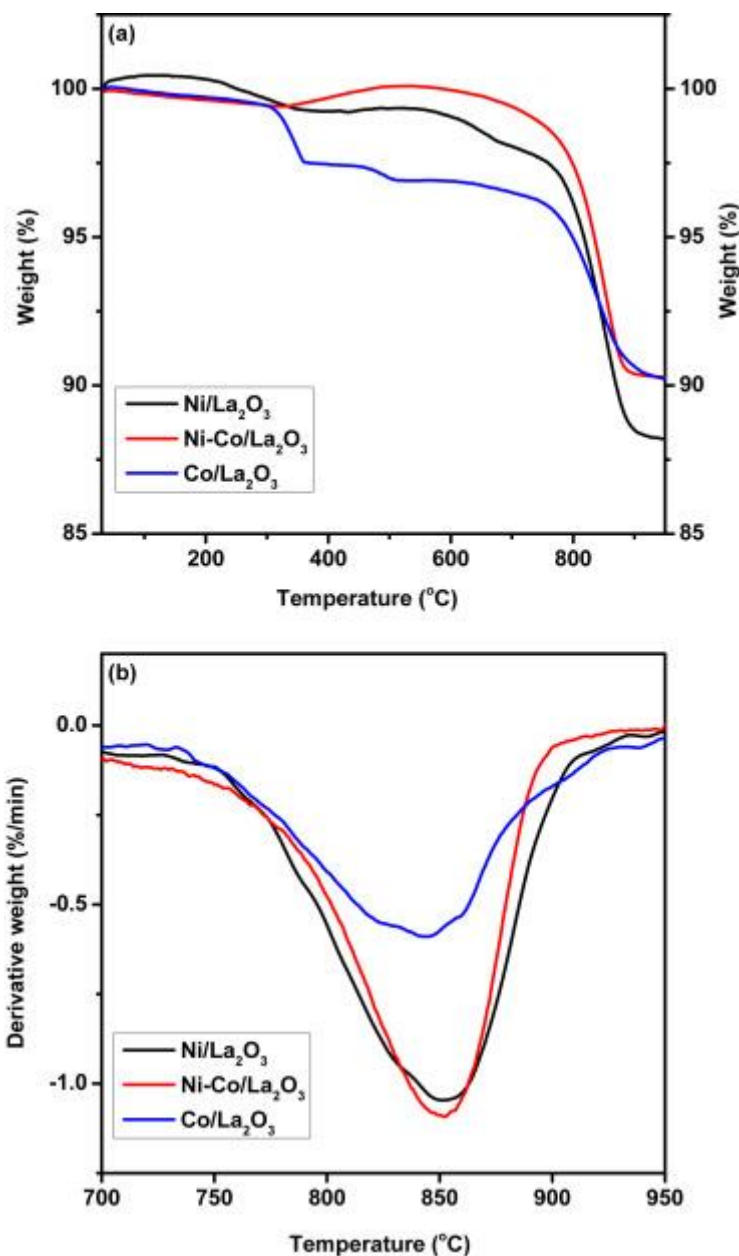
Fig. 2.3 (a) TGA and (b) DTA curves after 6 h of steam reforming for Ni/La$_2$O$_3$, Ni/Co/La$_2$O$_3$ and Co/La$_2$O$_3$ (Nabgan et al., 2016).

Apart from TG analysis, other thermal characterization methods, such as temperature programmed oxidation (TPO) and temperature programmed hydrogenation (TPH), are widely used for carbon

determination and quantification (Wu and Williams, 2010, Li et al., 2015, Quek et al., 2010, Becerra et al., 2001). TPO and TPH are usually carried out in a chemisorption device, in which the spent catalyst could be degassed to remove moisture and volatiles in a pre-treatment step. This is to weaken the interference from contaminants. In a TPO test, the sample is oxidized by the oxygen flow in a temperature-time process. The consumption of O_2 and production of CO_2 can change thermal conductivity of the effluent gas which is monitored via a thermal conductivity detector (TCD). A typical TPO profile is presented in Fig. 2.4.
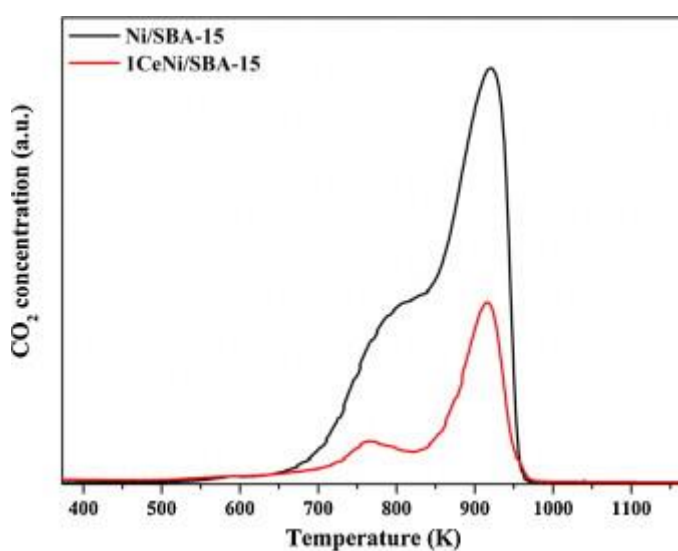
Fig. 2.4 A graphic example of TPO profiles (Li et al., 2015).

TPH (shown in Fig. 2.5) is similar to the TPO test, except that it uses the hydrogenation reaction as the means of carbon removal. Carbon deposits can also react with H_2 to produce CH_4. The difference between TPO and TPH is that the temperatures for carbon

species hydrogenation are normally distinguished from carbon oxidation. In the TPO test, oxygen is consumed during the metal species oxidation. For instance, in a steam reforming system, oxidized-Ni on spent catalyst surface can be reduced to Ni^0 during the reforming process. These Ni^0 can also be oxidized in the TPO test and commonly confused with the oxygen consumption of carbon gasification. Thus, in this aspect, TPH is more suitable for the carbon characterization of the spent catalysts derived from a reducing atmosphere reaction, while the TPO is more suited for materials derived from an oxidation reaction such as partial oxidation. However, in a steam reforming reaction, Ni species are usually not completely reduced and thus attention should be paid to the biased hydrogenation temperature. An extra H_2-TPR test can be carried out to determine the temperature limit for the reduction of any residual Ni^{2+} or Ni^{3+} species. Thus, any hydrogen consumption peaks in TPH occurring at a temperature range higher than that limit should be considered as disturbed data.
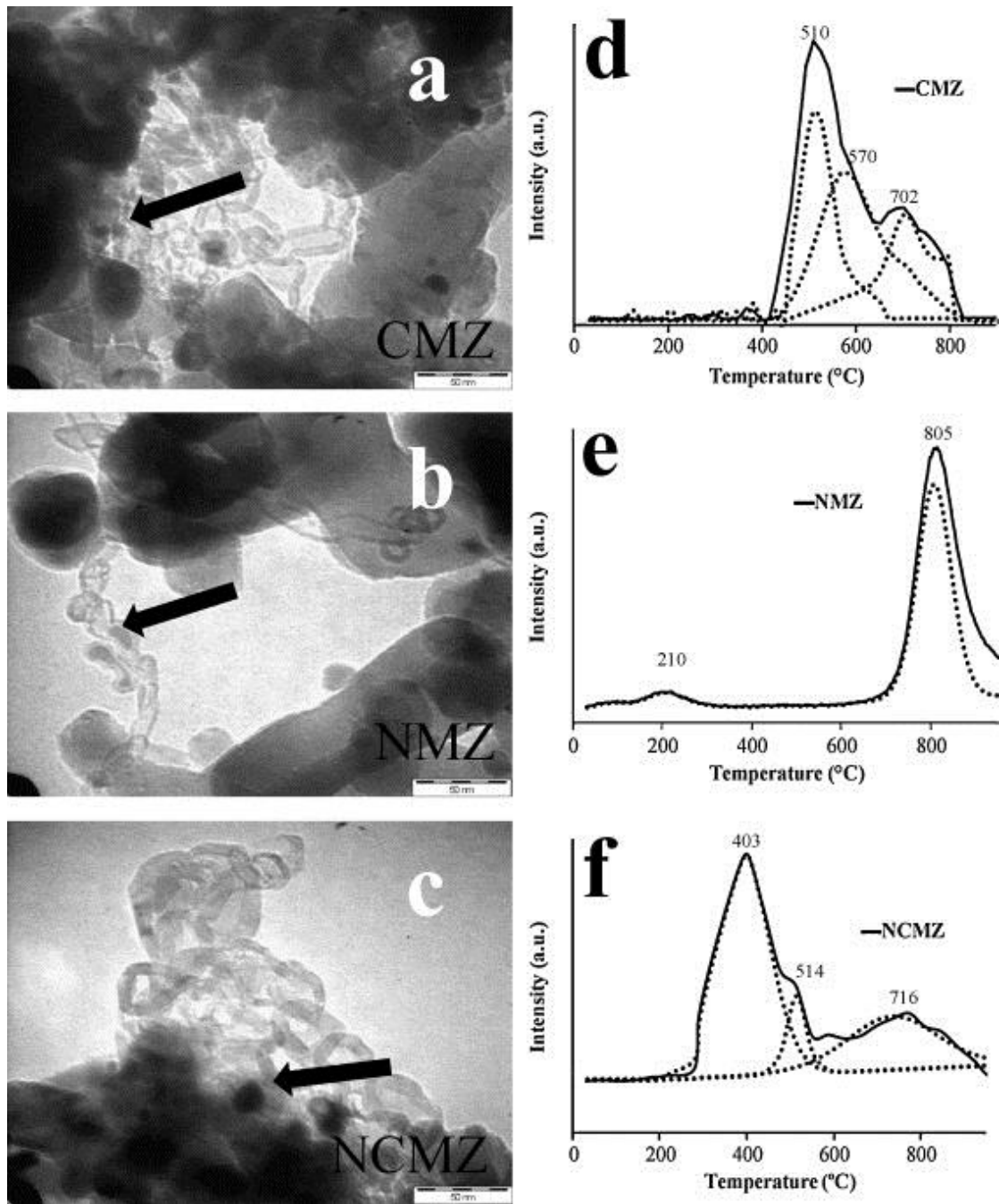
Fig. 2.5 Profiles of TEM and TPH (Fan et al., 2010).

As for the non-destructive methods, Raman spectroscopy is the most widely used method for carbon identification (Robertson, 2002, Li and Stair, 1997, Aguayo et al., 2011). In a typical Raman spectra profile (in Fig. 2.6), there are two main peaks at 1340 cm^{-1} and

1595 cm^{-1} denoted as D band and G band, respectively. The D band is attributed to the 'breathing' mode of disordered aromatic carbon whilst the G band is caused by the graphited carbon with highly ordered structure. Many studies suggested that the area ratio of D/G bands could represent the degree of carbon transformation from disordered structures to graphited structures (Robertson, 2002, Matthews et al., 1999). Thus, this ratio acts as an important marker to evaluate the carbon resistance ability of catalysts.
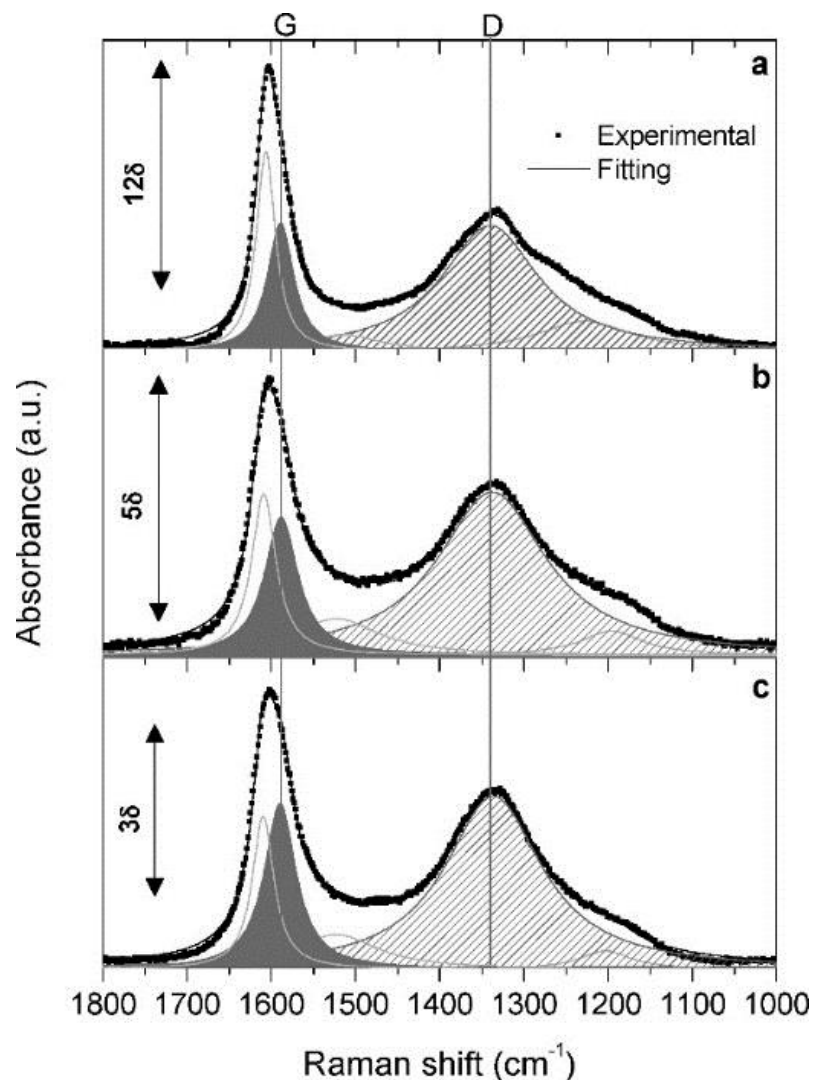
Fig. 2.6 Raman spectra of the coke deposited on the spent catalysts (Aguayo et al., 2011).

The properties of carbon are often characterized by X-ray photoelectron spectra (XPS). C 1s spectra was used to identify C-C, C-CO and CO^{3-} species and suggested that the content of C-C structure is closely linked to the filamentous carbon whilst the other two species are caused by spherical carbon (Kim et al., 2015). XPS was also employed to measure the existence of Ni_3C species (shown in Fig. 2.7), which is commonly regarded as a precursor of

filamentous carbon growth on Ni particles (Yu et al., 2014). Compared with thermal-tech (TPO, TPH), XPS method is widely preferred as it could detect the chemical bonds within the carbonaceous structures. Such detailed characterisation benefits the mechanism study of carbon formation. Furthermore, the TPO and TPH analysis only distinguish between the disordered carbon and the highly ordered carbon based on their gasification temperature range.

In summary, thermal-tech, such as TGA, TPO and TPH, is more suitable for the quantification of carbon deposition, while XPS could provide more information for a mechanism study of carbon formation. However, no single technology can provide a whole picture. Therefore, two or more methods should be applied for a systematic investigation of carbon deposition. The SEM and TEM techniques are also regularly used to examine the physical properties of carbon materials and their morphology on the surface of catalyst.
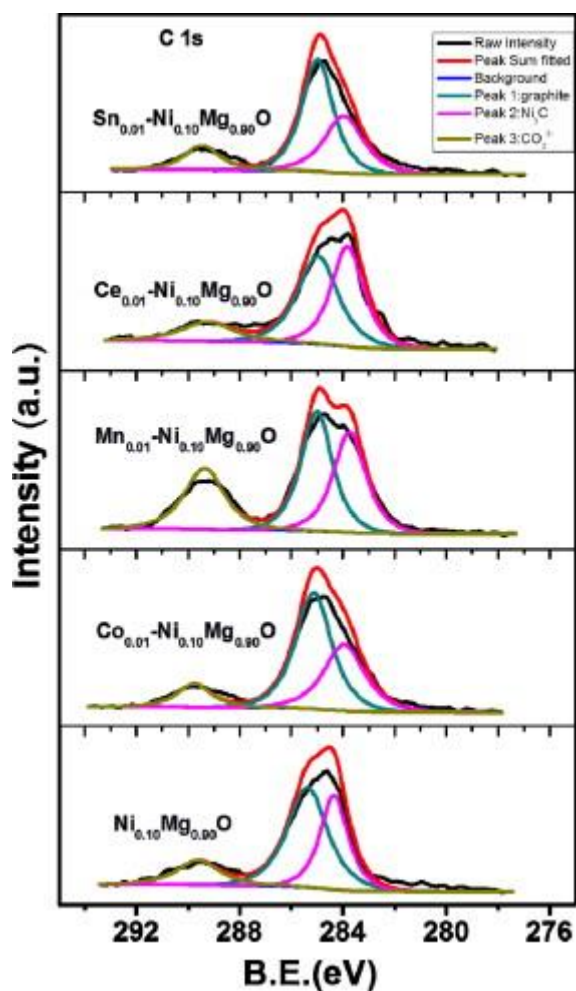
Fig. 2.7 C 1s XPS spectra of the spent NiMgO catalysts (Yu et al., 2014).

Methods for carbon mitigation

The mitigation of carbon deposition is one of the primary research priorities in the area of steam reforming (Bartholomew, 1982, Mattos et al., 2012, Trimm, 1999, Rostrup-Nielsen, 1984a). Several mitigation methods are discussed in this section: increasing steam/carbon ratio, modification of catalysts and size control of active metal. All these three approaches are used to minimise

carbon formation via either inhibition of carbon formation or increasing gasification rate of the deposited carbon.

Increasing steam/carbon ratio is regarded as the most direct way to slow the deactivation by coking. A higher steam/carbon ratio accelerates the gasification rate of deposited carbon species (C + $H_2O \rightarrow CO + H_2$), and subsequently reduce the amount of accumulated carbon. In addition, it is also discovered that the decomposition of acetate species and hydrogen production could be promoted under an excessive water environment according to DRIFTS study (de Lima et al., 2008). However, introducing more steam into a reforming system requires higher energy input and utility costs which will lead to lower efficiency. Some studies also suggested that certain steam/carbon ratio for carbon removal may slow down the kinetics of the reforming process (Bernardo and Trimm, 1979). This means that unilaterally increasing the steam input is not able to achieve a long-term stability. For example, the $Rh/CeZrO_2$ catalyst still encounters a significant deactivation after 7 h, even if it is carried out under a steam-ethanol ratio of 8. In addition, the steam gasification rate of $C\beta$ and $C\gamma$ is much slower than $C\alpha$. Thus, the steam may predominate carbon removal only when the polymerisation of $C\alpha$ could be minimised (Trimm, 1997). In other words, coking could be reduced via increasing of steam-carbon ratio, but this kind of control has rather great limitations, i.e.,

energy cost for water evaporation. Therefore, scientists and engineers are more inclined to use alkali or alkali containing support materials to accelerate the gasification of carbon.

Size control of active metal is an effective approach for carbon mitigation by inhibiting the mechanistic pathways of carbon formation. Rostrup-Nielsen et al. (Rostrup-Nielsen, 1984b) proposed that the ensemble of active sites required for steam reforming is in fact smaller than that needed for carbon formation. The decomposition of any carbonaceous intermediates would undergo the formation of CH_x before yielding monatomic $C\alpha$. The dissociative adsorption of CH_x and polymerization of $C\alpha$ requires ensemble of 6-7 nickel atoms, but steam reforming of CH_x only requires 3-4 nickel atoms (Mattos et al., 2012). Therefore, a critically small nickel particle could effectively increase the difficulty of the carbon nucleation.

A number of synthesis methods have been developed for the preparation of small metallic particles based on sol-gel and co-precipitation (Kugai et al., 2006, Galetti et al., 2008, Bussi et al., 2008, Luo et al., 2016). Sol-gel method was also used to prepare Ni/SiO_2 catalyst, which had a much smaller Ni particle size and higher dispersion compared to impregnated nickel catalysts as shown in Fig. 2.8(Wu and Williams, 2010). The TPO result also showed that the sol-gel catalyst only had 2.0wt% of carbon

deposition compared to the 27.4wt% of coke found in the impregnated catalyst. Although the suppression of coking can be achieved by controlling the size of metallic particles, maintaining the size of small particles is still an intractable issue, especially under a high reforming temperature and thus requires further investigation.
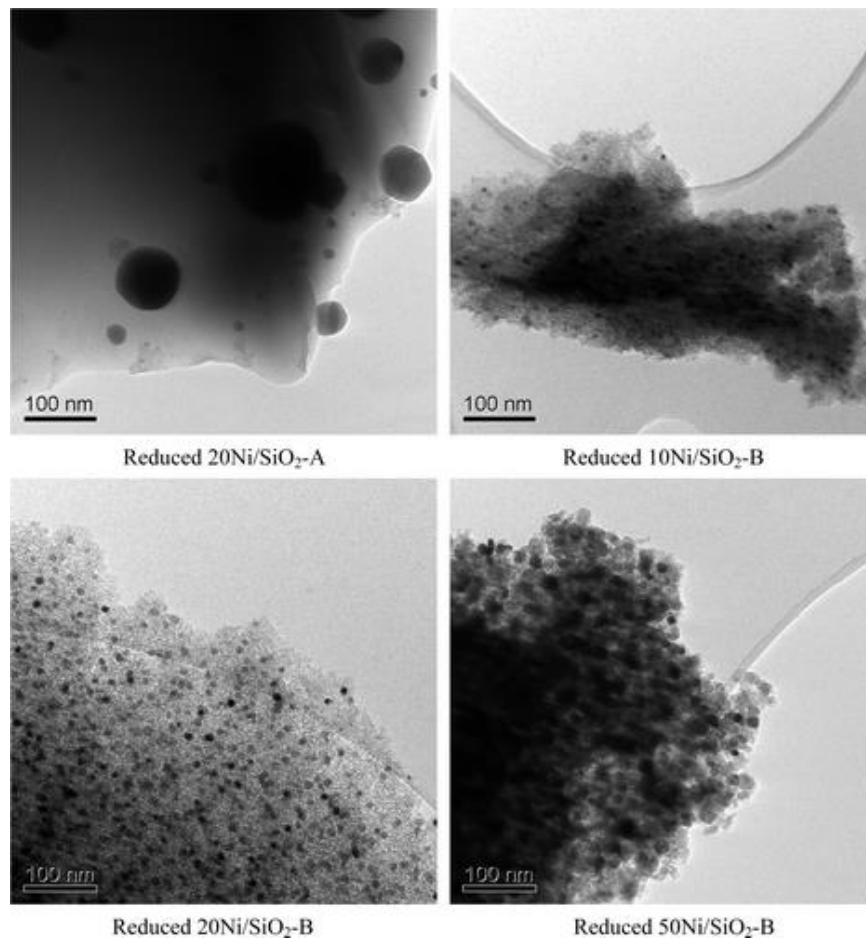
Fig. 2.8 Impregnated nickel catalyst: Ni/SiO₂-A; Sol–gel prepared nickel catalyst: Ni/SiO₂-B (Wu and Williams, 2010).

Modification of catalysts is to alter the nature of the catalysts, which can strongly influence the durability of steam reforming process. Recent good progress in steam reforming has been made

in the development of noble metal based catalysts (Liguras et al., 2003, Rioche et al., 2005, Cai et al., 2014). Compared with transition metals, noble metal catalysts have a lower steam reforming temperature within the range of 300-400℃ (Basagiannis et al., 2008). Low temperature suppresses the growth of active particles and naturally inhibits carbon formation. Meanwhile, WGSR is enhanced for higher hydrogen production under low temperature conditions. Rioche et al. (Rioche et al., 2005) carried out a series of tests using noble catalysts with various bio-oil model compounds and reported that Rh shows higher reforming activity compared to other noble metals, such as Pt and Pd. Similarly, Frusteri et al. (Frusteri et al., 2004) compared Rh with Ni and Co in an ethanol steam reforming test and found Rh is much superior. The Rh, supported by MgO, retained a conversion rate of ethanol above 95mol% for over 20 h, but both Ni/MgO and Co/MgO exhibited a significant deactivation by losing more than 30% of their initial activities. In terms of carbon deposition, it was observed that less than 1wt% of coke was formed on Rh/MgO, and a modest amount of coke, between 3-5wt%, was detected on Ni- and Co-catalysts. Such findings are attributed to the basic characteristics of the supporting material. The particle sizes of both spent Ni/MgO and Co/MgO increased from 7 nm to 20 nm and 14 nm, respectively. However, the average size of Rh particles remained at 10 nm with less than 10% increment even after 20 h of reaction. Apart from

being used as a single active element, noble metals are sometimes applied as the second metallic element. The Pt-Ni catalysts is proposed as a stable structure with improved activity and carbon resistance due to the strong interactions between Pt and Ni (Zhan et al., 2009, Parizotto et al., 2009, He et al., 2015). The beneficial effects of Pt was also studied in n-butane reforming by doping 0.2% of Pt onto 15%Ni/δ-Al$_2$O$_3$ catalyst and found that the addition of Pt increased the butane conversion from 66.7mol% to 99.3mol% with no carbon deposition detected (Avcı et al., 2004).

Although noble metals exhibit outstanding performance in terms of activity and anti-carbon properties, high price and low accessibility limit its extensive utilization. As such, a practical alternative is to modify the support materials by the addition of alkali metals (such as Na, K and Mg) to change the acid/base properties (Llorca et al., 2004, Vizcaíno et al., 2009, Roh et al., 2006). The reason is that base surface can suppress the carbon formation from the direct decomposition of methane and promote the carbon gasification with H$_2$O and CO$_2$. Vizcaíno et al. (Vizcaíno et al., 2008) found that the addition of Mg to a Ni/Al$_2$O$_3$ catalyst dramatically improve the performance of ethanol steam reforming. The molar ratio of Mg/Ni was varied between 0 and 4. The Ni/Mg/Al$_2$O$_3$ (Mg/Ni =1) showed 86.3mol% conversion of ethanol, which was 20% higher than that of Ni/Al$_2$O$_3$. The carbon resistance of Ni/Mg/Al$_2$O$_3$ (Mg/Ni =1) was

also promoted as the basic Mg element would neutralize acid sites on alumina and inhibit the formation of ethylene from ethanol dehydration. Ethylene is regarded as one of the carbon precursors in ethanol reforming and could easily cause coking by direct decomposition. The effects of Mg and Ca and their incorporation over $NiCu/SiO_2$ catalyst have been studied in steam reforming of ethanol (Carrero et al., 2010). The doped catalyst exhibited a much higher carbon resistant ability. The results of derivative TGA, XRD and Raman spectra all suggested that a smaller amount of highly ordered carbon was formed on the modified catalysts. This is attributed to the promotion of Cα gasification rate.

Recently, more research was carried out with rare earth oxides, especially CeO_2 and La_2O_3 as promoters (Kugai et al., 2006, Li et al., 2015, Yang et al., 2012). CeO_2 demonstrates an outstanding capability in the storage and release oxygen for the gasification of surface carbonaceous species and thus keeping the active sites free from carbon encapsulation (Liu et al., 2009, Mattos et al., 2012). Apart from that, the Ni-Ce system can alter the electronic and structural properties of Ni species as the strong metal-support interaction (SMSI) between Ni and Ce enables the stabilization of Ni particles and improves the reducibility of Ni^{2+} ions (Yu et al., 2014). In addition, Ce conveys a positive effect on the WGSR (Senanayake et al., 2011). La_2O_3 is conceived as one of the most widely used

rare earth metals and it could transformed into $La_2O_2CO_3$ species by the adsorption of CO_2 and hence provides CO_2 for carbon removal (Mattos et al., 2012).

2.5.2 Metal sintering

In steam reforming process, the active phase on catalyst plays an essential role on facilitating reactions. This is accompanied by a transformation of its texture, known as metal sintering. Sintering is embodied in the decrease of active surface area which is due to the growth of catalytic crystal particles and also the collapse of porous structures on active phase. Earlier studies have explained this thermal induced process via three principal mechanisms: 1) particle migration, 2) atom migration, and 3) vapour transportation at high temperature (Bartholomew, 2001).

The concept of Tammann temperature suggests that solid surface would have mobile species present at a critical temperature, under which metal sintering could be expected (Tammann temperature of Ni, 590 ℃) (Trimm, 1991). However, the common operating temperature for steam reforming is above 700 ℃. When temperature exceeds the Tammann temperature, the metal particles lose their thermal stability and migrate over to the support surface in the form of entire crystallite or metal atom. At even higher temperatures, metal particles start to release volatile metals which can be captured by larger particles. Therefore, using noble

metals as the active element can decrease the reaction temperature and hence act as a very effective way for resisting sintering (Frusteri et al., 2004).

Stabilization of metal particles can also be achieved by selecting proper supporting materials. One of the most successful methods is to employ MgO as the support which lead to the formation of NiO-MgO solid solution (Liu et al., 2011). Xu et al. (Hu, 2009) discovered that the growth of Ni particle is very difficult in a NiO-MgO structure after calcination at high temperatures. The H_2-TPR test demonstrated that it is difficult to reduce NiO in a NiO-MgO solid solution. Once the solid solution structure is formed, there is an "isolation effect" created by the MgO, which would inhibit the formation of Ni-Ni bond during the reduction process. Thus, this "isolation effect" can stabilize Ni particles inside the MgO lattices and prevent it from sintering. The NiO-MgO solid solution, prepared via co-precipitation and followed by hydrothermal treatment, showed an excellent anti-sintering ability where Ni particles size only increased 11.7% to 13.4 nm (Luo et al., 2016). On the other hand, the similar Al_2O_3-supported catalyst showed a significant size increment of nickel particle from 14.8 nm to 24.8 nm. The other widely accepted approach involves introducing ceria to the catalysts to form strong metal-Ce interactions, which can keep the active metals highly dispersed (Zhang et al., 2006, Cai et al., 2008b). Cai

et al. (Cai et al., 2008a) successfully synthesized a Rh/CeO$_2$ catalyst with nano Rh particles, with an average size controlled within the range of 1-3 nm after 70 h of reforming at 650 °C. Therefore, decreasing the reforming temperature or enhancing metal-support interaction can effectively inhibit metal sintering.

2.5.3 Sulphur poisoning

Sulphur poisoning is a common and inevitable problem in bio-oil steam reforming system. Previous reports suggested that the sulphur content in actual bio-oil was be up to 500 ppmw (Oasmaa and Czernik, 1999, Yan et al., 2010). However, the acceptable sulphur content for conventional catalysts needs to be controlled in ppb level. Poisoning is caused by a strong adsorption of sulphur on active sites which restrains them from catalysis. The adsorbed sulphur atoms can physically block the active step sites and possibly alter the neighbouring active sites electronically and weaken their abilities to dissociate reactant molecules (Bartholomew, 2001). In a reducing environment, S-metal bonds can be broken reversibly to produce H$_2$S but the driving force for desorption of sulphur is not strong enough, compared with sulphur chemisorption (Rostrup-Nielsen et al., 2002).

The sulphur poisoning can be mitigated by doping new elements, i.e., CuO, WO$_3$, which can either strip sulphur atoms from active metals due to its stronger binds with sulphur or accelerate the

sulphur removal by formation of H_2S (Azad and Duran, 2007, Sato and Fujimoto, 2007). Although the sulphur-CuO bond is much more stable thermodynamically, the active metal can still be poisoned once the CuO sites are fully occupied with sulphur. On the other hand, WO_3 is known to be a promoter for H_2S formation which has a very high chance of being captured again by other active metals. Therefore, continued studies on sulphur tolerance in steam reforming are still needed.

2.6 Summary and prospect

Steam reforming of bio-oil is one of the popular research focuses in bio-energy utilization. Numerous studies have been carried out in the steam reforming of bio-oil model compounds (i.e., ethanol, methanol, HAc,). However, more efforts are needed to develop reliable catalysts with stable performance, particularly in terms of high activity, anti-carbon deposition and poison immunity. Noble metals based catalysts appear to fulfil such criteria. However, the high price and limited accessibility will always be a conundrum. Besides, the additional weight of noble metals on catalyst needs to be controlled at an extremely low level whilst the regeneration of the catalysts remains feasible.

Meanwhile, the modification of supporting material could potentially alter the nature of catalyst and Ni-based catalysts appear to be a practical alternative. Methods, such as sol-gel, co-precipitation and

hydrothermal treatment, could be explored for the synthesis of novel materials. It is also of significant importance to employ stable structures such as solid solutions, bimetallic bonds and spinels for preparation of stable catalysts. In terms of anti-carbon improvements, rare earth oxides, such as CeO_2 and La_2O_3, need to be further studied.

Chapter 3. Experiments

This chapter details the methodologies and materials used in this study, including all the chemicals and equipment involved. The chemicals and procedures of catalyst synthesis are described in Section 3.1 and Section 3.2, while Section 3.3 details the different technologies used for material characterization as well as experimental parameters. In Section 3.4 and Section 3.5, the catalytic evaluation rig and catalytic reforming procedures are both amply described.

3.1 Chemicals

In this research, the purity of the chemicals used as raw materials for catalyst preparation and bio-oil model compounds were analytical grade (AR) or above. The details of chemicals used are summarized in Table 3-1.

Table 3-1 Details of chemicals used in this research.

No.	Chemical name	Formula	Application
1	Nickel (II) nitrate hexahydrate ($\geq$98.0%)	$N_2NiO_6 \cdot 6H_2O$	Catalyst synthesis
2	Magnesium nitrate hexahydrate ($\geq$99.0%)	$MgN_2O_6 \cdot 6H_2O$	Catalyst synthesis
3	Cerium (III) nitrate hexahydrate ($\geq$99.0%)	$CeN_3O_9 \cdot 6H_2O$	Catalyst synthesis

Table 3-1 continue

No.	Chemical name	Formula	Application
4	Lanthanum (III) nitrate hexahydrate ($La_2O_3 \geq 44.0\%$)	$LaN_3O_9 \cdot 6H_2O$	Catalyst synthesis
5	Cobalt (II) nitrate hexahydrate ($\geq 98.5\%$)	$CoN_2O_6 \cdot 6H_2O$	Catalyst synthesis
6	Polyethylene glycol (20,000 g/mol)	$HO(CH_2CH_2O)_nH$	Catalyst synthesis
7	Alumina particle	$\gamma\text{-}Al_2O_3$	Catalyst synthesis
8	Ammonium hydroxide solution (25-28%)	H_5NO	Catalyst synthesis
9	Methanol ($\geq 99.5\%$)	CH_4O	Bio-oil model compound
10	Ethanol ($\geq 99.0\%$)	C_2H_6O	Bio-oil model compound
11	Acetic acid ($\geq 99.8\%$)	$C_2H_4O_2$	Bio-oil model compound/catalysis synthesis
12	Phenol ($\geq 99\%$)	C_6H_6O	Bio-oil model compound
13	Quartz sand (Ø 2-3 mm)	SiO_2	Catalytic bed structure
14	Deionized water (Treated by Milli-Q purification system)	H_2O	Catalyst synthesis/steam reforming
15	Hydrogen gas (99.999%)	H_2	Catalyst activation process
16	10 vol% Hydrogen gas in Argon	H_2/Ar	H_2-TPR
17	Nitrogen gas (99.999%)	N_2	Carrier gas in multi-applications
18	Carbon dioxide (99.99%)	CO_2	CO_2-TPD
19	Argon (99.999%)	Ar	Chemisorption experiments

3.2 Procedures for catalyst preparation

The details of procedure and chemicals for preparation of each catalyst are described in their corresponding chapters. The general processes of each operating method are discussed below.

3.2.1 Impregnation method

In this study, active metals, such as nickel and cobalt, were loaded onto support materials via impregnation method. In this process, a certain amount of metal precursor ($Ni(NO_3)_2 \cdot 6H_2O$) was firstly dissolved in excess deionized water. Subsequently, support was added to the impregnant, which was then heated and kept at 60 ℃. The liquid was continuously stirred for 3 h until the mixture became sufficiently dry to be transferred. The volume of water was controlled at 3 times of the volume of support material.

Compared with common incipient wetness impregnation method, this method prevents non-even dispersion of active metals on the support surface. The proposed method can also heat the impregnant in a unique system. The heating of mixture can accelerate the elimination of adsorbed gas inside pore structure, and it is beneficial to the penetration of precursor into the pore structure of support material.

3.2.2 Precipitation method

The precipitation method was applied for the synthesis of MgO support, bimetallic supports (like Ce/MgO, La/MgO) and NiMgO catalyst. Ammonia was employed as the sedimentation agent and was added into the precursor solution at room temperature via continuous dropwise addition. As for the preparation of NiMgO catalyst, both Ni^{2+} and Mg^{2+} ions were introduced for co-precipitation. Particularly for the Ni^{2+} ions, aging process was required at 40℃ for 6 h to remove excessive NH^{4+} ions.

3.2.3 Hydrothermal treatment

The hydrothermal treatment was employed to alter the surface texture of pristine synthesized materials, including the increase of their surface area and pore volume (Perez-Hernandez et al., 2013). The precipitated slurry was first transferred into a 1 L Teflon-lined stainless steel autoclave (shown in Fig. 3.1), and kept at 100 ℃ for 24 h. The treated slurry would then be filtered and washed before proceeding to the next stage.

Fig. 3.1 Photograph of the hydrothermal reactor.

3.3 Characterization of catalysts

3.3.1 N$_2$ adsorption-desorption

Textural structure of samples were characterised using the Micrometrics ASAP-2020. In each analysis, approximately 200 mg of the catalyst were degassed at 300 ℃ for 5 h under high vacuum for the removal of moisture and other adsorbed gases. The specific surface area was determined following the BET method whilst the pore size distribution was estimated following the BJH method.

3.3.2 X-ray diffraction

Powder X-ray diffraction (XRD) patterns were acquired using a Bruker D8 Advance with a Cu X-ray tube (λ = 1.5406 Å) operated at 40 kV and 40 mA. The 2θ was scanned from 10° to 90° (resolution of 0.01°) (Shi et al., 2014). The calcined or reduced sample needed to be grinded into fine powder and layered onto the sampler with a flat and tight surface.

3.3.3 H$_2$-temperature programmed reduction/desorption (H$_2$-TPR and H$_2$-TPD)

The H$_2$-TPR and H$_2$-TPD were carried out in a temperature-controlled micro-reactor, which was connected to a thermal conductivity detector (Finetec, Finesorb 3010D) (Lim et al., 2016). In the TPR analysis, approximately 30 mg of fresh catalyst was placed in a U-shape quartz tube. The catalyst was heated to 300 ℃ in argon at a flow rate of 20 ml/min and was kept isothermal for 1 h before cooling down to ambient temperature. The catalyst was then heated from room temperature to 950 ℃ at a heating rate of 5 ℃/min in a reducing atmosphere (10vol% H$_2$ in argon). H$_2$ consumption was monitored by using an online thermal conductivity detector (TCD). Prior to TPD analysis, the catalyst was reduced in hydrogen at 600 ℃ for 4 h. During the desorption process, temperature was raised to 800 ℃ in argon at a heating rate of 5 ℃/min (Park et al., 2015).

3.3.4 CO$_2$-temperature programmed desorption (CO$_2$-TPD)

The CO$_2$-TPD experiments were carried out on a Finetec Finesorb 3010D for H$_2$-chemisorption tests. In the test, approximately 50 mg of catalyst was reduced at 600 ℃ for 4 h in a gas mixture of 10vol% of H$_2$ in argon. For the process of CO$_2$ adsorption, CO$_2$ (99.999vol%) was then introduced into the reactor at room temperature for 30 min. The gas was then switched to argon at a flow rate of 20 ml/min to purge off any excess CO$_2$ in the reactor and on the surface of catalysts. As soon as the signal of TCD became stable, temperature was raised to 600 ℃ to allow desorption to occur (Constantinou et al., 2012).

3.3.5 CO-temperature programmed desorption (CO-TPD)

The CO-temperature programmed deposition was also carried out on a Finetec Finesorb 3010D. Approximately 70 mg of sample was first reduced with in situ H$_2$ at 700 ℃ for 2 h. The inflow gas was then switched to high-purity argon (99.999vol%) to purge off the residual H$_2$. Meanwhile, the bed temperature was decreased to 300 ℃ and kept isothermal for an hour. The CO adsorption took place at room temperature for 30 min and followed by an argon-purging process until the thermal conductivity detector (TCD) signal became stable. On the other hand, the desorption was operated

from room temperature to 750 ℃ with a heating rate of 5 ℃/min (Hu and Ruckenstein, 1996).

3.3.6 High resolution transmission electron microscopy (HRTEM)

The morphology of fresh and spent catalysts was characterised using a high-resolution transmission electron microscope (HRTEM; JEM-2100F, JEOL, Japan, 200 kV). The sample was dispersed in ethanol, and then transferred onto a copper grid prior to HRTEM analysis. The size distribution of Ni particle was determined from the measurements of more than 100 particles from several TEM images (Lim et al., 2016).

3.3.7 Thermogravimetric analysis (TGA)

A thermogravimetric analyzer (NETZSCH, model STA449F3) was used to quantify the amount of carbon deposition on the used catalysts. In each test, around 20 mg of catalyst was kept at 105 ℃ for 20 min, before it was heated to 1000 ℃ at a heating rate of 10 ℃/min (Carbajal-Ramos et al., 2016).

3.3.8 Temperature programmed hydrogenation (TPH)

The carbon species deposited on spent catalyst was characterized via the temperature-programmed hydrogenation (TPH). The spent catalyst was purged with argon at 150 ℃ for 1 h and then cooled down to ambient temperature. Prior to hydrogenation, the gas was

switched to 10vol% of H_2 in argon at a flow rate of 20 ml/min. The temperature was then raised from room temperature to 950 ℃ at a rate of 5 ℃/min. The on-line TCD was used to monitor the composition of gas at the outlet (Quek et al., 2010).

3.3.9 Raman spectroscopy

Raman spectra from 1000 to 2000 cm^{-1} at ambient temperature were recorded by using a Renishaw inVia-reflex equipped with a 532 nm-wavelength laser. Each catalyst was analysed more than 3 times at different positions to ensure representative sampling (Shi et al., 2014).

3.3.10 X-ray photoelectron spectroscopy

X-ray photoelectron spectroscopy (XPS) experiment was carried out using a Shimadzu Axis UltraDLD spectroscope to study the oxidation states of elemental species found on the catalysts surface under a vacuum condition of 10^{-9} Torr. A monochromatized Al Kα radiation source was selected along with the spectrum calibration of C 1s at 248.8 eV (Lim et al., 2016, Yu et al., 2014).

3.4 Catalyst evaluation

The catalyst performance was tested in a pilot scale catalyst evaluation system (CES), which is shown in Fig. 3.2 below. The system has five gas inlets controlled by five corresponding mass flow controllers. Nitrogen gas was used as a carrier gas. There is

also a liquid inlet controlled by a liquid piston pump (Optos series, Eldex Lab, Inc), which has a working range at 0-30 ml/min. During the reaction, water and reactant (like methanol, ethanol, or phenol) mixture liquid at various mole ratios could be pumped into the reactor.

The schematic diagram of the system is shown in Fig. 3.3. Gas inflow and liquid inflow would be mixed and evaporated adequately inside a pre-heater, which could then increase the temperature from room temperature to 300℃. The main reactor is a tube-shaped fixed bed with an inner diameter of 12mm. The maximum working temperature is 1000 ℃. There is a thermocouple inserted at the bottom of the reactor to measure the in situ temperature of catalyst bed. The outflow from the reactor is cooled by a cold trap before entering the gas-liquid separator. The separated gas is collected in a 1 L Tedlar bag and analyzed on an offline GC. There are also two balances dedicated to measure both the mass of liquid pumped in and mass of liquid collected after the reaction.
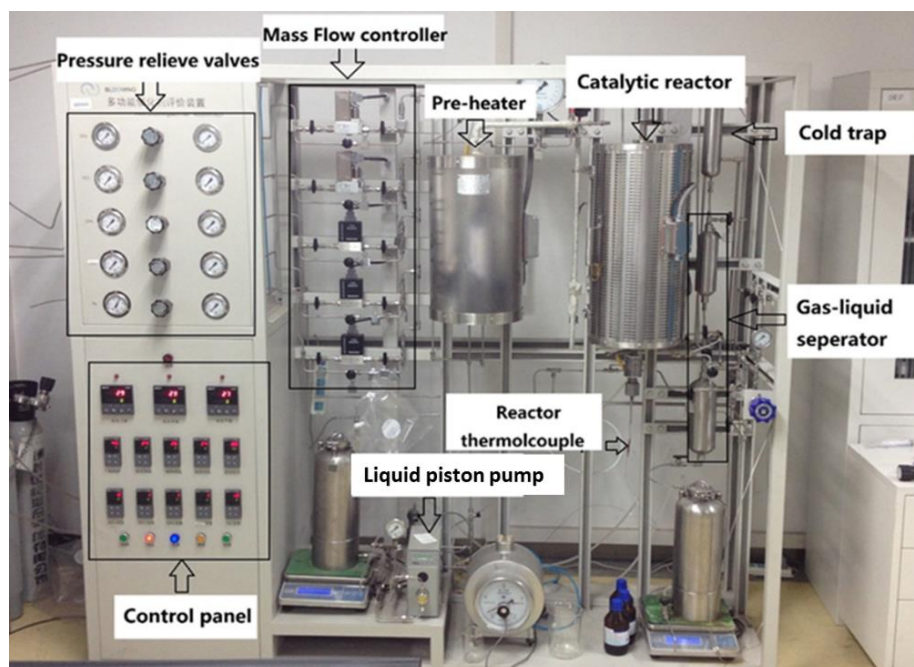
Fig. 3.2 Illustration of the catalytic evaluation rig.
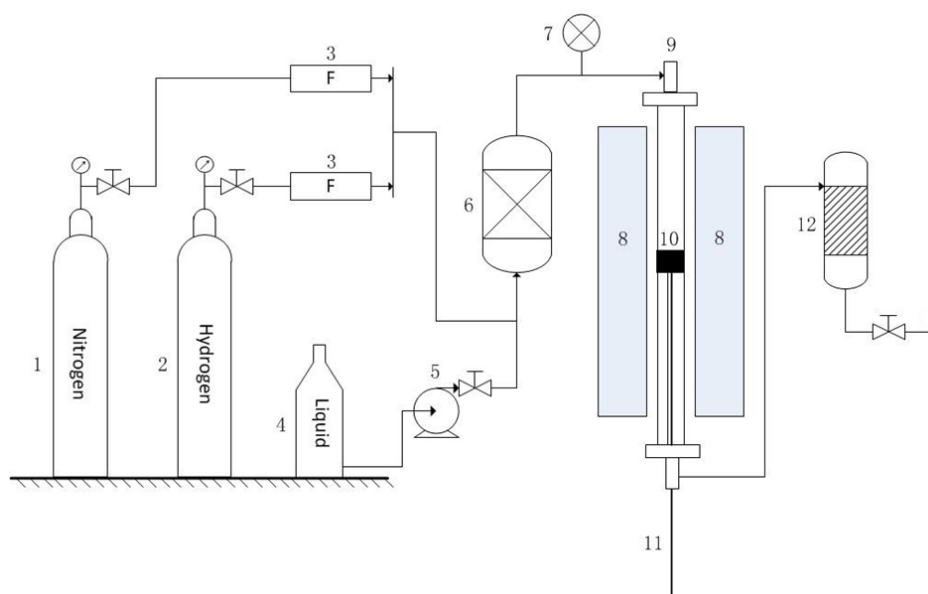
Fig. 3.3 Schematic diagram of the experimental apparatus (1) N₂ cylinder; (2) H₂ cylinder; (3) mass flowmeters; (4) liquid container; (5) syringe pump; (6) preheater; (7) pressure gauge; (8) heating unit; (9) reactor; (10) catalyst bed; (11) thermocouple; (12) cold trap.

3.5 Procedures of steam reforming testing

3.5.1 Steam reforming of methanol

Approximately 0.5 g of fresh catalyst was diluted with quartz sand (8 g, ⌀ 2-3 mm; Aladdin) and then placed on the top of a layer of quartz wool located in the middle of the reactor (310S stainless steel, I.D. = 12 mm). Prior to each test, the catalyst was reduced in situ with 400 ml/min of 25vol% H_2 in N_2 at 600 ℃ for 1 h. A mixture of water and methanol was pumped into the test rig at a flow rate of 1 ml/min (1 atm, room temperature) by using a liquid pump with a reproducibility of +/- 0.3% (measured at the flowrate of 1 ml/min). The pump was calibrated prior to each test and maintained on a regular basis to ensure its accuracy and consistency. Water and methanol mixture with 2 molar ratios (denoted as steam/carbon ratio= 1, 3) were adopted in this study, together with two different gas hourly space velocities (GHSV, 92,000 ml/g_{cat}·h and 114,000 ml/g_{cat}·h). The liquid mixture was evaporated in a preheater at 300 ℃ before being fed into the catalytic reactor. After passing through a cold trap, the effluent gas was collected by using a 1 L Tedlar bag and analysed using an off-line Gas Chromatograph (SHIMADZU, GC-2014) equipped with two TCDs and one FID. N_2 gas at a flow rate of 300 ml/min was used as the carrier gas in the reaction system. The flow rate of gaseous products (H_2, CO_2, CO and CH_4) was calculated based on the known flow rate of N_2 and

their relative concentration to N_2 which was determined by using GC. The calculation of methanol conversion was based on the flow rate of methanol introduced to the reaction system and the carbon balance. The concentration of other gases detected by the FID, such as ethane, was often very low and then neglected. The methanol conversion, selectivity of CO, H_2 yield and H_2/CO ratio were determined using following formula (Cortright et al., 2002, Deshmane et al., 2015):

$$CH_3OH \text{ conversion (mol\%)} = \frac{[CO_2]_{out}+[CH_4]_{out}+[CO]_{out}}{[CH_3OH]_{in}} \times 100 \text{ \%}$$

(eq 3.1)

$$CO \text{ selectivity (mol\%)} = \frac{[CO]_{out}}{[CO_2]_{out}+[CH_4]_{out}+[CO]_{out}} \times 100\% \qquad \text{(eq 3.2)}$$

$$CO_2 \text{ selectivity (mol\%)} = \frac{[CO_2]_{out}}{[CO_2]_{out}+[CH_4]_{out}+[CO]_{out}} \times 100\% \qquad \text{(eq 3.3)}$$

$$CH_4 \text{ selectivity (mol\%)} = \frac{[CH_4]_{out}}{[CO_2]_{out}+[CH_4]_{out}+[CO]_{out}} \times 100\% \qquad \text{(eq 3.4)}$$

$$H_2 \text{ yield (mol\%)} = \frac{[H_2]_{out}}{[CH_3OH]_{in}\times3} \times 100\% \qquad \text{(eq 3.5)}$$

$$H_2/CO \text{ ratio} = \frac{[H_2]_{out}}{[CO]_{out}} \qquad \text{(eq 3.6)}$$

3.5.2 Steam reforming of ethanol

For each test, 1 g of catalyst was first diluted by 15 g of quartz sand (Aladdin; 2-3 mm φ) which had been calcined prior to the mixing to remove any volatile contaminants. A thin layer of silica wool was placed underneath the catalyst bed to prevent loss of the catalyst

powder. A K-type thermocouple was placed along the central axis of the reactor to monitor the temperature of the catalytic bed. The outflow gas would pass through a cold trap and then be collected in a 1 L Tedlar bag for analysis off-line using a Gas Chromatograph (SHIMADZU, GC-2014). For each catalyst, its catalytic activity was tested at four different temperatures, i.e., 500 ℃, 600 ℃, 700 ℃ and 800 ℃. The composition of outflow gas was analysed 2 h after the temperature of the catalyst bed had become stable. As for the durability test, each catalyst was tested in the catalytic reforming carried out at 700 ℃ for 30 h. The catalytic evaluation system was operated under atmospheric pressure.

In this study, the yield of hydrogen gas was defined according to the stoichiometric reaction (in R 2.9):

$$\text{H}_2 \text{ yield (mol\%)} = \frac{\text{moles of H}_2 \text{ produced}}{\text{moles of inlet ethanol} \times 6} \cdot 100\% \qquad \text{(eq 3.7)}$$

Ethanol conversion ($X_{ethanol}$) was defined based on carbon balance:

$$X_{ethanol} \text{ (mol\%)} = \frac{\text{a sum of moles of converted carbon in outflow}}{\text{moles of input ethanol} \times 2} \cdot 100\%$$

(eq 3.8)

The yield of carbonaceous gases, such as CO_2, CO and CH_4, was calculated as:

$$\text{Carbonaceous gas yield (mol\%)} = \frac{\text{moles of gas produced}}{\text{moles of input ethanol} \times 2} \cdot 100\%$$

(eq 3.9)

3.5.3 Steam reforming of phenol, acetic acid and model bio-oil

The procedure of steam reforming of phenol, HAc and model bio-oil are very similar, if not identical, to the steam reforming of ethanol. Same loading amounts of catalysts (1 g) and quartz sand (15 g) were applied. The inflow rate of liquid mixture was still fixed at 1 ml/min. The details of conversion and yield calculation for each compound were separately discussed in Chapter 6.

Chapter 4. Ni-based catalysts study for steam reforming of methanol (SRM)

4.1 Introduction

In this work, the MgO supporting materials was prepared via various methods and different preparation conditions. In the synthesis process, polyethylene glycol (PEG) acted as a surfactant to improve both specific surface area and total pore volume of MgO material. The optimal Ni loading was also investigated via steam reforming of methanol.

After that, several types of Ni_xMg_yO solid solutions in nano-scale, denoted as Ni_xMg_yO-impre, Ni_xMg_yO-hydro and Ni_xMg_yO-copre, for SRM were synthesized with three different procedures. Performance of these catalysts was evaluated at four different temperatures, i.e., 400, 500, 600 and 700 ℃, using a fixed-bed reactor under atmospheric pressure. The tests were undertaken under two steam/carbon ratios, i.e., S/C = 1 and S/C = 3. The novel Ni_xMg_yO solid solution (Ni_xMg_yO-hydro), which was further treated by a hydrothermal method, showed the highest methanol conversion efficiency and hydrogen yield at 97.4mol% and 58.5mol%, respectively, at 600 ℃ after 20 h.

The nature of both fresh and spent catalysts was characterized systematically by employing H_2-Temperature Programmed

Reduction/Desorption, X-ray Photoelectron Spectroscopy and CO_2-Temperature Programmed Desorption. TEM analysis also demonstrated that the average size of Ni particles in these solid solutions were at the region of 9.6 to 12 nm.

In addition, the evaluation on carbon deposition resistance showed that nano Ni_xMg_yO-hydro had no detectable carbon deposition under a steam carbon ratio of 3. The outstanding carbon deposition resistance of Ni_xMg_yO-hydro was attributed to the "isolation effect" of the Ni_xMg_yO solid solution structure, which restricts Ni nano particles from aggregation. The high basicity of the surface of Ni_xMg_yO-hydro catalyst also resulted in the enhanced CO_2 adsorption and therefore contributed to anti-carbon deposition by providing oxygen to promote the gasification reaction between carbon and CO_2.

4.2 Preliminary work

4.2.1 MgO synthesis

All the chemicals used in this research were analytical grade purchased from Sinopharm Chemical Reagent Co., Ltd. (Shanghai, China).

At the very beginning of this work, the preparation methods and different synthesis conditions were compared for making MgO supporting materials, which was to obtain a novel nano-scale MgO

with high specific surface area and large pore volume. The synthesis factors and methods for each prepared MgO sample and their corresponding denoted names were explained and listed:

- Nonhydro-MgO: MgO was synthesized by precipitation method. 0.2 mol $Mg(NO_3)_2 \cdot 6H_2O$ dissolved in deionised water was mixed with 250 ml of 5 wt% ammonia solution at room temperature. After filtration, the solid material was dried in air at 105 ℃ for 12 h and then calcined in air at 600 ℃ for 4 h.

- Hydro-MgO: The participated $Mg(OH)_2$ slurry was additionally treated with hydrothermal treatment at 100 ℃ for 24 h before filtration. For the hydrothermal treatment, the suspended solution needed to be transferred into a Teflon-lined autoclave.

- Hydro-MgO (low A): 2.5wt% ammonia solution was used in the process.

- Hydro-MgO (high T): A higher temperature, 200 ℃, was used as the hydrothermal reaction temperature.

- Hydro-MgO (ethanol): Ethanol was conducted as the dissolvent to instead of deionized water.

- Hydro-MgO (PEG): PEG was added as the surfactant.

The texture structure features of MgO prepared via different conditions were shown in Table 4-1. That hydrothermal treatment exhibited the promotion effect on the increment of surface area. The conduction of high temperature and low concentration ammonia did not alter the surface area obviously. It also showed that the addition of surfactant PEG substantially improved surface area and total pore volume. The reason is that PEG has a larger average molecular weight (20,000 g/mol), these large molecules normally occupy a lot of space inside the MgO powder during its growth (Higginbotham et al., 2003). After calcination of the support, the PEG was evaporated and left behind a porous structure with a larger surface area and pore volume.

Table 4-1 Surface properties of MgO materials.

	BET surface area (m^2/g)	Average pore size (nm)	Total pore volume (cm^3/g)
Nonhydro-MgO	14.2	17.1	0.060
Hydro-MgO	24.9	7.9	0.049
Hydro-MgO (low A)	22.7	14.0	0.080
Hydro-MgO (high T)	19.7	18.8	0.092
Hydro-MgO (ethanol)	25.4	18.1	0.114
Hydro-MgO (PEG)	37.4	10.9	0.102

4.2.2 The study of Nickel loading weight in SRM

Nickel loading is a very important factor for Ni-based catalyst. It not only affects catalytic performance, but also has a close relevance with the deactivation of catalyst. In addition, the nickel loading also decides the nickel particle size distribution and degree of dispersion, which subsequentially affects the reaction activity and stability of the catalyst (Li et al., 2012). High nickel loading usually leads to a good catalytic activity at initial stage of the test. As the time going, the deactivation of the catalyst becomes more severe due to particles sintering and coke deposition. Thus, finding an appropriate amount of nickel loading is very necessary for the development of catalyst.

The aim of this research was to find out an optimal nickel loading weight for the Hydro-MgO (PEG) support. The experiment tested Ni/MgO catalysts with five different Ni loadings: 1%Ni/MgO, 5%Ni/MgO, 10%Ni/MgO, 15%Ni/MgO and 20%Ni/MgO. Each test was operated at 600 ℃ and lasted for 8 hours with a high space rate at 113,800 ml/g_{cat}·h and low steam/carbon ratio of 3. The tests were focused on the catalytic activities and their stabilities in 8 h processing.
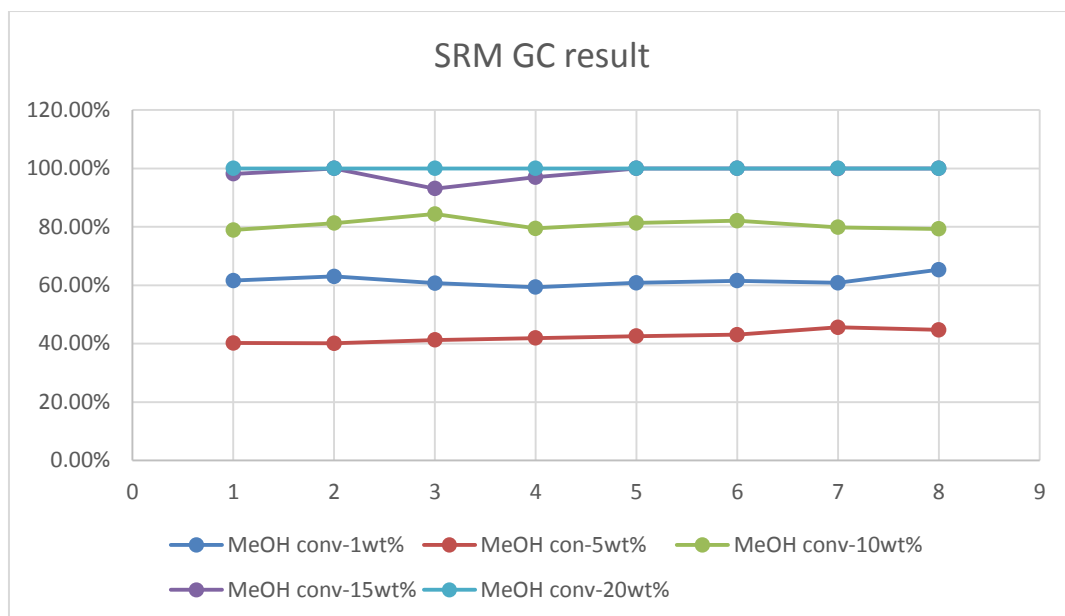
Fig. 4.1 Methanol conversion over Ni catalysts with different nickel loadings.
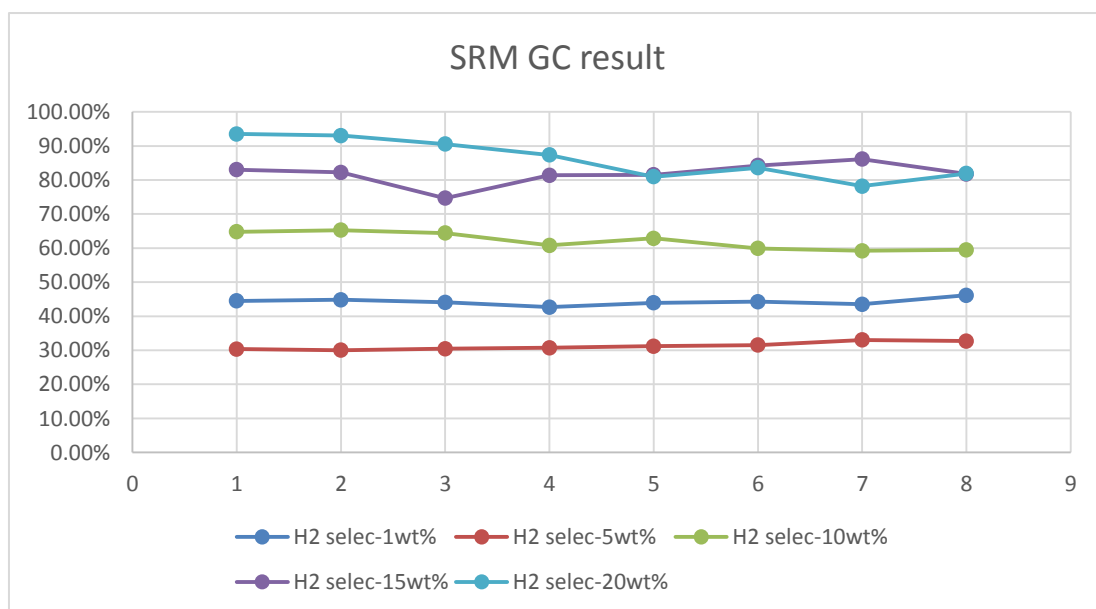
Fig. 4.2 Hydrogen selectivity over Ni catalysts with different nickel loadings.

Fig. 4.1 shows the methanol conversion for each catalyst. It could be observed that conversion rate increased with the increase in

nickel loading, except for 1%Ni/hydro-MgO. This suggests that higher nickel loading results in more active sites on the surface of catalyst, and this leads to a higher conversion. However, the conversion rate of 1%Ni/hydro-MgO was greater than that of 5%Ni/-hydro-MgO. This result suggests that the catalyst with approximately 1wt% of nickel loading might have a better nickel particle dispersion and smaller size. In Fig. 4.2, the initial H_2 yields of 5 catalysts had a same ranking with their methanol conversion rate. One difference was H_2 yield of the 20%Ni/hydro-MgO droped from 93.5mol% to 80mol% in 8 hours. The other 4 catalysts all kept stable activity in 8 hours' test.

4.3 Synthesis of different Ni_xMg_yO solid solutions

In this study, three different nano Ni_xMg_yO solid solutions were prepared using three different methods. The preparation of the first type of Ni_xMg_yO catalyst started from the preparation of MgO support by precipitation of $Mg(NO_3)_2 \cdot 6H_2O$ with ammonia at room temperature followed by drying in air at 105 ℃ for 12 h and calcination in air at 600 ℃ for 4 h. The catalyst containing 10wt% nickel in Ni_xMg_yO solid solution was achieved via incipient wetness impregnation using aqueous solution of $Ni(NO_3)_2 \cdot 6H_2O$ impregnated onto the MgO support at room temperature. The catalyst was subsequently dried at 105 ℃ for 12 h, and then calcined in air at 600 ℃ for 4 h. This catalyst was denoted as Ni_xMg_yO-impre.

The second type of Ni_xMg_yO catalyst was prepared by following a similar procedure as described previously. The only difference was the added hydrothermal treatment of the catalysts at 100 ℃ for 24 h after precipitation. This catalyst was denoted as Ni_xMg_yO-hydro.

The third type of Ni_xMg_yO catalyst was prepared by co-precipitation of $Mg(NO_3)_2·6H_2O$ and $Ni(NO_3)_2·6H_2O$ in an ammonia solution at controlled concentration, followed by aging at 40 ℃ for 6 h. The aged mixture was then dried in air at 105 ℃ for 12 h, calcined in air at 600 ℃ for 4 h, and treated hydrothermally following the same hydrothermal process as the preparation of Ni_xMg_yO-hydro. This catalyst was denoted as Ni_xMg_yO-copre.

In addition, 10wt% Ni/γ-Al_2O_3 was prepared for comparison purpose using incipient wetness method. The γ-Al_2O_3 support was purchased from V-SK Co., Ltd., which had a BET surface area about 200 m^2/g. Before the impregnation process, the alumina support was calcined at 600 ℃ for 8 h to remove its surface contaminants. The impregnation was conducted under room temperature. The sample was then dried at 105 ℃ for 12 h and calcined in oxidizing atmosphere at 600 ℃ for 4 h. This catalyst was denoted as Ni_xAl_yO.

4.4 Characterization of pristine Ni_xMg_yO solid solution catalysts

4.4.1 XRD analysis

XRD patterns of fresh, reduced and spent catalysts are shown in Fig. 4.3. From the XRD spectrum, it is clear that the nickel crystal structure had peaks close to that of the MgO crystal. This was due to their identical lattice type and similar ionic radius value (Chen et al., 1998). The peaks of nickel phase have increments of 0.6°, 0.8°, and 0.81°, compared with MgO at $2\theta \approx 62.64°$, 75.00°, and 79.00° (Hu and Ruckenstein, 1997). In Fig. 4.3(B)-(D), no double structure was found associated with the five major peaks, which were assigned as MgO at 37°, 43°, 62°, 75° and 79° (Furusawa and Tsutsumi, 2005). This proves the formation of Ni_xMg_yO solid solution in all three Ni_xMg_yO systems as a result of the excellent mutual solubility of these two metal oxides (Tang et al., 1998, Chen et al., 1998, Furusawa and Tsutsumi, 2005, Hu and Ruckenstein, 1997).
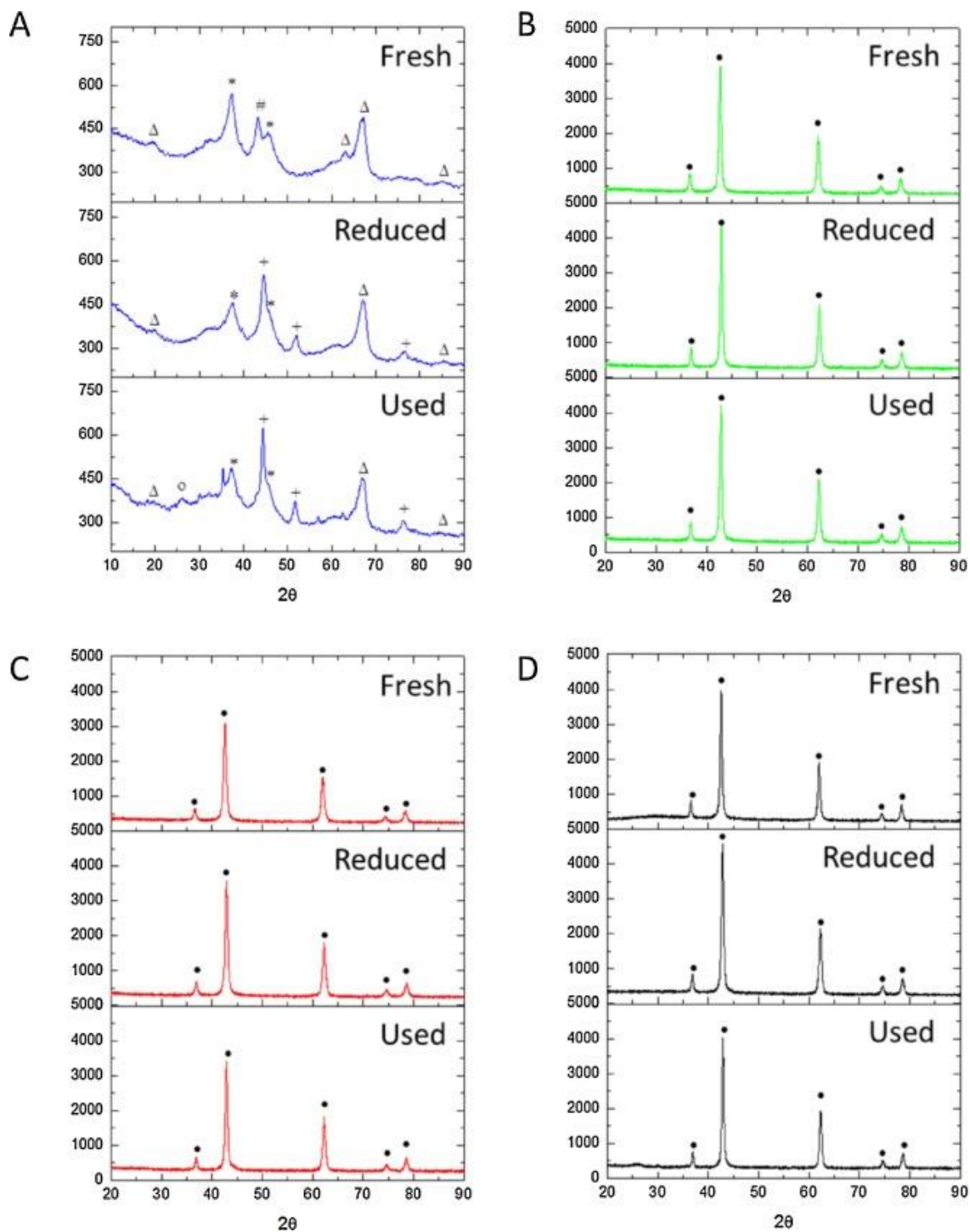
Fig. 4.3 X-ray diffraction patterns of fresh, reduced, and spent catalysts (A) Ni$_x$Al$_y$O, (B) Ni$_x$Mg$_y$O-copre, (C) Ni$_x$Mg$_y$O-hydro, (D) Ni$_x$Mg$_y$O-impre, Δ: γ-Al2O3; ∗: NiAl2O4; +: Ni; #: NiO; ο: ordered carbon; •: NiO/MgO.

4.4.2 N$_2$ physiosorption isotherm analysis

From Fig. 4.4(A), it can be seen that the sorption isotherm of Ni$_x$Al$_y$O catalyst was Type IV. Its big hysteresis loop was associated with the capillary condensation in mesopores (>2 nm and <50 nm) and the large surface area (Sing. et al., 1985). From Fig. 4.4(B), it is clear that its pore width varied between 1.9 nm and 31.7 nm. The isotherm curves of the other three catalysts can be categorized as Pseudo-Type II isotherm. This type of isotherm indicates slit-shaped pores or aggregates of platy particles existed on these catalysts (Sing, 1995). It is worth noting that there were two hysteresis loops on the sorption isotherm of Ni$_x$Mg$_y$O-copre, which suggests that there were two types of pores with different sizes. This observation is consistent with the pore size distribution of Ni$_x$Mg$_y$O-copre shown in Fig. 4.4(B). The existence of both small pores (<2 nm) and mesopores in Ni$_x$Mg$_y$O-copre could enhance the "confined effect" to resist metallic Ni particles from sintering, which could then contribute to the mitigation of carbon deposition (Fan et al., 2010, Sun et al., 2010).
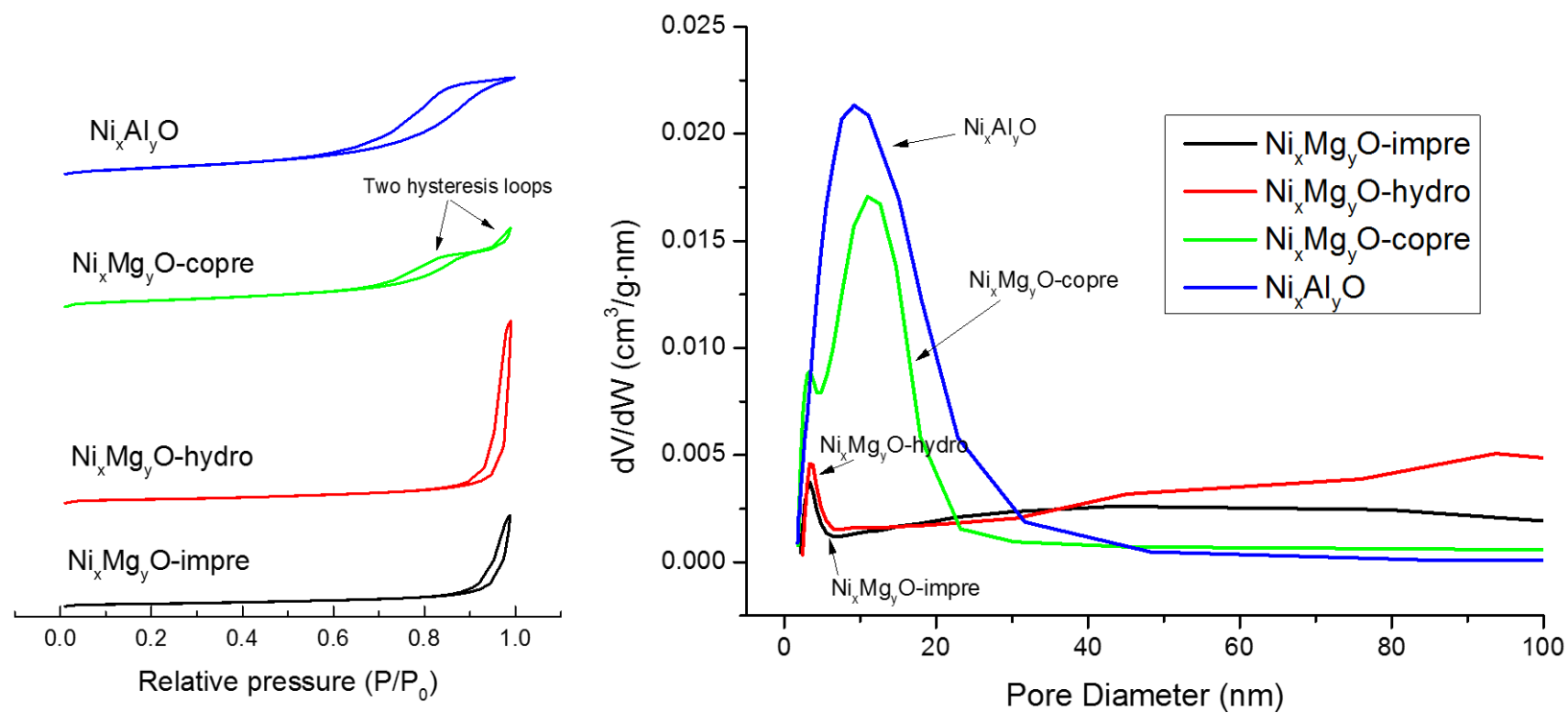
Fig. 4.4 (A) N₂ physisorption isotherms for fresh catalysts; (B) Pore size distribution of fresh catalysts.

4.4.3 H$_2$-TPR analysis

H$_2$-TPR experiment was conducted to investigate surface Ni species and the interactions between Ni species and support materials. Fig. 4.5 shows the TPR profiles of calcined catalysts. It can be seen that the main peak of Ni species in Ni$_x$Al$_y$O was found to be at 792 ℃, which is assigned as the temperature for oxidized Ni particles to be reduced from NiAl$_2$O$_4$ spinel (Wu et al., 2013). The TCD signal at temperatures below 600 ℃ was weak. The TPR results verified the formation of NiAl$_2$O$_4$ spinel with a very small amount of free Ni species in the Ni$_x$Al$_y$O catalyst (Wu et al., 2012, Sánchez et al., 2010). All the Ni$_x$Mg$_y$O-copre, Ni$_x$Mg$_y$O-hydro, and Ni$_x$Mg$_y$O-impre catalysts showed their strongest peaks at a temperature higher than 800 ℃, which was ascribed as the temperature for the reduction of Ni cations from the Ni$_x$Mg$_y$O solid solution (Wang et al., 2009). The Ni cations were diffused into MgO lattice (Torres and Liu, 2012) for the three MgO based catalysts. Since the reduction temperature and the reforming test temperature were both 600 ℃, this temperature was not high enough for oxidized Ni particles in the MgO matrix to be reduced. This is the reason why no noticeable peaks for metallic Ni were found from the XRD spectrums of Ni$_x$Mg$_y$O catalysts. However, low intensity peaks of Ni species were evident for the three Ni$_x$Mg$_y$O catalysts in the temperature range of 450-650 ℃. This suggests that Ni particles were highly dispersed

under MgO subsurface (Tang et al., 1998) and were in nano-scale. This is why these Ni species were not identified in the subsequent XRD analysis, as described in Section 4.6.1. These highly dispersed nano-scale Ni particles could potentially contribute to the good catalytic reforming performance of these Ni_xMg_yO catalysts.
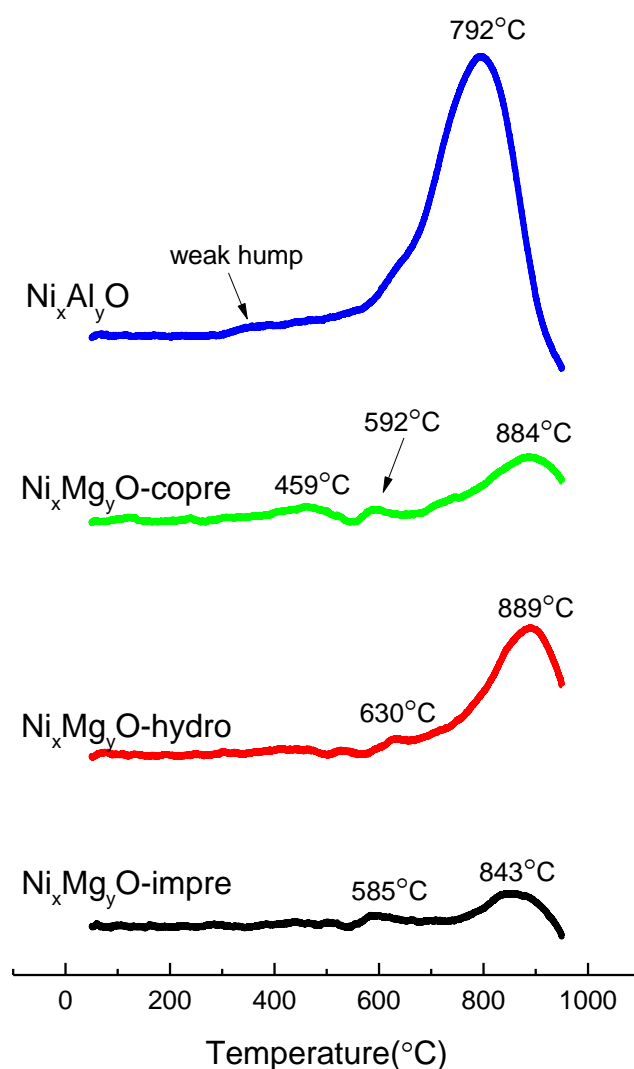
Fig. 4.5 H$_2$-Temperature programmed reduction profiles of fresh catalysts.

4.4.4 H$_2$-TPD analysis

H$_2$-TPD experiment was also carried out to investigate Ni species on the reduced catalysts after 4 h hydrogen reduction at 600 ℃. Two types of hydrogen desorption peaks can identified in Fig. 4.6 The temperature peak in the range of 150-300 ℃ is assigned as T$_L$, and the peak in the range of 300-600 ℃ is assigned as T$_H$. It is generally believed that T$_L$ corresponds to the existence of large Ni particles on the surface or subsurface, and T$_H$ indicates the presence of small Ni particles in the subsurface (Wang et al., 2009). It can be seen from Fig. 4.6 that the main peak of Ni$_x$Al$_y$O catalyst located at 248 ℃, with a high intensity and a narrow width. This suggested the existence of large Ni crystallites on the surface of the support of Ni$_x$Al$_y$O, which were larger than Ni particles in Ni$_x$Mg$_y$O catalysts. The strong peaks for Ni$_x$Mg$_y$O catalysts suggested the Ni crystallites did exist on the subsurface of the catalysts were in much smaller size. This further confirmed the existence of nano-scale Ni particles, which is consistent with what was found based on TPR tests. It is speculated that these nano-scale Ni particles are highly dispersed in the MgO matrix. The strong interactions between Ni particles and MgO resulted in an "isolation effect" to prevented Ni aggregation from happening (Hu, 2009). These would then contribute to the outstanding catalytic performance, carbon deposition resistance and stability of these Ni$_x$Mg$_y$O solid solutions.
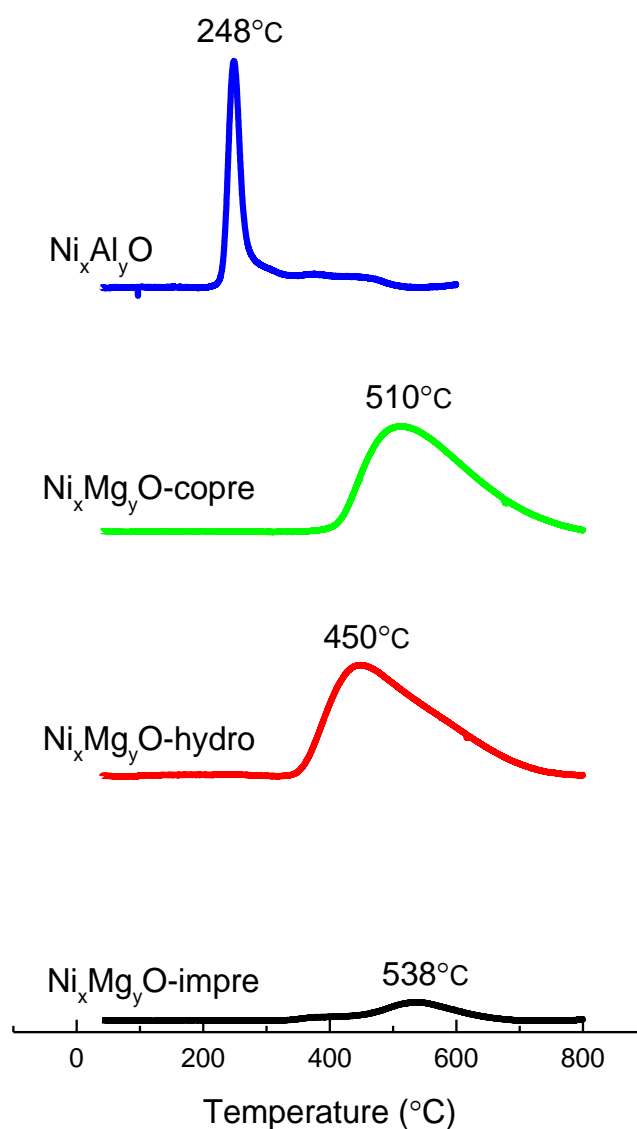
Fig. 4.6 H₂-Temperature programmed desorption profiles of reduced catalysts.

4.4.5 TEM analysis

The TEM images of catalysts studied are shown in Fig. 4.7 The Ni_xAl_yO catalyst, as shown in Fig. 4.7(A), had an average metal particle size about 14.8 nm (as shown in Table 4-2), which is in consistence with what was reported by others (Wang and Lu, 1998a,

Koo et al., 2008). The analogy in terms of morphology between Ni_xMg_yO-impre and Ni_xMg_yO-hydro was also observed, which was attributed to their similar synthesis procedure. The MgO particles were all sub-nanoparticles, which are smaller than 200 nm. The average size of Ni particles in Ni_xMg_yO-hydro was 10.1 nm, which is slightly larger than Ni particles in Ni_xMg_yO-impre (average size 9.6 nm). The Ni_xMg_yO-copre catalyst also demonstrated porous MgO nanosheets with an average Ni particle size of 12.0 nm, which is very similar to the earlier work conducted by Zhu et al. (Zhu et al., 2006). Due to the largest Ni crystallites in Ni_xAl_yO, it would result in poor carbon deposition resistance, whilst Ni_xMg_yO-hydro had the smallest Ni particle size and was expected to show better carbon deposition resistance.

Table 4-2 Metal particle size and dispersion from TEM for both fresh and spent catalysts.

Catalyst	Ni particle size of fresh catalyst (nm)	Ni Particle size of spent catalyst (nm)	Particle size increment (%)	Ni dispersion fresh catalyst (%)
Ni_xMg_yO-impre	9.6	20.2	110.4	6.9
Ni_xMg_yO -hydro	10.1	15.1	49.5	6.6
Ni_xMg_yO -copre	12.0	13.4	11.7	5.5
Ni_xAl_yO	14.8	24.8	67.6	4.5

The metal dispersion (D_M) was also calculated based on the size of particles determined from TEM images using Vannice's equation (Zhang et al., 2008):

$$D_M = 6 \times 10^7 \frac{V_M}{A_M} \frac{1}{d\ (nm)} \qquad \text{(eq 4.1)}$$

Where d is the average diameter of a metal particle in nm, V_M is the bulk atomic volume of metals (for Ni, $V_M = 1.10 \times 10^{-23}$ cm^3), A_M is the area of an atom (for Ni, $A_M = 1.0 \times 10^{-15}$ cm^2) (Wacke et al., 2011). Metal dispersion of materials is shown in Table 4-2. It can be seen that different preparation methods resulted in the difference in Ni dispersion in different Ni_xMg_yO solid solution. Since Ni_xMg_yO-impre and Ni_xMg_yO-hydro had relatively higher metal dispersion, it was expected that these two catalysts would have better catalytic performance as well as anti-carbon deposition property than the other catalysts.
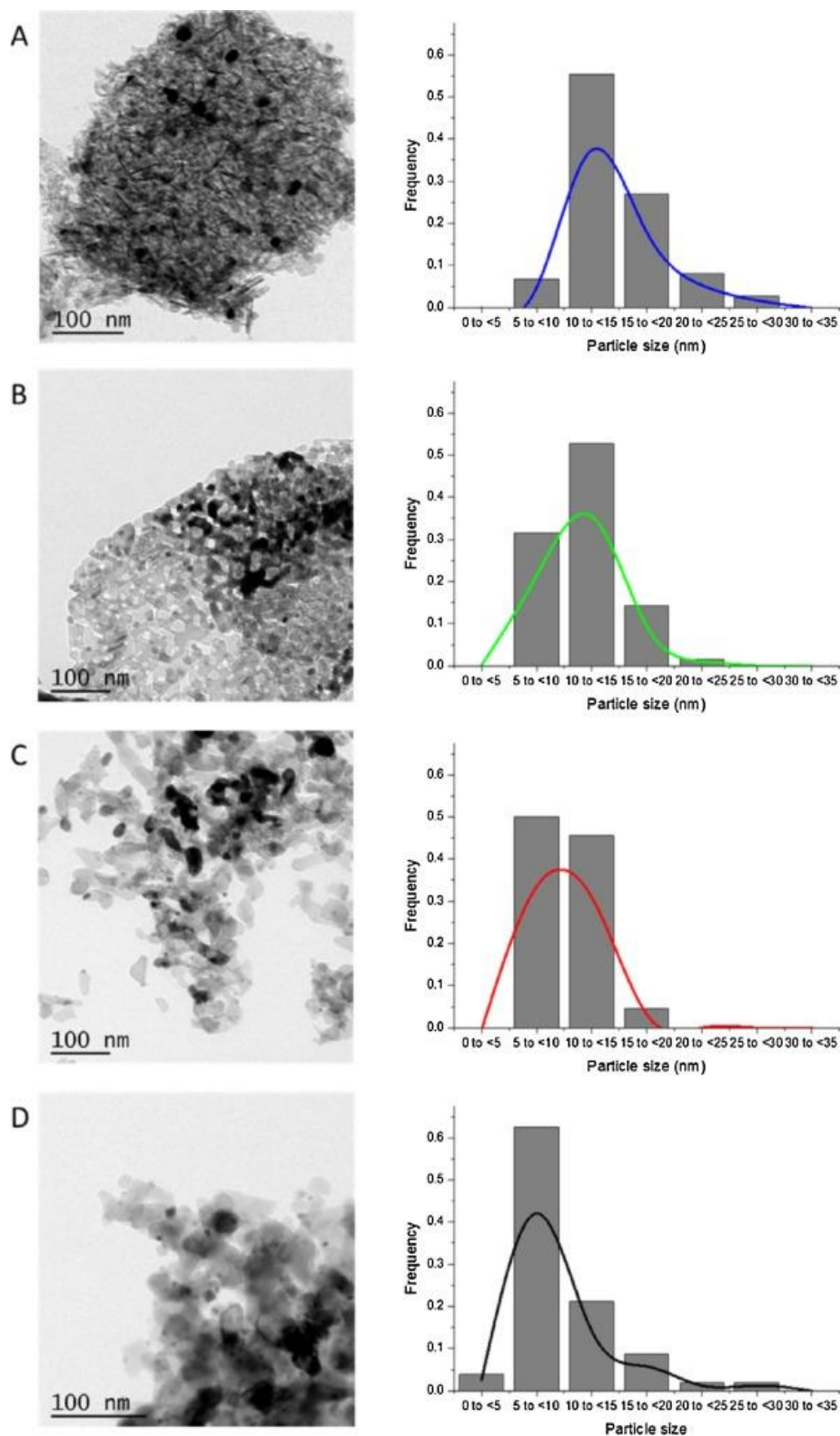
Fig. 4.7 TEM images and Ni particle size distribution of reduced catalysts (A) Ni$_x$Al$_y$O, (B) Ni$_x$Mg$_y$O-copre, (C) Ni$_x$Mg$_y$O -hydro, (D) Ni$_x$Mg$_y$O-impre.

4.4.6 CO$_2$-TPD analysis

Normally, CO$_2$-TPD analysis can show the strength of Lewis basicity and the number of basic sites on the surface of catalysts (Fan et al., 2008, Yuan et al., 2009). Theoretically, more basic sites could promote the chemisorption of CO$_2$, which accelerates the reverse Boudouard reaction (C + CO$_2$ → 2CO). On the other hand, the excessive CO$_2$ on the surface could also suppress the adsorption of CH$_4$ and CO, which hindered carbon formation via the decomposition of methane and CO hydrogenation.

The CO$_2$-TPD profiles of these catalysts are shown in Fig. 4.8. For individual catalysts, their desorption peaks present in two temperature ranges. The first peaks for these Ni$_x$Mg$_y$O catalysts were in a broad low temperature range from 100 to 450 ℃, which was associated with the weak basic sites (Babu. et al., 2008, Bergadà et al., 2008). Their second desorption peak located at a temperature above 500 ℃, which was assigned as moderate basicity sites. For Ni$_x$Al$_y$O catalyst, the first desorption temperature is in the range of 100-300 ℃, and the moderate basic site peak shifted to a lower temperature (413 ℃). According to the area of these peaks, the total basicity of catalysts was in the order of Ni$_x$Mg$_y$O-hydro > Ni$_x$Mg$_y$O-impre > Ni$_x$Mg$_y$O-copre > Ni$_x$Al$_y$O, which suggests Ni$_x$Mg$_y$O-hydro would show the best carbon resistance by promoting CO$_2$ adsorption to enhance reverse Bourdard Reaction.
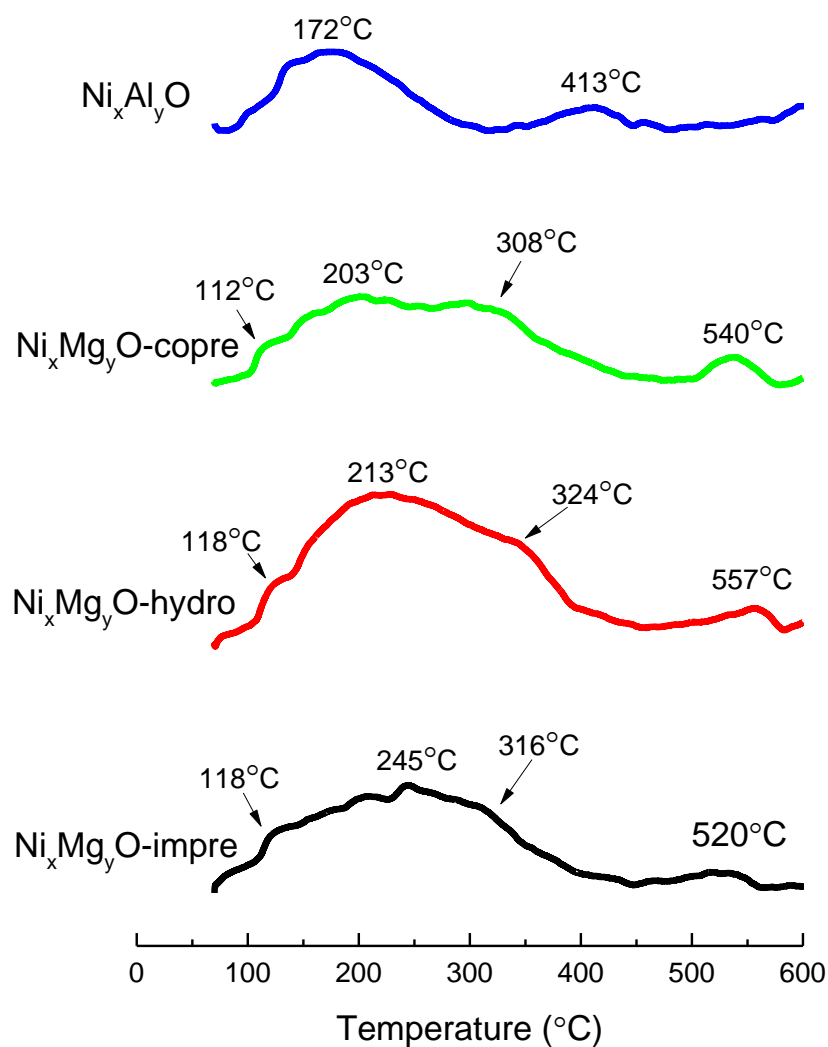
Fig. 4.8 CO$_2$-Temperature programmed desorption of reduced catalysts.

4.5 Methanol steam reforming over Ni$_x$Mg$_y$O solid solution catalysts

It can be seen from Fig. 4.9(A) that the conversion efficiency increased with the increase in temperature for each catalyst. Ni$_x$Al$_y$O

exhibited the highest conversion efficiency of 24.1mol% at 400 ℃, and reached 100mol% conversion at 600 ℃. The Ni_xMg_yO-hydro had a higher initiation temperature for reforming compared with Ni_xAl_yO, which could be attributed to its higher reduction temperature. The Ni_xMg_yO-impre and Ni_xMg_yO-copre showed similar methanol conversion, which was much lower than that of Ni_xAl_yO catalysts. Their low performance at low temperatures could be attributed to the lower reducibility as shown in TPR tests, which suggested that less amount of Ni particles was reduced. The H_2-TPD results also indicated most Ni species were dissolved deeply inside the MgO matrix and subsequently left only small amount of Ni particles at the subsurface (H_2 desorption peak temperature >500 ℃) to participate in the reaction. However, when the reaction temperature was raised to 700 ℃, all three Ni_xMg_yO catalysts achieved 100mol% methanol conversion. The reason could be that, at high temperatures, the kinetic energy of methanol molecules was high enough to diffuse deeper into the Ni_xMg_yO matrix. Thus, more oxidized Ni particles at the deeper layers of the Ni_xMg_yO catalysts become available for catalytic reactions. The H_2 yield, as shown in Fig. 4.9(B), is consistent with methanol conversion efficiency. High temperature (>600 ℃) favored H_2 production via methanol decomposition and carbon gasification reactions. In Fig. 4.9(C), the H_2/CO ratio decreased with the increase in temperature. The reason for this was that high temperature favored both reverse water-gas

shift reaction (WGSR) and reverse Boudouard reaction (C + CO_2 →
2CO), which lead to an excessive yield of CO (Zhang et al., 2007a,
Fidalgo et al., 2010). Fig. 4.9(D) shows the selectivity of both CO
and CO_2 at 600 ℃ for the 4 catalysts. All the three Ni_xMg_yO catalysts
showed higher CO yield and lower CO_2 yield compared with Ni_xAl_yO
catalyst. It might be due to the higher CO_2 capture ability of
Ni_xMg_yO solid solution that resulted in a greater amount of CO_2
being adsorbed, and subsequently accelerated the reverse
Boudouard reaction and mitigated carbon deposition.

Table 4-3 Methanol conversion and H_2 yield after 20 h steam reforming at different steam carbon ratios.

	Steam/carbon ratio	Methanol conversion (mol%)	H_2 yield (mol%)
Ni_xMg_yO-impre	3	55.3	30.0
Ni_xMg_yO - hydro	3	97.4	58.5
Ni_xMg_yO -copre	3	66.2	38.0
Ni_xAl_yO	3	97.1	61.6
Ni_xMg_yO-impre	1	51.4	29.0
Ni_xMg_yO - hydro	1	58.3	33.8
Ni_xMg_yO -copre	1	57.5	33.6
Ni_xAl_yO	1	51.1	28.8
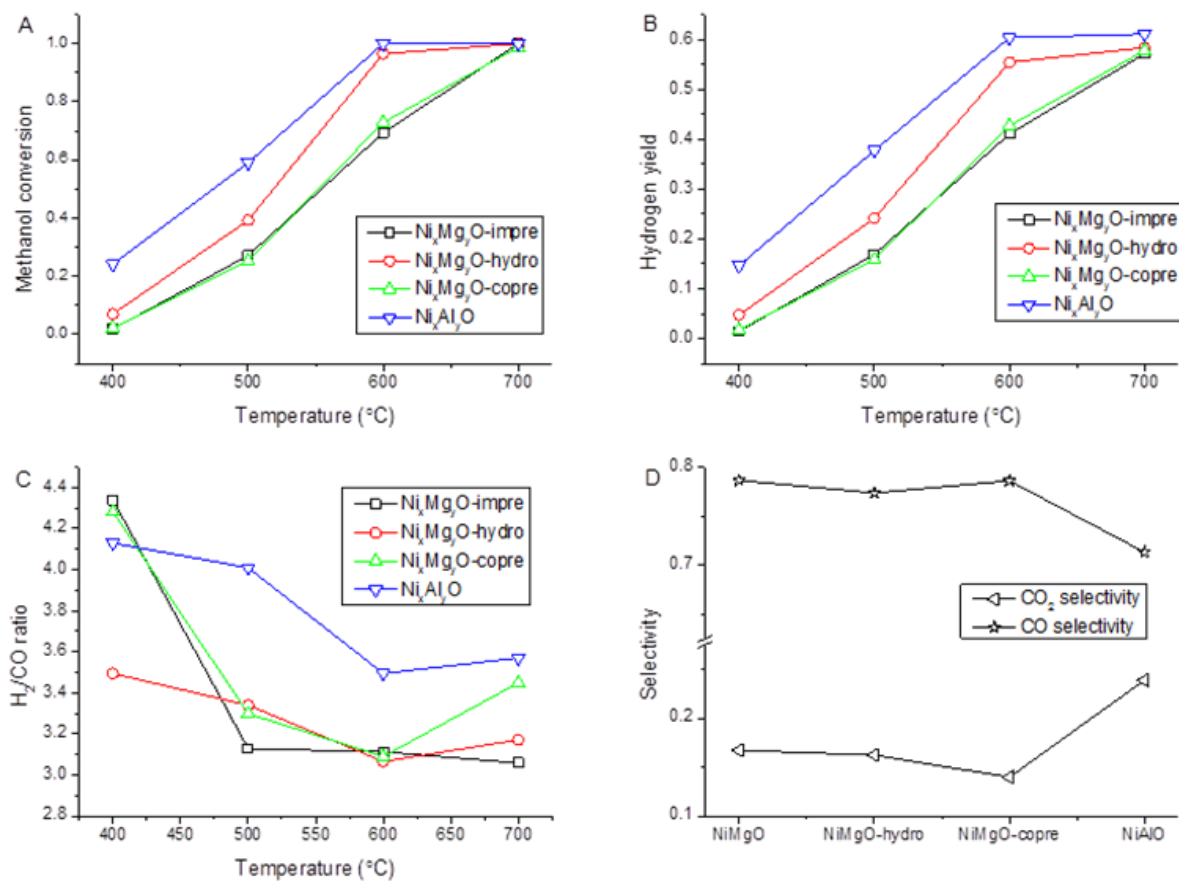
Fig. 4.9 Methanol steam reforming performance of catalysts (reaction condition: P = 1 atm, GHSV=114,000 ml/gcat·h, Steam/Carbon = 3)

The durability tests of catalysts were also carried out at two different S/C ratios. The methanol conversion efficiency and H_2 yield after 20 h test were shown in Table 4-3 and Fig. 4.10. In this study, the S/C ratio was 3 and the flow rate of methanol was kept as 0.86 ml/g_{cat}·min (GHSV at 114,000 ml/g_{cat}·h). After 20 hours' testing, Ni_xMg_yO-hydro and Ni_xAl_yO still exhibited outstanding stability with around 97mol% of methanol conversion and their hydrogen yield remained as 58.5mol% and 61.6mol%, respectively. For both Ni_xMg_yO-hydro and Ni_xAl_yO, the final H_2 yield increased, compared with their initial yields as shown in Fig. 4.10. This observation could be attributed to the gradual reduction of oxidized Ni particles from MgO matrix and $NiAl_2O_4$ spinel during reforming.

However, it was also observed in this study that methanol conversion of Ni_xMg_yO-impre and Ni_xMg_yO-copre decreased about 14.1mol% and 6.7mol% respectively compared with their corresponding fresh catalysts. The reason for the deactivation could be the slow surface restructuring, which alter the chemisorption behaviour on the surface of the catalysts or the number of active sites. This conclusion is also supported by the BET results, which showed that t-plot micropore volume of these two catalysts decreased significantly. The micropore volume of the spent Ni_xMg_yO-copre was less than half of its fresh catalyst. For the Ni_xMg_yO-impre catalyst, the micropore volume decreased

significantly from 0.00469 cm^3/g to 0.00059 cm^3/g. The catalytic performance of the Ni_xMg_yO-hydro was compared with catalysts by other researchers and summarized in Table 4-4 (Patel and Pant, 2006, Wang et al., 2007, Gao et al., 2008, Jones and Hagelin-Weaver, 2009, Huang et al., 2009). The commonly used catalysts for the steam reforming of methanol were mostly Cu-based and were used at temperatures below 300 ℃. It can be seen that only the La_2CuO_4 catalyst showed similar performance of Ni_xMg_yO-hydro prepared in this study. The other catalysts and the two commercial catalysts were not as good as Ni_xMg_yO-hydro in terms of methanol conversions. Compared with the two layers of $Ni/Ce-ZrO_2$ and Ni/YSZ catalysts, which achieved a hydrogen yield of 51.0mol% at 700 ℃ after 10 hours' testing, and 58.6mol% at 750 ℃ (Laosiripojana and Assabumrungrat, 2007), the Ni_xMg_yO solid solution developed in this study also showed better performance (hydrogen yield 58.5mol% at 600 ℃). In term of hydrogen production activity, Ni_xMg_yO-hydro showed the highest rate, which again proved the outstanding performance of this catalyst.

In order to investigate performance under harsh conditions and to understand carbon deposition resistant ability of these catalysts, tests were also conducted at a low S/C ratio (S/C = 1)and a much higher methanol input rate of 1.38 ml/g_{cat}·min (GHSV at 92,000 ml/g_{cat}·h). The methanol conversion and hydrogen yield were listed

in Table 4-3. Under these conditions, the conversion efficiency of all the catalysts was lower than 60mol% after 20 h test. The lowest conversion of Ni_xAl_yO (at 51.1mol%) was associated with severe carbon deposition (28.8wt% carbon deposition in total). The Ni_xMg_yO-hydro, which had a high basicity, kept its high catalytic activity with good carbon resistance ability (1.5wt% carbon deposition in total). The better performance of Ni_xMg_yO-copre compared with Ni_xMg_yO-impre could be attributed to its moderate increase in the size of Ni particle by 11.7%, while the size of metal particle of Ni_xMg_yO-impre increased by 110.4%. Based on the results at S/C ratio = 1 and 3, NixMgyO-hydro was the best catalyst with better carbon deposition resistance and durability.

Table 4-4 Comparison of catalytic performance of different catalysts.

Catalyst	Temperature (℃)	Methanol conversion (mol%)	Activity ($\mu mol_{H2}/g_{cat}\cdot s$)	Hydrogen yield (mol%)
Cu/Zn/Al (Patel and Pant, 2006)	260	76	203	-
Cu/ZnO (Wang et al., 2007)	240	71	59	-
La_2CuO_4 (Gao et al., 2008) (nanofiber or powder)	400	100	280	-
Cu/Zn/Al2O3 (Jones and Hagelin-Weaver, 2009) (commercial)	260	60	-	-

Table 4-4 continue

Catalyst	Temperature (°C)	Methanol conversion (mol%)	Activity ($\mu mol_{H2}/g_{cat} \cdot s$)	Hydrogen yield (mol%)
Cu/Zn/Al2O3 (Huang et al., 2009) (commercial)	300	57	-	-
Ni/Ce-ZrO$_2$ + Ni/YSZ (Laosiripojana and Assabumrungrat, 2007)	700	-	-	51.0
Ni$_x$Mg$_y$O -hydro	600	97	620	58.5
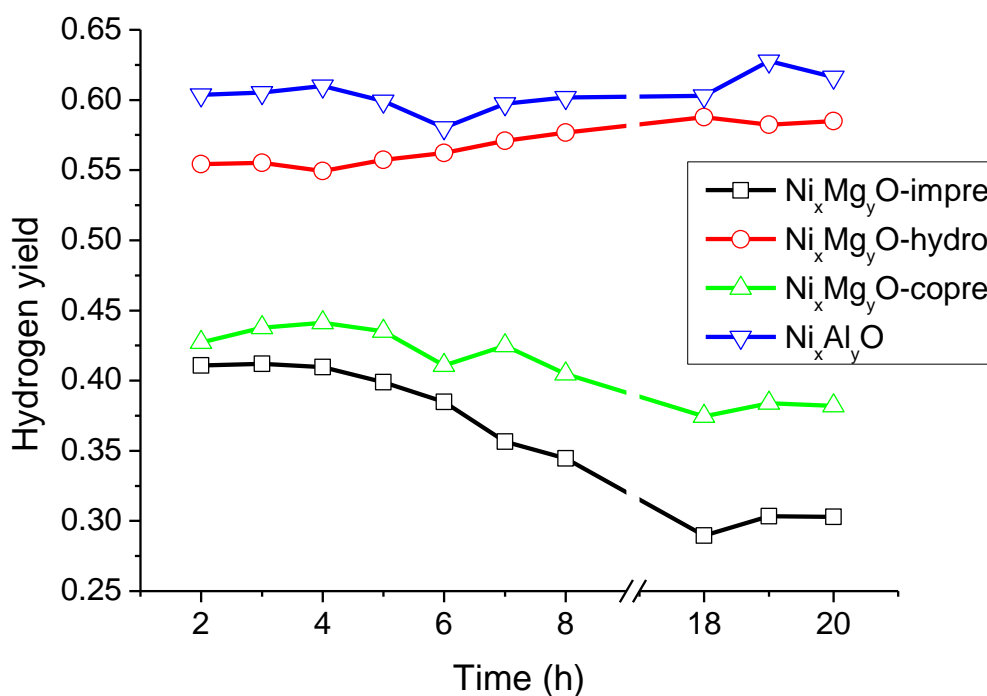
Fig. 4.10 H$_2$ yield at 600 °C as a function of time on stream (reaction condition: P=1 atm, GHSV=114,000 ml/g$_{cat}$·h, Steam/Carbon = 3).

4.6 Characterization of spent catalysts.

4.6.1 XRD analysis

Based on the comparison of fresh, reduced and spent catalysts of these three Ni_xMg_yO catalysts (in Fig. 4.3), it is clear that no noticeable difference was found except some small changes in peak intensity. This demonstrated the outstanding thermal stability of Ni_xMg_yO solid solutions prepared in this study. In addition, no peaks of metallic Ni ($2\theta = 44.6°$, $51.3°$, and $76.1°$) were identified for all reduced and spent catalysts of Ni_xMg_yO-copre, Ni_xMg_yO-hydro, and Ni_xMg_yO-impre (Wu et al., 2013). These results suggested that oxidized Ni particles in MgO matrix were not reduced to elemental Ni after the reduction process at 600 ℃. Even after the 20 h durability tests, Ni particles were still fixed inside the MgO matrix. The main reason for this is the strong metal support interaction effect (SMSI) of Ni_xMg_yO solid solution (Wu et al., 2013). For Ni_xAl_yO catalyst (Fig. 4.3(A)), both γ-Al_2O_3 and $NiAl_2O_4$ were identified on the XRD spectra of the catalyst (Al-Ubaid and Wolf, 1988, Zhao et al., 2015). The 3 characteristic peaks for metallic Ni particles were detected in both reduced and spent catalysts. This result indicates that the bonding crystal force inside the Ni_xMg_yO solid solution is stronger than that of Ni_xAl_yO structure. The Ni particles in Ni_xAl_yO structure normally contribute to the activation of catalysts at the initial stage of the reaction. Due to the weak

bonding force, these free Ni particles could overcome the surface crystal forces and aggregate to form larger size Ni crystallites during reforming process, which would worsen carbon deposition issues and accelerate the deactivation of catalysts. It can therefore be concluded that Ni_xMg_yO solid solution might be more stable and show a better catalytic durability than the Ni_xAl_yO catalyst. For the spent Ni_xAl_yO catalyst, a small peak around 26.6°, which was attributed to the formation of ordered carbon, was detected (Xing et al., 2013, Li et al., 2015). This indicates severe carbon deposition occurred on the surface of the Ni_xAl_yO catalyst.

4.6.2 N$_2$ physiosorption isotherms

Textural structure of reduced catalysts and spent catalysts after 20 h testing was summarized in Table 4-5. Compared with Ni_xMg_yO-impre, the hydrothermal treatment resulted in a 60% increase in surface area, the highest total pore volume and micropore volume for Ni_xMg_yO-hydro. Normally, a larger surface area helps improve metal dispersion on the surface of the catalyst, and a higher micropore volume enhances the adsorption of reactants. These improvements subsequently contribute to a higher catalytic performance of the catalyst. The Ni_xMg_yO-copre had an even higher surface area and it could be attributed to its porous structure, which was confirmed by TEM analysis in Section 3.5. The alumina catalyst showed the highest surface area, due to its typical mesostructure.

Normally, apart from surface area and total pore volume, micropore volume is another key factor associated with metallic agglomeration (Liu et al., 2014). A higher micropore volume helps alleviate metallic agglomeration and enhances gaseous exchange, which subsequently promotes reforming process (Lim et al., 2016). In Table 4-5, comparing the reduced catalysts with spent catalysts, the dramatic decrease in micropore volume of Ni_xMg_yO-impre from 0.00469 cm^3g^{-1} to 0.00059 cm^3g^{-1} suggests that the deactivation of the catalyst was due to its surface restructuring. However, for Ni_xMg_yO-hydro, no significant change in micropore was observed. This suggests that this catalyst was more durable and exhibited the least morphology changes after long-time testing, which was verified in Section 4.5.

Table 4-5 N$_2$ physisorption analysis results of reduced and spent catalysts.

Catalysts	State	Surface area (m^2g^{-1})	Total pore volume (cm^3g^{-1})	t-plot micropore volume (cm^3g^{-1})
Ni_xMg_yO-impre	Reduced	49.7	0.343	0.00469
	Spent	53.5	0.295	0.00059
Ni_xMg_yO-hydro	Reduced	79.8	0.841	0.00657
	Spent	71.6	0.768	0.00511
Ni_xMg_yO-copre	Reduced	54.0	0.364	0.00392
	Spent	52.5	0.339	0.00189
Ni_xAl_yO	Reduced	131.4	0.372	0.00390
	Spent	108.7	0.313	0.00261

4.6.3 TGA analysis

Normally, the burning of chars started at temperatures above 400 ℃ (Perez-Lopez et al., 2006, Wang and Lu, 1998b, Tsyganok et al., 2003). Therefore, in this study, the spent catalysts were heated in air to 900 ℃ to determine the quantity of carbon deposited on the catalysts, the results of which are presented in Table 4-6. When S/C = 3, Ni_xAl_yO experienced a moderate carbon deposition rate of 2.45 mg/g_{cat}·h although a conversion efficiency of 97.1mol% was achieved. This suggests a weak correlation between carbon deposition and the deactivation of the catalyst. For all Ni_xMg_yO catalysts, no carbon deposition was detected at 700 ℃. This finding is better than what was reported by other researchers (Laosiripojana and Assabumrungrat, 2007), in which 0.13wt% of carbon was deposited at 700 ℃. When steam/carbon was 1, the Ni_xMg_yO-hydro catalyst showed the lowest carbon deposition rate of 0.75 mg/g_{cat}·h. This could be attributed to its high basicity and the excellent performance in steam reforming. Both the Ni_xMg_yO-impre and Ni_xMg_yO-copre had slightly higher carbon deposition rates of 1.95 mg/g_{cat}·h and 2.10 mg/g_{cat}·h, respectively. The Ni_xAl_yO catalyst exhibited the highest carbon formation rate of 14.40 mg/g_{cat}·h. It was reported (Rostrup-Nielsen, 1974, Bitter et al., 1999) that basic supports supply more surface oxygen via CO_2 adsorption, which subsequently contributes to the removal of amorphous carbon. Fig. 4.11 shows the TGA-DSC profiles of the spent catalysts under a

steam-carbon ratio of 1. The peaks of DSC profile indicated that the burning temperature of the carbon species deposited on Ni_xAl_yO was higher than that of carbon formed on MgO support. This also suggests that more highly ordered carbon formed on the Ni_xAl_yO catalyst (Wu and Williams, 2010).
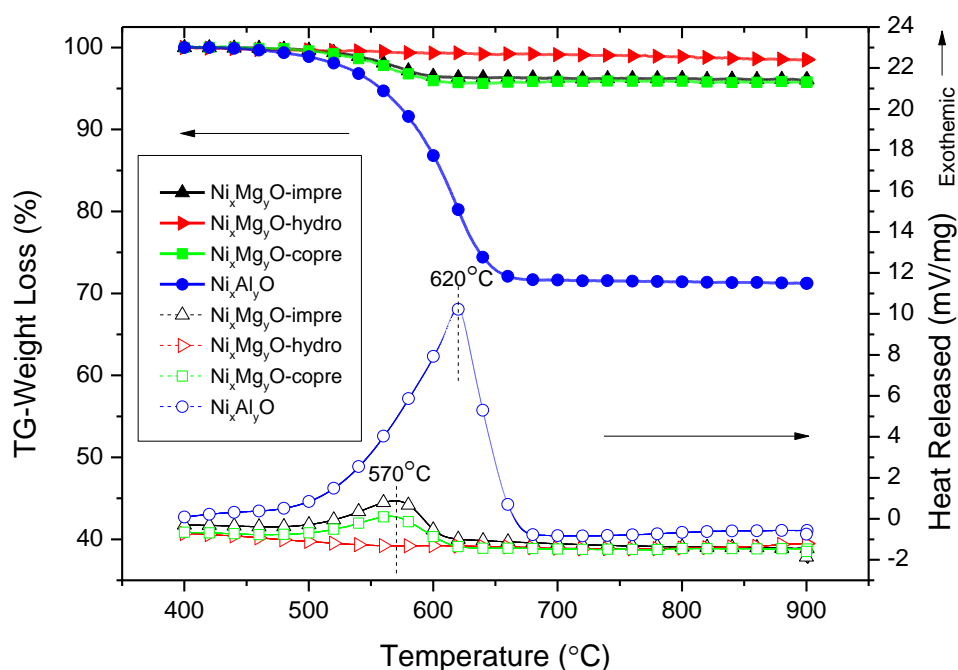
Fig. 4.11 TGA and DSC profiles for the spent catalysts after 20 h steam reforming (Steam/Carbon=1).

Table 4-6 Quantitative results from TGA for spent catalysts

after 20h testing.

Catalyst	Carbon deposition (mg/g$_{catalyst}$·h) at Steam/Carbon=3	Carbon deposition (mg/g$_{catalyst}$·h) at Steam/Carbon=1
Ni$_x$Mg$_y$O-impre	ND[a]	1.95
Ni$_x$Mg$_y$O -hydro	ND	0.75
Ni$_x$Mg$_y$O -copre	ND	2.10
Ni$_x$Al$_y$O	2.45	14.40

[a] ND denotes carbon deposition was not detectable on the spent catalyst.

4.6.4 Raman spectra

Raman spectra analysis was conducted to identify the types of carbon deposited on spent catalysts. Fig. 4.12 shows the Raman spectra in 1000-2000 cm^{-1} region, together with the value of D/G ratio on the top left of the figure, in which the G band (1595 m^{-1}) was attributed to the highly ordered carbon, while the D band (1340 m^{-1}) was attributed to the disordered aromatic carbonaceous structure. Normally, highly ordered carbon species is difficult to be burned (Vogelaar et al., 2007, Aguayo et al., 2011).

It can be seen that the Ni$_x$Mg$_y$O-hydro had the highest D/G ratio, which means carbon deposited on this catalyst was of less highly ordered carbon than the other three catalysts. Refer to the earlier study on carbon formation, the amorphous carbon, denoted as C$_\alpha$ and C$_\beta$, was formed initially via the directly decomposition of hydrocarbon or surface dissociation of carbonaceous gas

(Bartholomew, 2001). These are amorphous carbon and are relatively reactive and could be burned via reacting with free oxygen near the surface of the catalysts. Once the rate of combustion of C_α and C_β is lower than the rate of formation, the amorphous carbon would start to accumulate on the surface of the catalyst and start to turn into highly ordered carbon, which is less reactive (Bartholomew, 2001). Due to the high basicity, the surface of Ni_xMg_yO-hydro had more free oxygen originated from adsorbed CO_2 or H_2O, which accelerated the combustion rate of the surface amorphous carbon and subsequently suppressed the formation of highly ordered carbon during reforming process.

	D/G
Ni_xAl_yO	1.62
Ni_xMg_yO-copre	1.66
Ni_xMg_yO-hydro	1.99
Ni_xMg_yO-impre	1.67
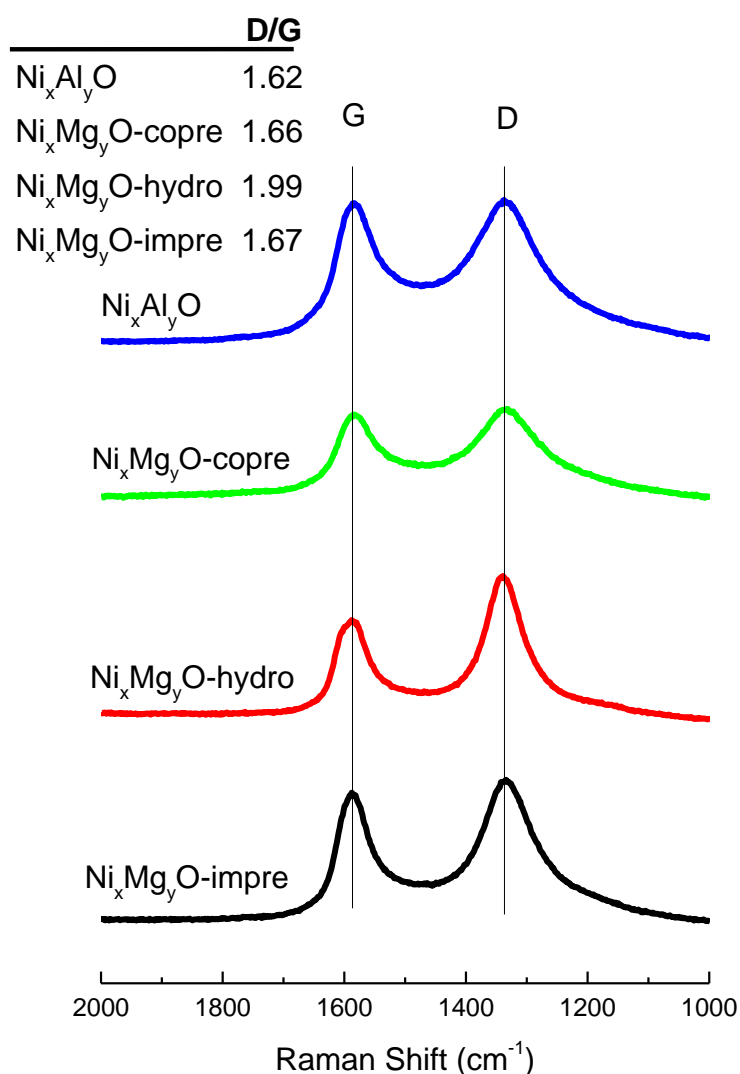
Fig. 4.12 Raman spectra of spent catalysts after 20 h steam reforming (Steam/Carbon=1).

4.6.5 Temperature programmed hydrogenation

TPH analysis was conducted in this study to distinguish different carbon species on the surface of spent catalysts. The results are illustrated in Fig. 4.13. Normally, carbon species with a hydrogenation temperature < 300 ℃ is very reactive amorphous carbon (α-carbon)(Fan et al., 2010), which is more reactive than β-

carbon with a hydrogenation temperature > 600 ℃ (Becerra et al., 2001). Carbon species with a hydrogenation temperature greater than 800 ℃ is assigned as γ-carbon, which is highly unreactive (Fan et al., 2010, Quek et al., 2010).

Four types of carbon species can be identified on the spent Ni_xAl_yO as there were four different hydrogenation temperatures, i.e. two peak temperatures at 221 ℃ and 644 ℃, and two shoulder peaks at around 500 ℃ and 800 ℃. It is generally believed (Bartholomew, 2001) that methanol decomposition and CO dissociation were the two main sources of α-carbon. The main peak at 644 ℃ represents filamentous carbon (highly ordered, less reactive). Similar carbon species was found on the Ni_xMg_yO-copre catalyst. However, the fraction of β-carbon formed was lower than that of Ni_xAl_yO catalyst.

The first peak identified in Ni_xMg_yO-hydro was for α-carbon. The hump of temperature range at 600-900 ℃ was due to the existence of both β-carbon and γ-carbon. This small oscillation indicates a small amount of highly ordered carbon formed on the spent Ni_xMg_yO-hydro, which also confirmed what was found in Raman analysis (Section 4.6.4). The identified hydrogenation peaks for the spent Ni_xMg_yO-impre were similar with those for the spent Ni_xAl_yO, except the missing peak at 644 ℃. It is normally believed that deactivation of Ni-impregnated catalysts was associated with the significant amount of inert γ-carbon (Wang et al., 2013). The low

catalytic performance of both Ni_xAl_yO and Ni_xMg_yO-impre at low steam feeding condition is consistent with this TPH test, which showed a significant portion of highly ordered carbon formed on Ni_xAl_yO and Ni_xMg_yO-impre catalysts.
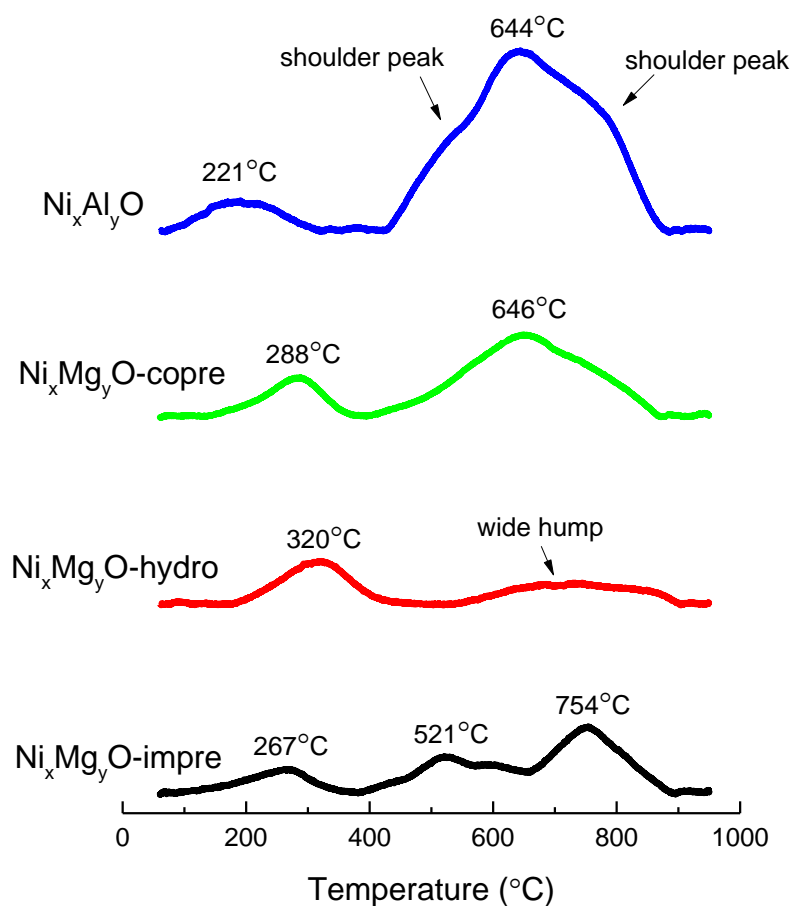
Fig. 4.13 Temperature programmed hydrogenation profiles for spent catalysts after 20 h steam reforming (Steam/Carbon=1).

4.6.6 TEM images of spent catalysts

To further investigate the morphology of carbon species deposited on the catalysts, the 4 spent catalysts, after 20 h reforming at S/C = 1, were characterized by using a TEM (as shown in Fig. 4.14). Carbon species was observed on the spent catalysts, except for Ni_xMg_yO-hydro. Fig. 4.14(A) and (D) shows carbon filament existed on both Ni_xAl_yO and Ni_xMg_yO-impre catalysts. The formation of filamentous carbon begins with sufficient dissolved carbon on the rear side of Ni particles (Rostrup-Nielsen and Trimm, 1977, Liu et al., 2002). When significant amount of carbon deposited on the surface of Ni particles, the access to active sites was blocked and the reforming reaction was inhibited (Fan et al., 2010, San-José-Alonso et al., 2009). Both the Ni_xAl_yO and the Ni_xMg_yO-impre catalysts showed carbon encapsulation phenomenon (highlighted in Fig. 4.14), which supported the findings in catalytic reforming that both catalysts exhibited relatively low conversion efficiency after 20 hours' test. In Fig. 4.14(B), it can be seen that a large amount of amorphous carbon formed on the Ni_xMg_yO-copre, but most of Ni particles were still intact within the MgO support and free from encapsulation by carbon deposition. Deactivation of reforming catalysts was also dependent on the type and location of carbon deposition (San-José-Alonso et al., 2009, Menon, 1990). In Fig. 4.14(B), no carbon was detected on the spent Ni_xMg_yO-hydro by

TEM observation, which suggested that Ni_xMg_yO-hydro was highly resistant to carbon deposition.

The sintering-sensitive nature of the catalysts was also investigated in this study. The average particle size and the size increment of catalysts after 20 h reforming at a low steam carbon ratio (S/C = 1) are shown in Table 4-2. The spent Ni_xMg_yO-copre had the smallest particle size, followed by Ni_xMg_yO-hydro with an average diameter of 15.1 nm. The high resistance to metallic sintering of Ni_xMg_yO-copre could be attributed to its "confined effect", which was mentioned in Section 4.4.2. The spent Ni_xMg_yO-impre and the spent Ni_xAl_yO catalysts showed an average particle size greater than 20 nm. This result is consistent with the significant deactivation of these two catalysts in low steam-to-carbon ratios as shown in Table 4-3.
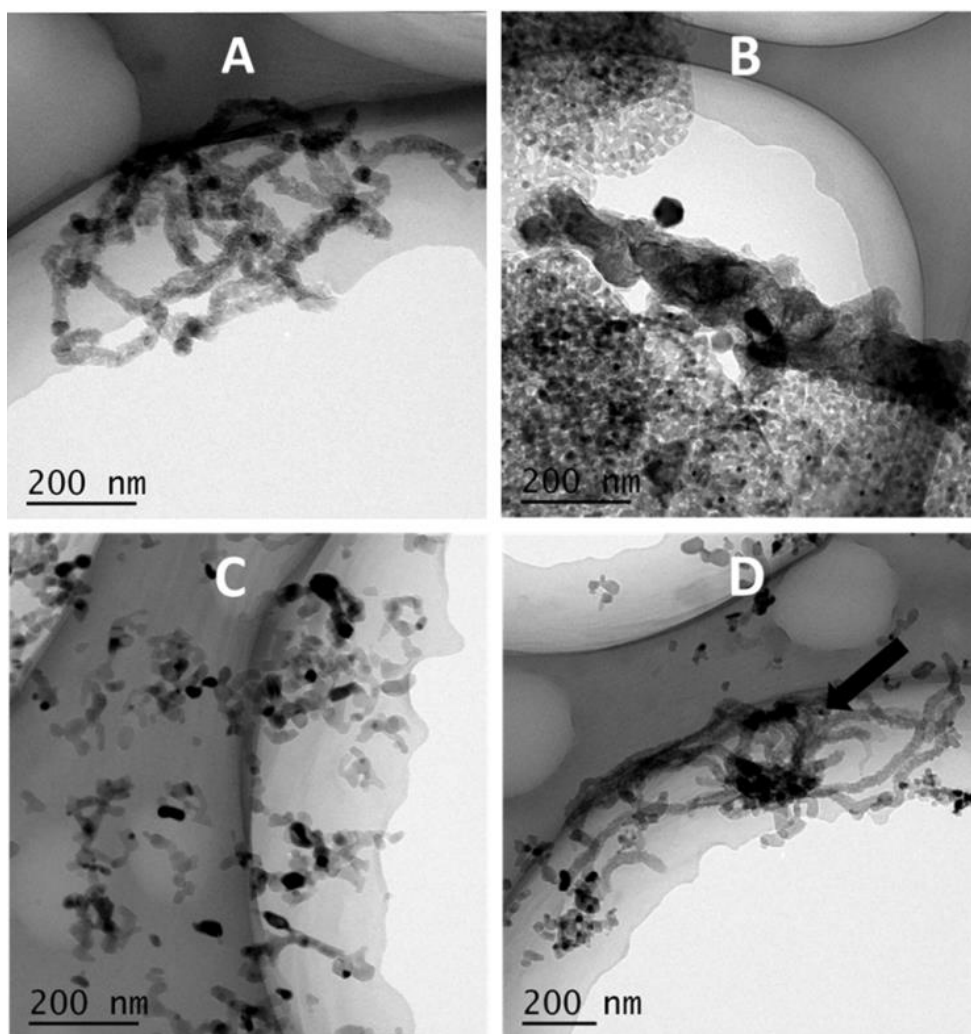
Fig. 4.14 TEM images for spent catalysts after 20 h steam reaction (Steam/Carbon=1) (A) Ni_xAl_yO, (B) Ni_xMg_yO-copre, (C) Ni_xMg_yO-hydro, (D) Ni_xMg_yO-impre.

4.6.7 X-ray photoelectron spectra

Apart from carbon characterization, the oxidation state of active compound Ni was studied to further explain the catalysts activity via XPS technology. The Ni 2p regions of XPS of both fresh and spent catalysts (after 20 h reaction with S/C=1) were displayed in Fig. 4.15 and 4.16 for comparison purpose. The deconvolution of Ni 2p

spectra were carried out by the Gaussian-Lorentzian curve-fitting method. The Ni^{2+} $2p_{3/2}$ was assigned to about 855 and 855.8 eV for Ni_xMg_yO solid solution and Ni/Al_2O_3, respectively (Yu et al., 2014, Natesakhawat et al., 2005). The broad satellite peak was around 7 eV above the main peak of Ni $2p_{3/2}$, which was due to the unscreened $\underline{c}d^8$ and screened $\underline{c}d^{10}\underline{L}^2$ final states (Oku and Hirokawa, 1977, Alders et al., 1996). Among the fresh catalysts, Ni_xMg_yO-impre was the only one that it had Ni^{3+} at 858.4 eV, which was oxidized from Ni^{2+} during calcination process. The content of Ni^{3+} on the fresh Ni_xMg_yO-impre was 5.6 times higher than the content of Ni^{2+}. Thus, the XPS analysis did give an in-depth comprehension of Ni species that different synthesized methods also affected the Ni oxidation states. But if compared the initial catalytic performance of Ni_xMg_yO-impre and Ni_xMg_yO-copre (in Fig. 4.9(A) and (B)), very similar catalytic activities of the both catalysts indicated the performance of catalysts after reduction were not really affected by their pristine oxidation states of Ni. Thus, simplex conclusion on catalyst performance, which only depended on the Nickel oxidation state, was dangerous to be made (Kim et al., 2015). Compared with fresh catalyst, the spent Ni_xMg_yO-impre displayed a very low trace of Ni 2p mass concentration, which meant the lack of the available Ni on the surface. This data supported the reforming tests results in Section 3.7 that the high degree deactivation of Ni_xMg_yO-impre was observed after 20 h test with a harsh condition of S/C=1 (in Table

4-3). For the spent Ni_xAl_yO, the Nickel particles were almost non-existent over the surface. This highly attenuation of Ni 2p spectra should be assigned to sever carbonaceous deposition, including carbon-layer covering of Ni and encapsulation of Ni. While, the spent catalysts of Ni_xMg_yO-hydro and Ni_xMg_yO-impre still shown strong trace of Ni 2p spectra without enclosed by carbonaceous species. This finding also supported their reasonable higher performance at harsh condition reaction. The metallic Ni^0 (about 852.7 eV) was not identified on the all three spent Ni_xMg_yO catalysts, which was consistent with the XRD results (in Section 3.1) (Yu et al., 2014). Combined with H_2-TPD analysis, it was believed that the most of Ni particles were existed at the catalysts subsurface, where oxidized Nickel was hardly to be reduced at the reaction temperature of 600 ℃.
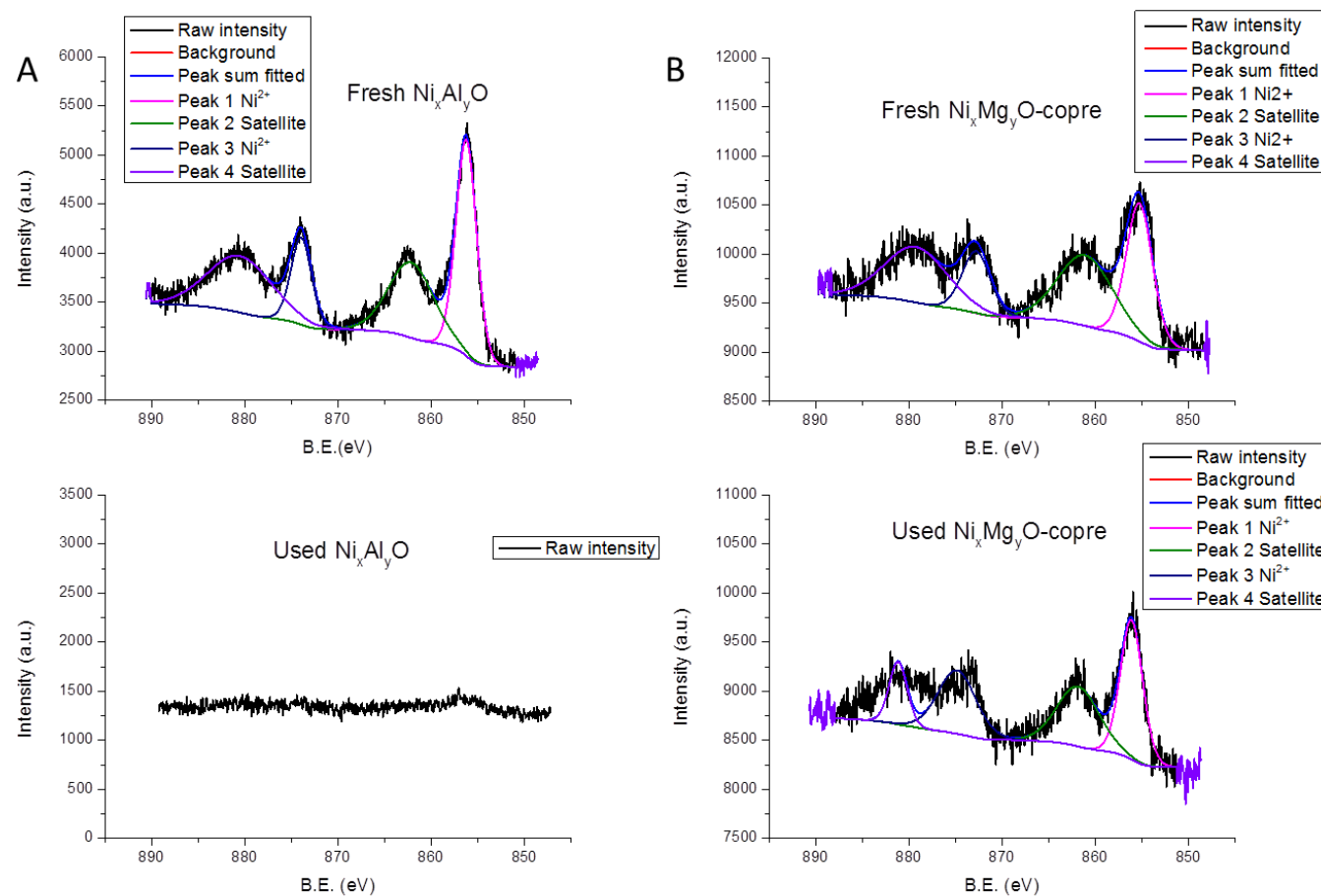
Fig. 4.15 Ni 2p spectra of both fresh and spent catalysts
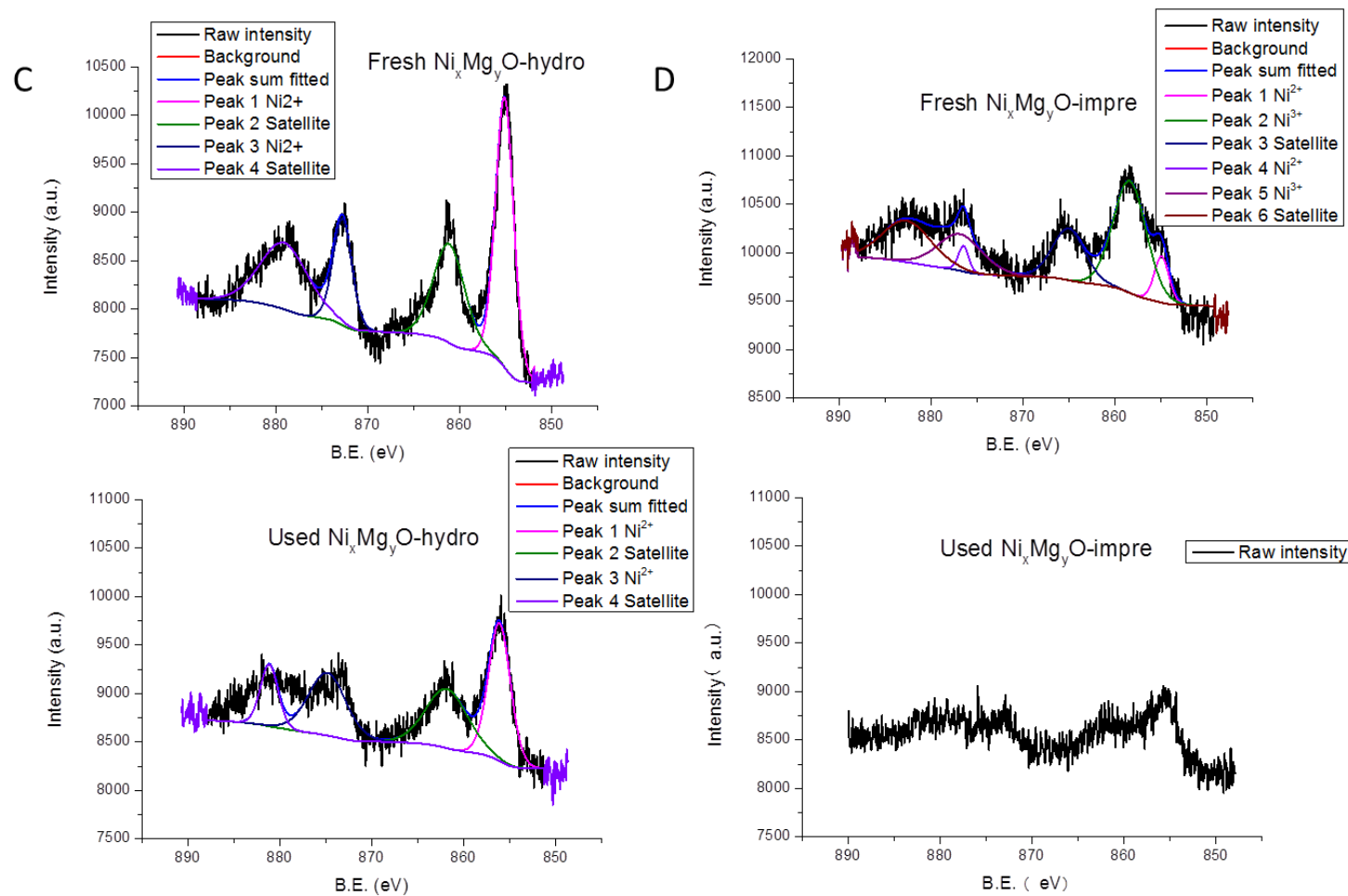
Fig. 4.16 Ni 2p spectra of both fresh and spent catalysts.

4.7 Summary

In this research, it is found that catalysts prepared using different preparation methods showed active phase in different crystal structures and nano Ni_xMg_yO solid solution were found in all three catalysts studied. The good dispersion of nano-scale NiO particles in the Ni_xMg_yO solid solution and the 'isolation effect' of MgO resulted in the formation of nano Ni crystallites in these catalysts after reduction. A stable catalytic performance of Ni_xMg_yO-hydro (97.4mol% conversion of methanol and 58.5mol% hydrogen yield) was maintained for 20 h at a steam-to-carbon ratio of 3. This high catalytic performance was attributed to its nano-scale active phase in Ni_xMg_yO matrix and its high micropore volume. The excellent anti-carbon deposition capability of this catalyst was attributed to the formation of solid solution that mitigated the agglomeration of Ni particles and the high total basicity of the MgO supports, which supplied sufficient oxygen from the adsorbed CO_2 and H_2O to burn off amorphous carbon.

Chapter 5. Screening of MgO-based binary metal oxides for ethanol steam reforming

5.1 Introduction

Hydrogen production via bio-oil reforming has captured much attention in recent decades, and it has the potential to eliminate risks and difficulties associated with hydrogen transportation and storage period (Md Zin et al., 2015, Cai et al., 2012a, Cortright et al., 2002). The catalytic reaction of sugar and bio-diesel combined fuel cell has been successfully demonstrated, however, its low power density and economic factors limited its further development (Chaudhuri and Lovley, 2003). Bio-ethanol is another promising alternative with high H/C ratio and low cost of production (Fang et al., 2015). Thus, steam reforming of ethanol (SRE) has been widely studied in recent decades (Md Zin et al., 2015, Mattos et al., 2012, Tippawan and Arpornwichanop, 2014).

In this chapter, Ni/MgO catalyst, together with Ni/MgO-based catalysts doped with Ce, La and Co, were synthesized for the steam reforming of ethanol (SRE). The mass fraction of promoter elements being loaded was measured by Inductively coupled plasma - atomic emission spectroscopy (ICP-AES). Other characterisation techniques such as N_2-physisorption, X-ray diffraction (XRD), H_2-temperature programmed reduction (H_2-TPR), CO-temperature programmed

deposition, X-ray photoelectron spectroscopy (XPS), Transmission electron microscopy (TEM), Thermogravimetric analysis (TG) and Raman spectra were employed to characterise the both fresh and spent catalysts. Catalytic performance and durability of these catalysts were investigated in a temperature region of 500-800 ℃ at atmospheric pressure. The reforming results showed that all the modified catalysts exhibited higher hydrogen yield, which was attributed to the enhancement of water-gas shift reaction (WGSR) and the inhibition of methanation, especially for the La-containing catalyst, which showed significantly improved selectivity at low temperatures (such as 500 ℃). For Ce and La promoted catalysts, the carbon deposition was suppressed due to the existence of oxygen vacancy and the distinct oxygen capture-release capability of the promoters.

5.2 Preparation of bimetallic catalysts

All the chemicals used in this research are of analytical grade and were purchased from Sinopharm Chemical Reagent Co., Ltd. (Shanghai, China). Four types of catalysts, i.e., Ni/MgO, Ni/Ce/MgO, Ni/La/MgO and Ni/Co/MgO, were prepared via hydrothermal treatment and impregnation method. The Ni/MgO catalyst were synthesized hydrothermally by following the process described elsewhere (Luo et al., 2016).

To prepare the doped catalysts, magnesium nitrate and nitrate of promoting element (Ce or La) were initially dissolved into deionized water at a controlled molar ratio. Ammonia solution (5wt%) was employed as sedimentation agent and was introduced to the solution dropwise with continuous stirring. The slurry therefore formed was then transferred into a Teflon-lined vessel for hydrothermal treatment for 24 h at 100 ℃ (Perez-Hernandez et al., 2013). The treated slurry was subsequently filtered and dried at 120 ℃ for 24 h, followed by calcination at 700 ℃ for 6 h. The calcined material was then impregnated with nickel via incipient wetness impregnation method at 60 ℃, and then dried at 120 ℃ for 24 h and calcination at 700 ℃ for 6 h again. The theoretical value of nickel loading was 10wt% in mass.

The Ni/Co/MgO catalysts were prepared in different ways, the reason was that it is difficulty to completely precipitate both $Ni(NO_3)_2 \cdot 6H_2O$ and $Co(NO_3)_2 \cdot 6H_2O$ at a high concentration of ammonia solution. For Ni/Co/MgO catalyst, MgO support was prepared following a hydrothermal method. The MgO support was then co-impregnated with nickel and cobalt under the same condition with the Ce- and La-promoted catalysts.

In this study, the Ce-containing catalysts with four different loadings, together with La-containing and Co-containing catalysts with three different loadings were prepared. Their element weight

percentages and denoted names were listed in Table 5-1. From the table, it showed obvious differences between theoretical values and measured values. The reasons for this included the loss of nickel element during impregnation, the loss of promoted elements during precipitation, and ICP measurement error. However, the nickel weights of all the catalysts were still controlled in the region of 8.2 ± 0.5wt%, which was acceptable. For the promoted elements, their compositions also followed a similar trend.

Table 5-1 Catalysts elemental analysis results.

Catalyst name	Theoretical element composition			Measured element composition[a]		
	Ni	Promoted element (Ce/La/Co)	Mg+O	Ni	Promoted element (Ce/La/Co)	Mg
NiMgO	10%	N/A	90%	8.4%	N/A	51.7%
1%Ce/NiMgO	10%	1%	89%	8.7%	0.6%	49.0%
2%Ce/NiMgO	10%	2%	88%	8.7%	1.7%	47.9%
3%Ce/NiMgO	10%	3%	87%	8.3%	2.3%	45.0%
4%Ce/NiMgO	10%	4%	86%	8.0%	3.0%	40.9%
2%La/NiMgO	10%	2%	88%	7.6%	1.7%	45.7%
4%La/NiMgO	10%	4%	86%	8.2%	3.6%	46.5%
6%La/NiMgO	10%	6%	84%	7.9%	5.4%	44.9%
2%Co/NiMgO	10%	2%	88%	8.2%	1.7%	45.4%
4%Co/NiMgO	10%	4%	86%	8.3%	3.4%	47.3%
6%Co/NiMgO	10%	6%	84%	8.6%	5.2%	44.7%

[a] *Measured by ICP-AES for the bulk composition, balanced by oxygen.*

5.3 Characterization of fresh bimetallic catalysts

5.3.1 N$_2$-physiosorption analysis

Structural features of the fresh catalysts were analysed via BET method. In Table 5-2, the fresh catalysts 3%Ce/NiMgO and 6%La/NiMgO showed a very similar surface property as NiMgO, which indicates the doping of Ce and La had no obvious effect on the morphology of the catalysts. This finding is also proved by their the same type of isothermal curves (Pseudo-type II isotherm) (Luo et al., 2016). However, the fresh 6%Co/NiMgO has much lower specific surface area and pore volume than the other catalysts. The difference between Co-containing catalyst and Ce/La-containing catalysts could be attributed to their distinct synthesis processes. For the co-precipitation method, Ce and La would be distributed both inside the MgO matrix and its surface as supporting materials. But in co-impregnation process, Co could only deposited on the MgO surface or sublayer. Therefore, for the Co-modified catalysts, more metallic ions were impregnated onto MgO surface and subsequently block porous structures and reduce surface area.

Table 5-2 Fresh catalysts surface morphology including specific surface area, total pore volume, micropore volume, and average pore size.

Catalysts	Surface area (m^2/g)	Pore volume (cm^3/g)	Micropore volume (cm^3/g)	Pore size (nm)
NiMgO	56	0.28	0.0059	20
3%Ce/NiMgO	52	0.29	0.0045	22
6%La/NiMgO	50	0.26	0.0046	21
6%Co/NiMgO	30	0.11	0.0026	15

5.3.2 XRD analysis

It can be seen from the powder XRD patterns of the fresh catalysts shown in Fig. 5.1 that NiO and periclase MgO exhibited the same structure as NaCl. Since no double structure peaks were observed, it means that the rocksalt structured solid solution formed due to the similar ionic radius and the same valence number of Ni and Mg ions (Chen et al., 1998, Luo et al., 2016). For the fresh Ce- and La-promoted catalysts, fluorite phase of CeO_2 and hexagonal phase of La_2O_3 were observed, and no perovskite structure of $LaNiO_3$ was detected at 32.3° and 57.3° (Yu et al., 2014, Sutthiumporn and Kawi, 2011). The immiscibility of MgO and rare earth elements resulted into a weak intensity of the rocksalt phase peak. The small CeO_2 and La_2O_3 particulates, dispersed on the surface of the support, could increase the reducibility of surface nickel ions by altering nickel electronic property, which might improve nickel activity in SRE. For the fresh Co-promoted catalyst, it had the same pattern as

NiMgO without double peaks and no Co_3O_4 diffraction peaks were observed regardless of the cobalt existence. It can be inferred that Co^{2+} highly dispersed into MgO lattice and formed NiCoMgO solid solution, which was attributed to the similar ionic radius for Co^{2+}, Ni^{2+} and Mg^{2+} and their excellent mutual solubility (Ji et al., 2001, Choudhary et al., 2005). Strong affinity of Ni-O-Co in NiCoMgO solid solution would increase the reduction temperature of Ni significantly. This effect was also confirmed by comparison analysis of XRD spectrum of the spent catalysts in Section 3.6.1.
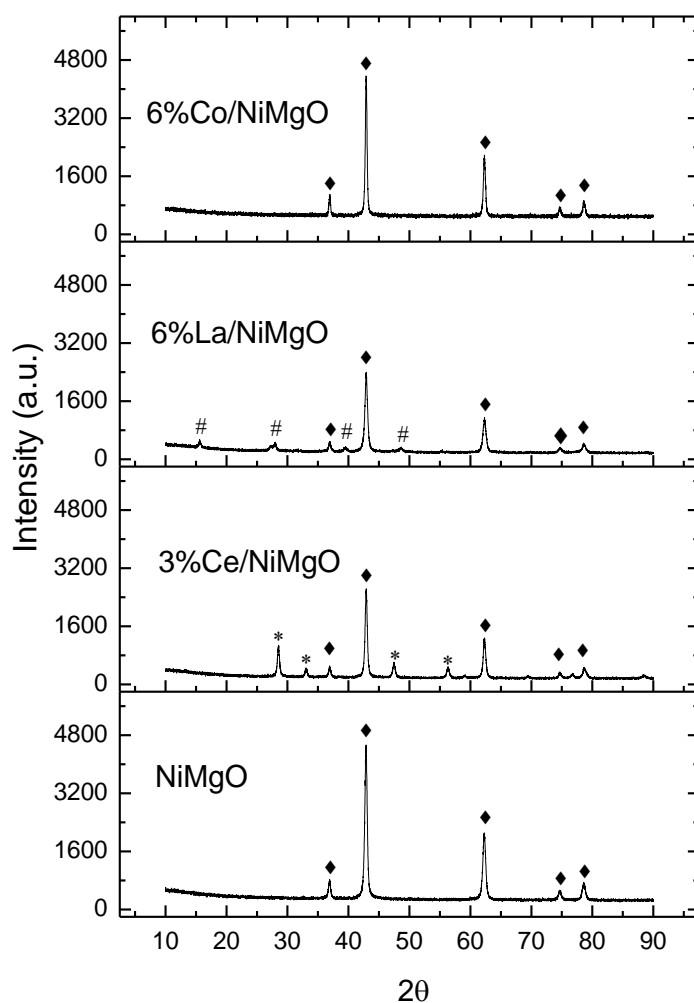
Fig. 5.1 X-ray diffraction patterns of fresh catalysts after calcination at 700 ℃, (◆): NiO or MgO, (∗): CeO₂, (#): La₂O₃.

5.3.3 H₂-TPR analysis

The reducibility of surface metal ions and the interactions between nickel ions and the support were studied by using H_2-TPR analysis. The results are shown in Fig. 5.2. According to the area of the reduction peaks, the reducibility of nickel species of all the three modified catalysts decreased, which suggested that the promoter

particles in the catalysts might have partially covered the surface Ni ions and there might be some strong interaction between Ni ions and the promoter elements. In Fig. 5.2, it is obvious that the Co-modified sample 6%Co/NiMgO showed the lowest intensity of TCD signal and a different reduction temperature compared with the other catalysts. Due to the fact that Ni and Co were co-impregnated during the preparation process, the affinity between Ni and Co was strong enough to restrain the reduction at temperatures below 700 ℃. At approximately 170 ℃, the small humps, which were observed at all three Co-containing catalysts (shown in Fig. A1), were identified as the free oxygen connected with NiMgO facets (Yu et al., 2014). For the NiMgO catalyst, the main peak (at 889 ℃) was attributed to the reduction of Ni^{2+} ions dissolved inside the MgO lattice as the formation of Ni_xMg_yO solid solution (Wang et al., 2009). The broad shoulder peak at 630 ℃ or above was confirmed as the reduction of Ni^{2+} ions at sublayers in previous work (Luo et al., 2016). For the 3%Ce/NiMgO and 6%La/NiMgO catalysts, the notable peaks at lower temperatures, i.e., 416 and 449 ℃, were also detected.

The existence of these reduction peaks in the region of 400-500 ℃ could be explained by two reasons. The first reason could be the reduction of surface CeO_2 and La_2O_3 particles. At this temperature, both CeO_2 and La_2O_3 particles could be reduced by H_2 to some

extent (Zhou et al., 2005, Trovarelli et al., 1992, Fuentes et al., 1997). The second reason might be the reduction of uncovered Ni^{2+} ions at the outermost layer with square pyramidal coordination or the reduction of NiO that has no interaction with the MgO surface (Furusawa and Tsutsumi, 2005, Parmaliana et al., 1990). On the other hand, the reduced CeO_2 and La_2O_3 particles would provide extra electrons which could migrate to the neighbouring Ni^{2+} sites and make NiO easier for reduction (Pillai and Deevi, 2006, Yu et al., 2014, Kim et al., 2015).

The broad shoulder peaks at 668 ℃ and 730 ℃ could be explained by the reduction of Ni^{2+} at sublayers (Yu et al., 2014, Wang et al., 2009), which was the same as the situation of the shoulder peak of NiMgO at 630 ℃. For 3%Ce/NiMgO and 6%La/NiMgO, these broad shoulder peaks could also be attributed to the reduction of CeO_2 and La_2O_3 particles dispersed on the surface (Zhou et al., 2005, Bernal et al., 1997).
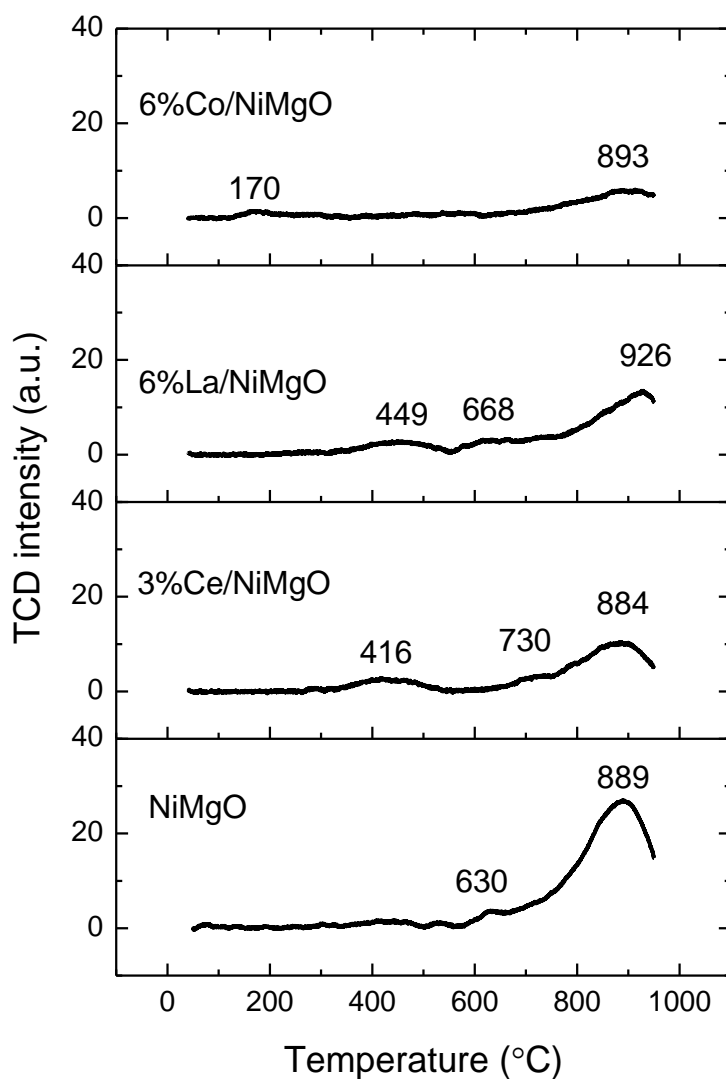
Fig. 5.2 TPR profiles of the fresh catalysts.

5.3.4 Further investigation on the catalyst surface

In order to further study the surface Ni species, XRD experiment was conducted again to investigate the reduced catalysts, which were treated in a flow of 25vol% H_2 in N_2 at 700 °C for 2 h. It is clear in Fig. 5.3 that no Ni^0 crystalline for all the catalysts was observed. This result suggests that, in H_2-TPR test, the peaks at

400-500 ℃ for Ce/La-containing catalysts were mainly due to the reduction of CeO_2 and La_2O_3 nanoparticles.
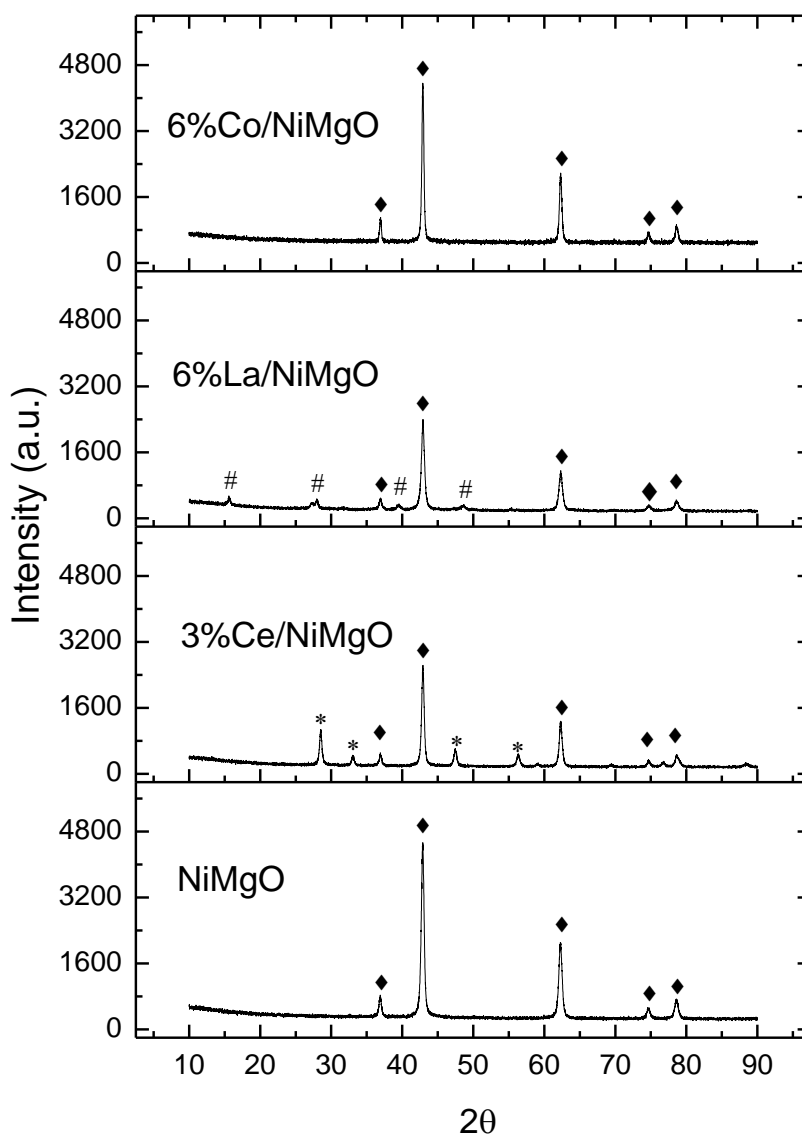
Fig. 5.3 X-ray diffraction patterns of reduced catalysts after reduction with 25vol% H_2/N_2 at a flow rate of 400 ml/min at 700 ℃ for 2h, (◆): NiO or MgO, (∗): CeO_2, (#): La_2O_3.

Based on the results of XRD analysis and H_2-TPR tests, NiMgO catalyst and Ce/La-containing catalysts had reduction peaks in the temperature range of 450-650 ℃. Due to the coverage effects of the addition of Ce and La, the total hydrogen consumption intensities of Ni^{2+} ions decreased for 3%Ce/NiMgO and 6%La/NiMgO. However, the peak intensity of Ce/La containing catalysts at 450-650 ℃ was significantly stronger than that of the NiMgO. Since there was no evidence of the existence of Ni^0 on the reduced Ce/La containing catalysts in XRD profiles, it is convinced that the reduction peaks at 450-650 ℃ were mainly attributed to the reduction of surface CeO_2 and La_2O_3. In the case of NiMgO, low intensity humps, in the temperature range of 450-650 ℃, was due to the existence of a small amount of Ni^{2+} ions on the surface, which was verified in previous research (Luo et al., 2016). However, no peaks for these reduced Ni^0 particles appeared on the XRD pattern of the reduced NiMgO catalyst. The reason for such should be that Ni^0 particles were highly dispersed or the formation of small size Ni^0 crystals (< 5 nm). It cannot be detected by the XRD (Tang et al., 1998, Kugai et al., 2006).

5.3.5 CO-TPD

It has already been proved that the primary site for CO adsorption is Ni^0 crystal but not the MgO (Hu and Ruckenstein, 1996). In the study of CO-Temperature programmed desorption was carried out

to find out the interactions between Ni and CO molecules. In Fig. 5.4, the desorption peaks observed on these NiMgO materials could be divided into three groups. The peaks at low temperature (< 200 ℃) are ascribed to the desorption of CO molecules with weak bonds with Ni species (Pillai and Deevi, 2006, Monteiro et al., 1995). The second peak group, located in a higher temperature region (200-350 ℃), is attributed to strongly bonded CO molecules (Pillai and Deevi, 2006). The broader peaks, desorbed at temperatures above 400 ℃, are associated to the formation of much higher bond strength between Ni species and CO molecules. Moreover, for the adsorption of CO on the Ni_xMg_yO solid solutions, it is believed that the substance desorbed below 200 ℃ was molecular CO adsorbed on the smooth nickel crystal planes (α site), while the high temperature (around 550 ℃) desorbed CO was adsorbed on the stepped nickel surface (β site) by dissociative adsorption (Hu and Ruckenstein, 1996). The board peaks above 400 ℃ could also be attributed to the formation of CO_2 due to the WGSR of CO and hydroxyl groups and the oxidation of CO by the subsurface NiO (Hu and Ruckenstein, 1996, Zhu et al., 2004, Kang et al., 2014).

Generally, the reducibility of CO is stronger than H_2, therefore the H_2-reduced catalysts might still have NiO on the subsurface to be reduced by CO during the desorption process. Compared the modified catalysts with the pristine NiMgO, the amount of CO

desorbed at low temperature ($< 400 ℃$) did not vary significantly because of their similar nickel content. Ce- and Co-containing catalysts showed higher intensity peaks above $400 ℃$. The likely reason for such is that Ce and Co promoted the adsorption of CO and consequently increased the formation of CO_2 via WGSR. For the Ce-modified catalysts, surface CeO_2 was much easier to release oxygen for CO oxidation and also to capture oxygen from dissociated water (Lin et al., 2003). However, the addition of La did not promote CO_2 desorption at the temperature above $400 ℃$, which could be ascribed to the CO_2 fixation via the formation of $La_2O_2CO_3$ compound (Gu et al., 2015). This was also confirmed in the XRD analysis of the spent La-modified catalysts (in Section 3.6.1).
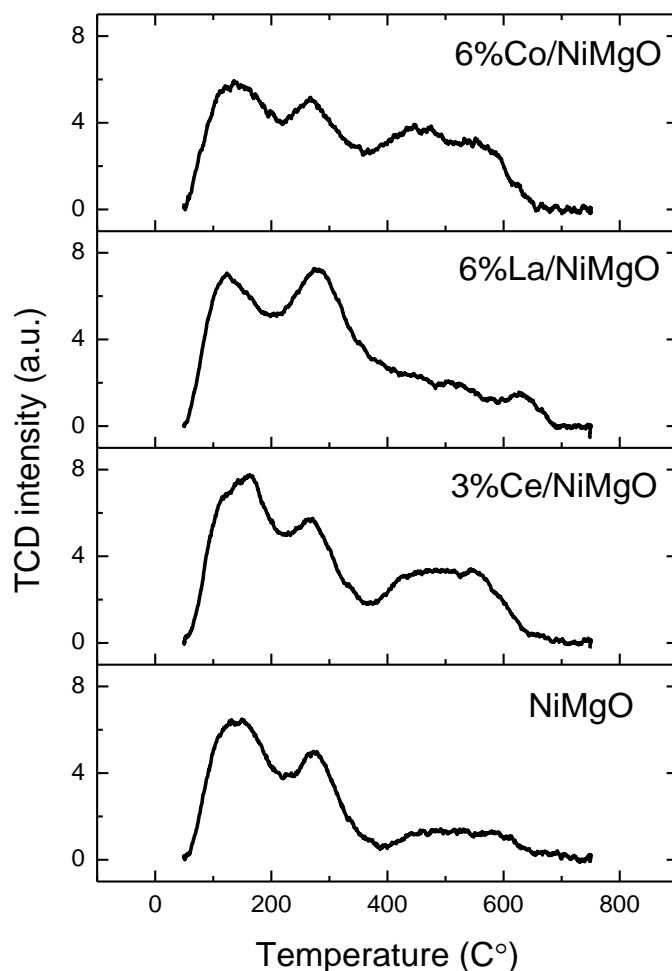
Fig. 5.4 CO-Temperature programmed deposition profiles of the H$_2$-reduced catalysts at 700 ℃ for 2 h.

5.4 Ethanol steam reforming performance of bimetallic catalysts

5.4.1 Hydrogen yields

Table 5-3 shows the performance of the catalysts in terms of H$_2$ yield, ethanol conversion and carbonaceous gas (CO$_2$, CH$_4$ and CO) yield. The hydrogen yield is a vital factor for the evaluation of the

performance of catalytic reforming catalysts. In the steam reforming of ethanol, one mole of ethanol can produce six moles of hydrogen molecules according to the stoichiometry of SRE reaction (R1). However, some free hydrogen atoms might participate in the methanation reaction (the reverse of R8), and WGSR (R5) would be inhibited at a certain extend. As a result, the unmodified NiMgO catalyst showed relatively low selectivity in hydrogen yield compared with other modified catalysts. At low temperatures, i.e., 500 ℃, the NiMgO catalyst only resulted in a H_2 yield of 12.5mol%, while the other catalysts had considerably higher H_2 production rates, especially the La-containing catalysts (2%La/NiMgO and 4%La/NiMgO), which had the H_2 yield of 53.0mol% and 52.8mol%, respectively. The two major initial steps of SRE are ethanol dehydrogenation to acetaldehyde (R3) and ethanol dehydration to ethylene (R4) (Mattos et al., 2012). The reason for the outstanding hydrogen productivity of La-modified catalysts at 500 ℃ was believed to be the lack of suitable acidic sites on La_2O_3 surface, which suppressed the dehydration reaction and led to the formation of acetaldehyde (R3) (Fatsikostas and Verykios, 2004). Compared with ethylene, acetaldehyde would undergo steam reforming to produce hydrogen at a lower temperature (around 450 ℃) (Vaidya and Rodrigues, 2006). At higher temperatures (600, 700 or 800 ℃), the initial H_2 yield of modified catalysts were all above 66.7mol% except the 6%Co/NiMgO at 600 and 700 ℃, while the highest yield

138

for NiMgO was 55.7mol% even at 800 ℃. Thus, it can be concluded that the doping of Ce, La and Co as promoters improved hydrogen yield. Among these promoters studied in this research, Lanthanum is the most effective promoter.

Moreover, the 3%Ce/NiMgO, 2%La/NiMgO and 2%Co/NiMgO were selected as the best catalysts for the 30 h long-term tests since they exhibited the highest hydrogen yield (80.3mol%, 74.3mol% and 81.8mol% respectively) among different loadings. The results of long-term tests are shown in Table 5-3. Normally, the catalytic performance of steam reforming catalyst decreases as a result of metal sintering (causing active particles size growth) and carbon deposition (causing active metal particles encapsulation) coupling with surface defects blocking (Bartholomew, 2001). But in this study, some catalysts, for instance, 3%Ce/NiMgO, 2%La/NiMgO and 2%Co/NiMgO, showed even higher hydrogen yield rates at the final stage of these long-term tests compared with the yields at initial stages. The reason for this observation could be the slow reduction of active metal oxides from the support matrix. At the early stages of the SRE, some of the nickel ions were still in their oxidized state and dispersed inside the MgO matrix, which were not reduced to form active sites during the hydrogen reduction process. These Ni^{2+} ions were slowly reduced during the reforming process due to the higher H_2 concentration in gas phase, which enhanced the reduction

of Ni^{2+}. Thus, more newly reduced Ni^0 sites formed during the course of the SRE process proceeded, which resulted in the formation of more catalytic activities and subsequently led to higher H_2 yields. This deduction was also confirmed by the XRD analysis the spent catalysts after long-term SRE tests (Fig. A1, A2 and A3). The diffraction peak of Ni^0 appeared in the XRD spectrums of spent catalysts, which was not previous observed for freshly reduced catalysts.

For Co-containing catalysts, both Ni and Co particles can act as active components. However, the hydrogen yields of catalysts at the broad temperature range (500-800 ℃) decreased with the increase in cobalt loading. It is believed that the addition of cobalt into NiMgO catalyst enhanced the Ni-O-Co affinity and made the reduction of Ni more difficulty, which subsequently led to fewer active sites formed after reduction. By comparing H_2-TPR patterns of Co-containing catalysts with different cobalt loadings (shown in Fig. A1 (C)), the intensity of hydrogen consumption peaks decreased with the increase in cobalt loading. This affinity effect was also confirmed by the XRD analysis of the spent Co-promoted catalysts, which showed that Ni^0 was only observed for 2%Co/NiMgO, and no Ni^0 was identified for both 4%Co/NiMgO and 6%Co/NiMgO (shown in Fig. A4 (B)).

5.4.2 Conversion of Ethanol

For the conversion of ethanol, it is clear (in Table 5-3) that the non-modified NiMgO catalyst showed a much lower ethanol conversion of 21.5wt% at 500 ℃ compared with the modified catalysts, especially the 2%La/NiMgO, which had a conversion of 73.0wt%. These results were consistent with their hydrogen production rate. On the contrary, the ethanol conversion of the NiMgO catalyst at 700 ℃ after 30 h testing was 90.7wt%, which was the highest among all the catalysts. There are two possible reasons for this high ethanol conversion of the NiMgO catalyst. Firstly, the temperature (at 700 ℃) is high enough to thermodynamically favour the reforming of ethanol (Mattos et al., 2012). Secondly, it is believed that the addition of the promoter elements (Ce, La and Co) in the catalysts would partially cover surface Ni and reduce the number of active sites on the catalysts slightly, which has been confirmed by H_2-TPR test in this study. In addition, the average ethanol conversion (at 700 ℃, after 30 h testing) of three Co-promoted catalysts was 89.6wt%, which was higher than those of the Ce- and La-promoted catalysts (87.4wt% and 86.9wt%, respectively). The reason for this is that Co^{2+} in the lattice of MgO could also demonstrate its catalytic effect on ethanol conversion (Ji et al., 2001).

Table 5-3 Ethanol steam reforming results.

Catalyst	T(℃)	H$_2$ yield (mol%)	X$_{ethanol}$ (mol%)	CO$_2$ yield (mol%)	CH$_4$ yield (mol%)	CO yield (mol%)
NiMgO	500 (2 h)	12.5	21.5	2.1	7.0	13.4
	600 (2 h)	41.5	84.5	8.3	19.4	56.9
	700 (2 h)	55.0	90.8	24.1	16.6	50.2
	800 (2 h)	55.7	89.1	34.9	19.8	34.4
	700(30 h)	62.2	90.7	29.8	12.1	48.9
1%Ce/NiMgO	500 (2 h)	39.3	48.5	27.9	10.1	10.5
	600 (2 h)	76.0	83.1	58.5	6.0	18.5
	700 (2 h)	77.7	81.2	53.5	1.0	26.8
	800 (2 h)	80.0	89.7	52.0	3.6	34.2
	700(30 h)	77.2	87.7	52.9	4.9	30.1
2%Ce/NiMgO	500 (2 h)	47.3	59.2	38.7	12.9	7.6
	600 (2 h)	80.3	85.8	61.9	4.0	19.9
	700 (2 h)	81.3	86.6	55.7	0	30.9
	800 (2 h)	75.3	89.3	49.4	6.2	33.7
	700(30 h)	79.5	86.4	54.3	1.3	30.9
3%Ce/NiMgO	500 (2 h)	41.0	49.8	31.8	10.9	7.1
	600 (2 h)	79.5	88.1	62.3	7.3	18.6
	700 (2 h)	79.8	84.8	54.7	1.0	29.2
	800 (2 h)	81.8	89.3	52.2	0.6	36.5

Table 5-3 continue

Catalyst	T(℃)	H$_2$ yield (mol%)	X$_{ethanol}$ (mol%)	CO$_2$ yield (mol%)	CH$_4$ yield (mol%)	CO yield (mol%)
	700(30 h)	80.3	87.1	55.9	2.1	29.1
4%Ce/NiMgO	*500 (2 h)*	35.0	38.7	26.2	6.6	5.9
	600 (2 h)	76.3	84.8	58.4	6.4	20.1
	700 (2 h)	81.3	87.5	55.1	0.9	31.5
	800 (2 h)	78.7	88.0	48.6	1.7	37.7
	700(30 h)	75.7	88.5	47.1	4.3	37.1
2%La/NiMgO	*500 (2 h)*	53.0	73.0	35.6	14.8	22.6
	600 (2 h)	74.2	85.4	58.7	9.4	17.4
	700 (2 h)	72.5	79.4	49.1	3.3	27.0
	800 (2 h)	76.8	85.5	46.9	0.9	37.8
	700(30 h)	74.3	84.4	53.2	5.7	25.6
4%La/NiMgO	*500 (2 h)*	52.8	70.5	36.1	13.0	21.4
	600 (2 h)	73.3	86.8	53.9	8.8	24.1
	700 (2 h)	66.7	85.2	46.4	11.3	27.5
	800 (2 h)	66.8	87.4	45.1	12.3	30.1
	700(30 h)	70.7	88.5	49.2	10.6	28.7
6%La/NiMgO	*500 (2 h)*	40.0	52.4	25.6	9.9	16.9
	600 (2 h)	71.0	86.2	49.7	9.0	27.6
	700 (2 h)	67.3	85.9	46.0	10.9	29.0
	800 (2 h)	68.0	88.1	45.6	11.5	31.0

Table 5-3 continue

Catalyst	T(℃)	H_2 yield (mol%)	$X_{ethanol}$ (mol%)	CO_2 yield (mol%)	CH_4 yield (mol%)	CO yield (mol%)
	700(30 h)	70.8	87.9	48.3	10.2	29.4
2%Co/NiMgO	500 (2 h)	40.0	50.8	28.5	11.7	10.7
	600 (2 h)	77.7	84.8	59.3	5.6	19.9
	700 (2 h)	78.5	83.5	52.3	0	31.2
	800 (2 h)	79.7	86.9	49.4	0	37.5
	700(30 h)	81.8	89.5	56.1	2.3	31.1
4%Co/NiMgO	500 (2 h)	18.8	20.7	12.1	4.1	4.6
	600 (2 h)	71.0	80.4	54.5	8.3	17.6
	700 (2 h)	74.3	79.4	51.3	2.1	26.0
	800 (2 h)	76.2	87.0	47.6	2.8	36.7
	700(30 h)	78.8	89.1	53.9	4.8	30.4
6%Co/NiMgO	500 (2 h)	8.0	7.8	3.2	1.7	2.9
	600 (2 h)	42.7	56.0	23.4	9.5	23.0
	700 (2 h)	63.3	88.7	34.3	12.0	42.3
	800 (2 h)	67.8	91.7	41.8	12.7	37.2
	700(30 h)	62.0	90.1	26.5	11.1	52.4

5.4.3 Investigation of carbonaceous gas yields

The mechanism for the high ethanol conversion but low hydrogen production of the NiMgO catalyst was further investigated by comparing the gases yields with the other three representative

catalysts at 700 ℃. In Fig. 5.5, all the modified catalysts had similar tendency in the yield of gas products. They all showed lower methane yield, which suggested the methanation reaction (the reverse of R6) was inhibited. The restriction of methanation would contribute to a higher hydrogen gas yield. On the other hand, the modified catalysts had a higher carbon dioxide yield and a lower carbon monoxide yield, which indicated that WGSR was enhanced to produce more hydrogen. The result of CO-TPD test in this study also proved that the addition of Ce and Co increased the interactions between Ni and CO, which favored the WGSR. It can be concluded that both the enhancement of WGSR and the inhibition of methanation contributed to the higher hydrogen yield when Ce-, La- and Co-containing catalysts were used.
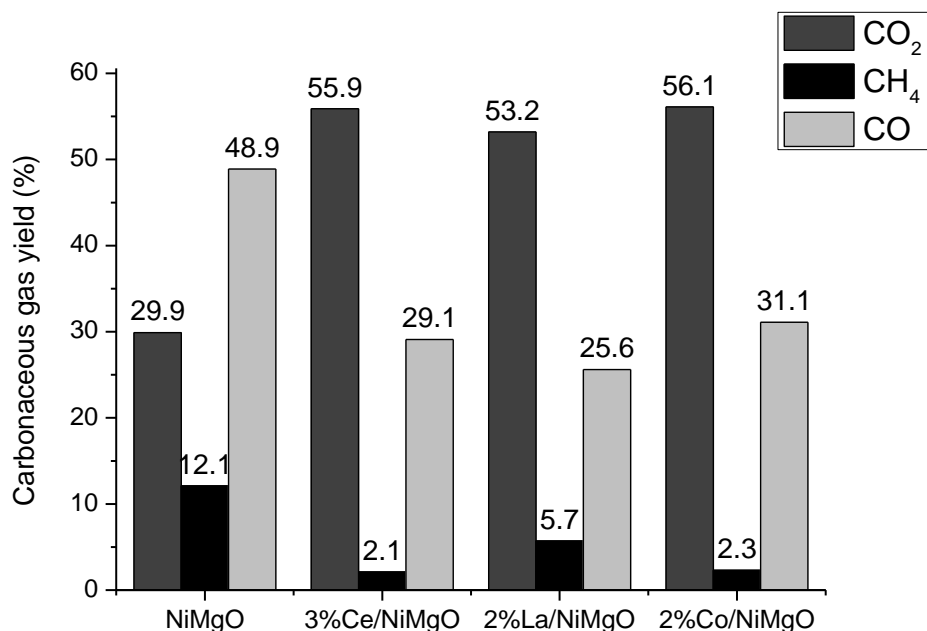
Fig. 5.5 Carbonaceous gases yields of catalysts at 700 ℃ after 30 h ethanol steam reforming test.

5.5 Evaluation of carbon deposition

5.5.1 TGA analysis

The amount of carbon deposition on the spent catalysts was investigated by using a TG-analyser. In Fig. 5.6, all the modified catalysts showed better carbon deposition resistant ability compared with the NiMgO. The doping of Ce and La expedited carbon removal rate, especially for the 3%Ce/NiMgO, 2%La/NiMgO and 4%La/NiMgO, which exhibited excellent catalytic reforming performance with less than 1wt% of carbon deposition after 30 h tests. In Fig. A5, the burning temperature for non-modified NiMgO and 1%Ce/NiMgO was within the range of 500-650 ℃, which

corresponded to the burning of graphited carbon (Wu and Williams, 2010, Wang et al., 2013). While the temperature for weight loss of the other Ce-containing catalysts was below 400 ℃. This could be attributed to the combustion of very active amorphous carbon (Rezaei et al., 2006). The cerium oxide and its high oxygen storage capacity provided highly mobile oxygen atoms for carbon removal due to reversible change of its oxidation state ($Ce^{4+} \rightleftharpoons Ce^{3+}$). Over La-containing catalysts, the formation of acetaldehyde (Reaction 3) during the catalytic reforming process was enhanced (Fatsikostas and Verykios, 2004), which helped restrain carbon formation. Acetaldehyde had a very low coking activity, while ethylene (Reaction 4) could easily cause carbonaceous residues and catalyst poisoning via polymerization (Vaidya and Rodrigues, 2006, Cai et al., 2013). The other reason for the excellent carbon deposition resistance of La-modified catalysts was the formation of $La_2O_2CO_3$ on the Ni particles (Shi et al., 2011). This lanthanum oxycarbonate species removed carbon deposited on the surface by providing CO_2 as a reactant (Fatsikostas et al., 2002). For Co-containing catalysts, the introducing of the second active constituent Co also accelerated the gasification of the surface deposited carbon. However, the excessive amount of Co (for example, 6%Co/NiMgO) led to a strong affinity between Ni and Co, which inhibited carbon removal. The anti-carbon deposition ability of the tested catalysts was found to be in the order of Ce/NiMgO $\approx$ La/NiMgO/ > Co/NiMgO > NiMgO.
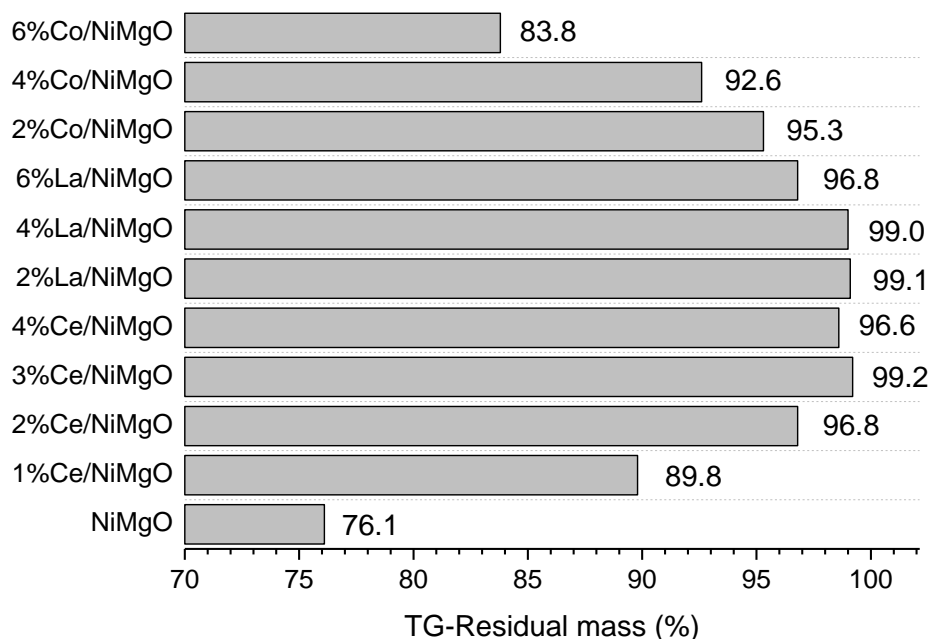
Fig. 5.6 TG-residual mass of the spent catalysts after 30 h steam reforming of ethanol.

5.5.2 Raman spectra

To qualitatively and quantitatively evaluate carbon deposits, Raman spectrum of the catalysts after 30 h reaction at 700 ℃ was examined. Fig. 5.7 illustrates spectra in the region of 800-3200 cm^{-1}. The second distinctive band at wavenumber in the range of 1596-1562 cm^{-1} (G line, labelled for graphite) corresponded to the stretching vibration of sp^2 sites in C=C chains or in hexagonal rings (Robertson, 2002, Tsaneva et al., 2014). Nevertheless, the first band at wavenumber in the range of 1329-1344 cm^{-1} (D line, labelled for disordered graphite) was only due to the sp^2 sites in six fold rings (Robertson, 2002). Based the magnitude of peak intensity

in Fig. 5.7, both spent NiMgO and 6%Co/NiMgO exhibited stronger integrated intensity compared with the spent 3%Ce/NiMgO and 6%La/NiMgO. This result is in consistence with TGA data, especially the extremely low carbon deposition on 3%Ce/NiMgO. For qualitative purpose, the calculation of microcrystalline planar size L_a, which could represent the graphitized structure proportion in the total formed carbon, was conducted using following equations (Llorca et al., 2002).

$$L_a = C(\lambda_L) \, (I_G/I_D)^{-1} \qquad \text{(eq 5.1)}$$

$$C(\lambda_L) = C_0 + \lambda_L \cdot C_1 \qquad \text{(eq 5.2)}$$

Where I_G/I_D is the ratio of two peaks area, and the coefficient $C(\lambda_L)$ must be estimated depending on the excitation laser wavelength (eq 5.2), where λ_L was 532 nm in this experiment. C_0 and C_1 were identified to be $-$ 126 Å and 0.033 (Matthews et al., 1999). By comparing the L_a value in Table 5-4, the catalyst 3%Ce/NiMgO had the lowest value, which suggested the lowest amount of graphitized structure. This result further confirmed the finding of the TGA test that the carbon burning temperature of 2-4%Ce/NiMgO catalysts shifted to the lower temperature due to the formation of more amorphous carbon deposits.
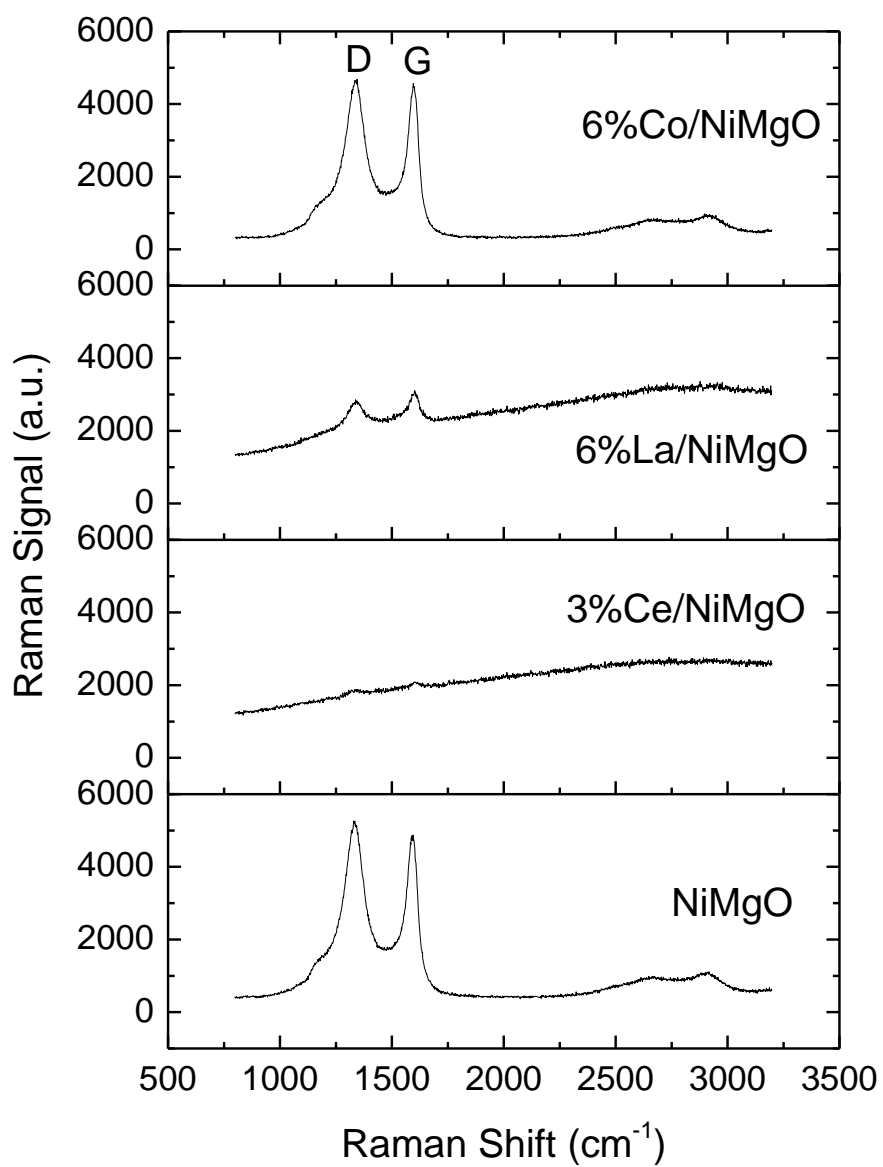
Fig. 5.7 Raman spectra of spent catalysts after 30 h reforming testing.

Table 5-4 Raman spectra data and parameter collected after peak deconvolution.

Catalysts	Peak label[a]	Peak position (cm^{-1})	FWHM (cm^{-1})	L_a (nm)
NiMgO	D (65%)	1329	115	2.7
	G (35%)	1596	67	
3%Ce/NiMgO	D (70%)	1334	51	2.1
	G (30%)	1599	39	
6%La/NiMgO	D (65%)	1337	99	2.7
	G (35%)	1602	51	
6%Co/NiMgO	D (64%)	1344	115	2.8
	G (36%)	1596	63	

[a] The values in parentheses represent the percentage area of each peak after deconvolution.

5.5.3 XPS study of C 1s

The XPS technique was also applied to elucidate the nature of carbon species on the surface of spent catalysts at the C 1s region (Fig. 5.8 and Table A-2). Normally, the main peak and the other two attached shoulders are associated with following carbon species: 285.0 ± 0.2 eV for graphite (Yu et al., 2014); 285.8 ± 0.2 eV for "defects" or crystalline imperfections (Estrade-Szwarckopf, 2004, Montero et al., 2015); 288-291 eV for CO_3^{2-} species on MgO surface (Hiroshi Onishi, 1987). It has been observed that the spent 3%Ce/NiMgO had the lowest intensity of graphite peak (Fig. 5.8 (B)), while that peak of the spent NiMgO showed the highest intensity (Fig. 5.8 (A)). This result suggests a good resistance ability of anti-filamentous carbon formation, which was due to the

existence of CeO_2 and its significant surface oxygen storage and release capability for the fast gasification of carbonaceous species. This finding also supports the conclusion drawn from the TGA analysis and Raman spectra analysis. The composition of broad CO_3^{2-} peak (Table A-2), calculated from peak area, suggested the spent 6%La/NiMgO had the highest CO_2 adsorption on its surface. The reason for this could be ascribed to the surface La_2O_3, which transformed into $La_2O_2CO_3$ by adsorption of CO_2 (Sutthiumporn and Kawi, 2011).
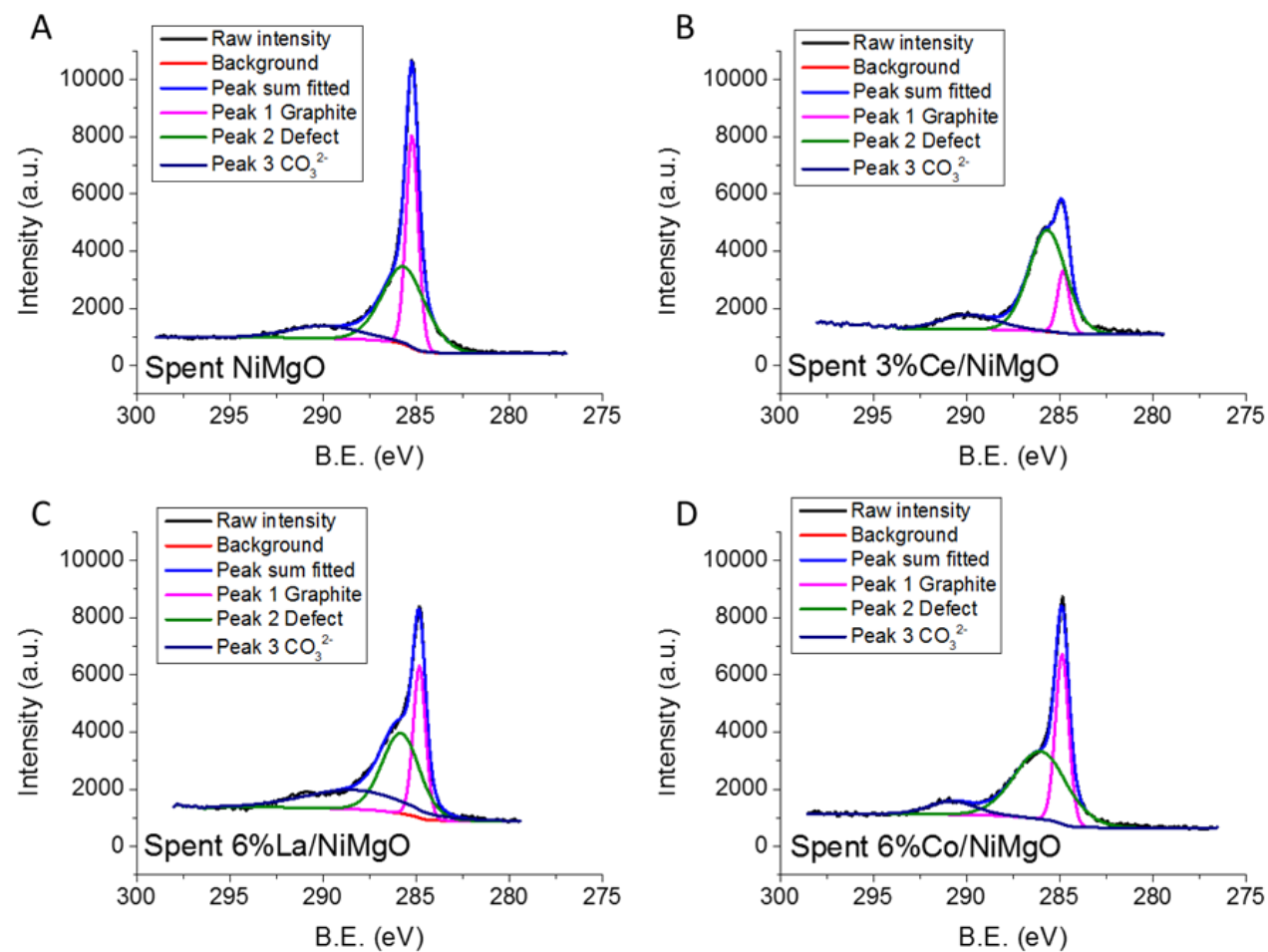
Fig. 5.8 C 1s spectra of spent catalysts after 30 h reaction.

5.6 Characterization of spent catalysts

5.6.1 XRD analysis of the spent catalysts

Several techniques were employed for the characterization of the spent catalysts (after 30 h reaction). In Fig. 5.9 (A), no carbonaceous diffraction peak was found in all the used catalysts except for NiMgO, for which there was a broader peak around 26.6°. It indicated the existence of a significant amount of highly ordered carbon (Xing et al., 2013). This peak was also in agreement with the TGA analysis and confirmed a serious carbon deposition issue for the NiMgO. Ni^0 was observed on the patterns of all the spent catalysts, expect for the 6%Co/NiMgO. In previous work (Luo et al., 2016), the Ni^0 was not identified on the spent catalysts surface. It was caused by the strong bonding force of MgO matrix and the lower reduction temperature (600 °C). However, in this study, the reduction temperature and reforming temperature were both at 700 °C, at which Ni^{2+} ions in the subsurface layers of the MgO lattice was reduced after 30 h reaction (Wang et al., 2009). Furthermore, in the H_2-TPR results, the main reduction peaks of most catalysts started at a temperature around 700 °C. On the other hand, no Ni^0 was found existed on 6%Co/NiMgO during the XRD analysis also suggested the strong affinity of Ni and Co. Compared the Co/NiMgO catalysts with different Co loadings in Fig. A4 (B), 2%Co/NiMgO was the only catalyst showing the presence of Ni^0. The interactions

between Ni and Co were enhanced by the increase in Co loading, in which the reduction temperature of Ni^{2+} ions increased simultaneously. The other difference between the fresh and used catalysts was that the diffraction peak of lanthana species (La_2O_3) on the used 6%La/NiMgO catalyst was weakened. It could be associated with the dissolution of La_2O_3 into MgO matrix. This incorporation could improve the mobility of the lattice oxygen for burning of carbon deposited on the surface (Chen et al., 1998). In addition, in Fig. 5.9 (B), small variations were found on the spent 6%La/NiMgO at the 2θ range of 45-55 °, while the diffraction pattern of both the fresh and reduced 6%La/NiMgO was relatively flat at that 2θ range and the diffraction of La_2O_3 near 48 ° disappeared. These variations confirm the existence of $La_2O_2CO_3$ with relatively content in the catalyst system (Sutthiumporn and Kawi, 2011).
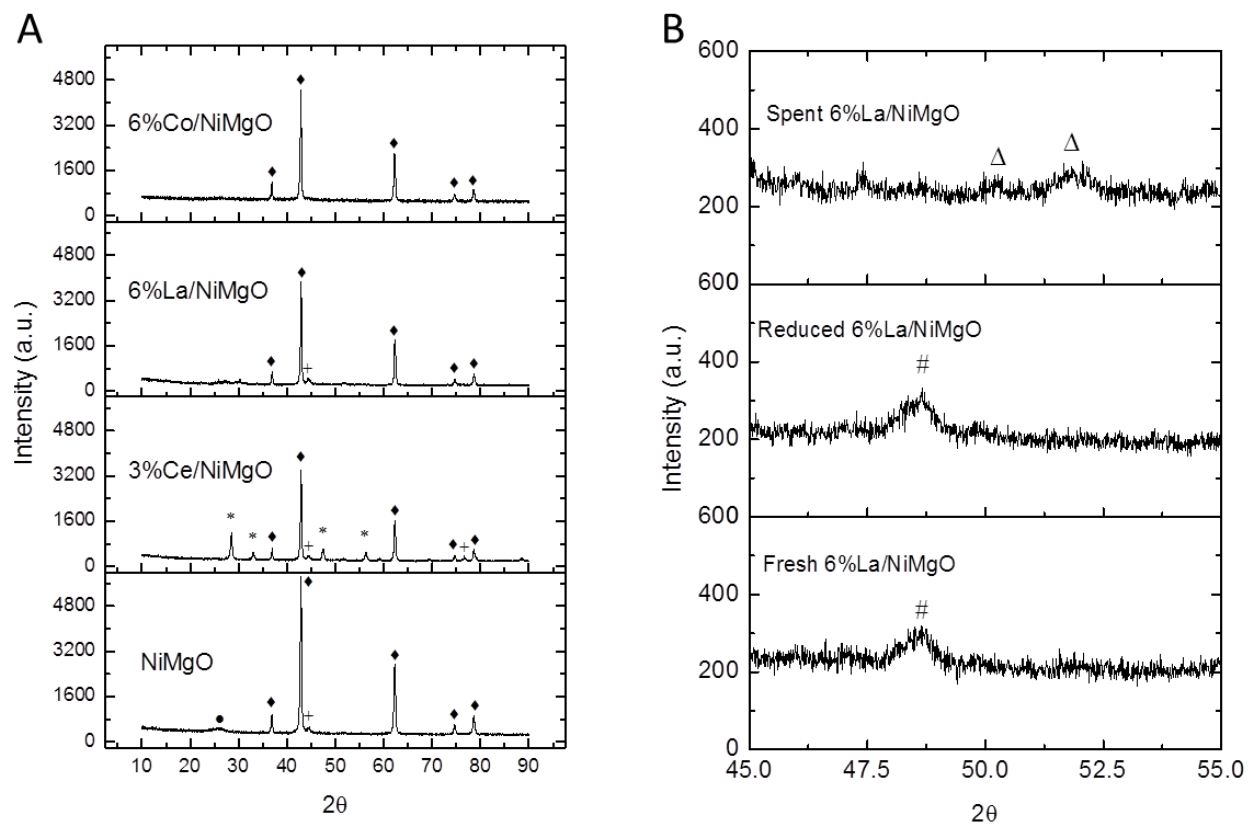
Fig. 5.9 X-ray diffraction patterns of spent catalysts after 30 h reaction at 700 ℃, (◆): NiO or MgO, (∗): CeO₂, (#): La₂O₃, (+): Ni⁰, (●): Carbon, (Δ): La₂O₂CO₃.

5.6.2 TEM analysis

TEM (Fig. 5.10) analysis showed a similar morphology of these four spent catalysts, except the 6%Co/NiMgO. The platelet size of 6%Co/NiMgO was obviously larger than the other three catalysts. This platelet agglomeration could occur during the calcination process and reaction period. The main reason of this effect was the excellent mutual solubility of Co, Ni and Mg, which was also mentioned in Section 3.2. This effect consequently led to the lowest specific surface area of the fresh 6%Co/NiMgO (shown in Table 5-2). It is noteworthy that distinct Ni particle was hardly observed on the spent 6%Co/NiMgO. This indicated the non-existence of Ni^0 due to the stable affinity of Ni-O-Co. The filamentous carbons were designated by arrows in Fig. 5.10 (A), (C) and (D). The spent catalyst 3%Ce/NiMgO was the only one, which was free from graphited carbons. This is also consistent with the results of Raman spectra.
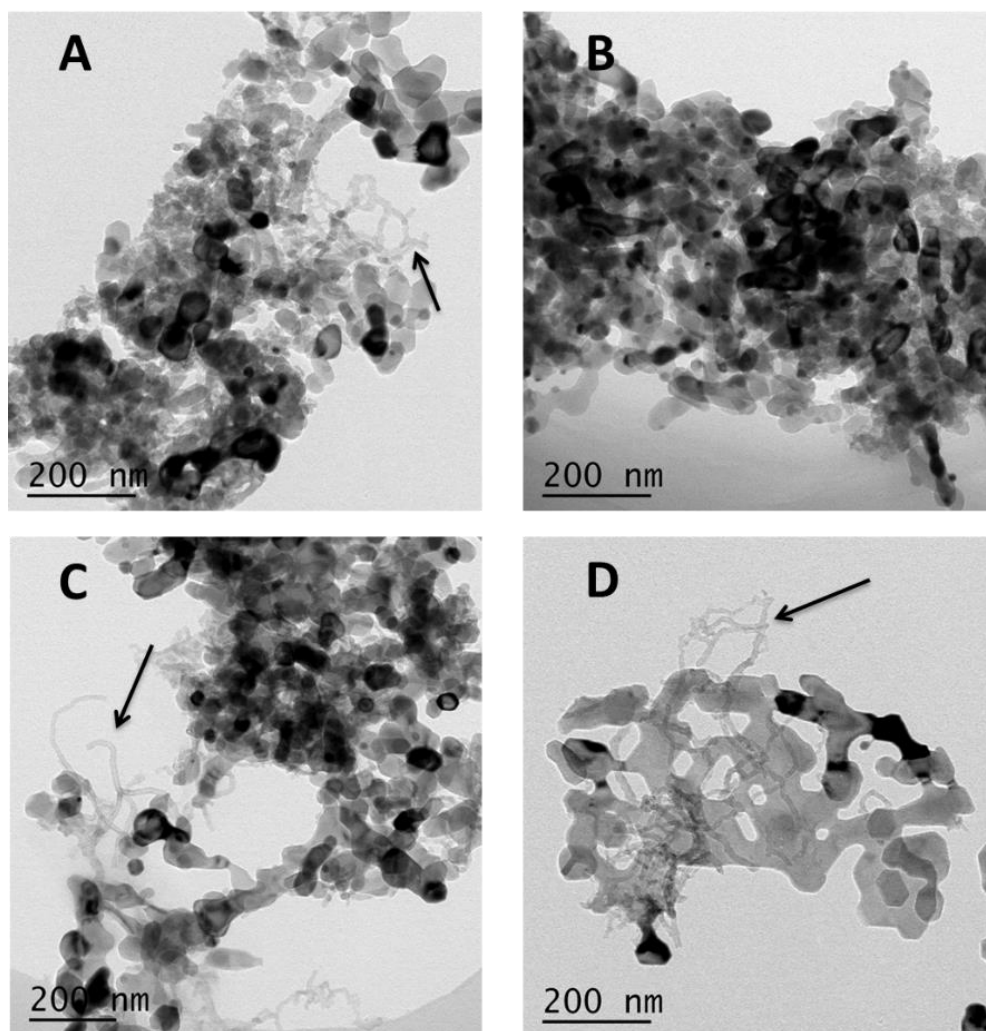
Fig. 5.10 TEM images of spent catalysts after 30 h reaction, (A) NiMgO, (B) 3%Ce/NiMgO, (C) 6%La/NiMgO, (D) 6%Co/NiMgO.

5.6.3 N_2-physiosorption analysis of the spent catalysts

N_2-physisorption analysis was employed again to test the spent catalysts after 30 h reaction (shown in Table 5-5). The surface area of fresh catalysts were in the region of 50 ± 5 m^2/g, except the 4%Co/NiMgO and 6%Co/NiMgO catalysts. From this result, you could deduce that the addition of Ce and La would not damage the

morphology of the Ni_xMg_yO solid solution, but the addition of Co in high loading weight (> 2wt%) would cover porous structures on the catalyst surface.

Normally, the specific surface area and pore volume of the spent catalysts decrease compared with those of fresh catalyst. This could be linked to carbon deposition blockage and surface metal restructure after the reduction and reforming test. However, the surface area of some spent catalysts increased compared with their fresh states, for example NiMgO, 1%Ce/NiMgO, 4%Co/NiMgO and 6%Co/NiMgO. Based on TGA analysis and BET data, it was believed that the formation of considerable amount of porous carbon structure (carbon deposition > 7wt%) on the surface of these catalysts was the primary reason of increments of surface area and pore volume. The highly ordered carbon structure was transformed from the accumulated disordered carbon (Forzatti and Lietti, 1999). Therefore, 7wt% of carbon deposition weight could be considered as a boundary to estimate whether there is a certain amount of highly ordered carbon formed on the catalyst.

Table 5-5 Surface morphology of the catalysts

catalysts	Surface area (m^2/g)	Pore volume (cm^3/g)	Micropore volume (cm^3/g)	Pore size (nm)
NiMgO				
Fresh NiMgO	56	0.28	0.0059	20
Used NiMgO	138	0.47	0.0090	14
Ce-modified NiMgO				
Fresh 1%Ce/NiMgO	47	0.23	0.0049	19
Used 1%Ce/NiMgO	63	0.21	0.0043	14
Fresh 2%Ce/NiMgO	49	0.38	0.0042	31
Used 2%Ce/NiMgO	33	0.10	0.0024	12
Fresh 3%Ce/NiMgO	52	0.29	0.0045	22
Used 3%Ce/NiMgO	37	0.12	0.0024	13
Fresh 4%Ce/NiMgO	49	0.31	0.0044	25
Used 4%Ce/NiMgO	32	0.11	0.0044	14
La-modified NiMgO				
Fresh 2%La/NiMgO	52	0.37	0.0043	29
Used 2%La/NiMgO	29	0.12	0.0025	16
Fresh 4%La/NiMgO	49	0.29	0.0041	24
Used 4%La/NiMgO	26	0.07	0.0018	10
Fresh 6%La/NiMgO	50	0.26	0.0046	21
Used 6%La/NiMgO	25	0.08	0.0020	12
Co-modified NiMgO				
Fresh 2%Co/NiMgO	46	0.20	0.0049	18

Table 5-5 continue

catalysts	Surface area (m^2/g)	Pore volume (cm^3/g)	Micropore volume (cm^3/g)	Pore size (nm)
Used 2%Co/NiMgO	32	0.11	0.0021	14
Fresh 4%Co/NiMgO	30	0.11	0.0053	15
Used 4%Co/NiMgO	41	0.18	0.0046	17
Fresh 6%Co/NiMgO	30	0.11	0.0026	15
Used 6%Co/NiMgO	68	0.30	0.0040	18

5.6.4 XPS study

The surface Ni oxidation states were investigated by using XPS. Both reduced and spent catalysts were analysed to compare the initial and final state of the catalysts. The Ni 2p spectra and deconvolution details are illustrated in Fig. 5.11, Table A-2 and Table A-3. The spectra of Ni 2p of 6%La/NiMgO was not evident due to the overlapping of Ni 2p and La 3d. The binding energies of Ni^0, Ni^{2+} and Ni^{3+} in Ni_xMg_yO solid solution are ca. 853.0 eV, 854.8 eV and 856.7 eV (Yu et al., 2014). For the reduced catalysts, no Ni^0 was observed for all the three catalysts. This has already been confirmed by the XRD patterns of the reduced catalysts. The reduction for 2 h at 700 ℃ still could not overcome the bonding forces of Ni-O-MgO sites. For the spent catalysts, NiMgO exhibited a substantial attenuation on the intensity of the Ni 2p, compared with 3%Ce/NiMgO. The reason could be firstly, the catalyst surface endured severe deposited carbon, which formed a carbon layer and

covered the surface Ni ions; and on the other hand, the surface restructuring of NiMgO during the reforming test could also embed the surface Ni into MgO matrix. Ni^0 was observed on both spent NiMgO and spent 3%Ce/NiMgO, which was consistent with the XRD result. However, in Table A-2, the different Ni^0 and Ni^{2+} surface atomic compositions of both spent catalysts also demonstrated that the chemical environment of surface Ni changed after the doping of Ce. For the spent 3Ce%/NiMgO, 12.4 mol% of Ni^0 was on the catalyst surface, while this figure was 19.1 mol% for the spent NiMgO. However, if took the total number of Ni sites into account, the spent 3%Ce/NiMgO (5.38wt% total Ni on the surface) had more Ni^0 sites than the spent NiMgO (2.85wt% total Ni on the surface). The larger number of the Ni^0 sites on the spent 3%Ce/NiMgO should be attributed to its good carbon resistance ability and the strong metal-support interactions (SMSI) between NiO and CeO_2. The surface CeO_2 could be partially reduced under reducing atmosphere. In the meantime, the spare electrons on Ce^{3+} can migrate to the neighbouring Ni^{2+} ions. These abundant electrons can reduce the oxidation state of the Ni^{2+} ions (Kim et al., 2015). The presence of Ce^{3+} was also confirmed via Ce 3d spectra in Fig. 5.12 (A) (Men et al., 2004).
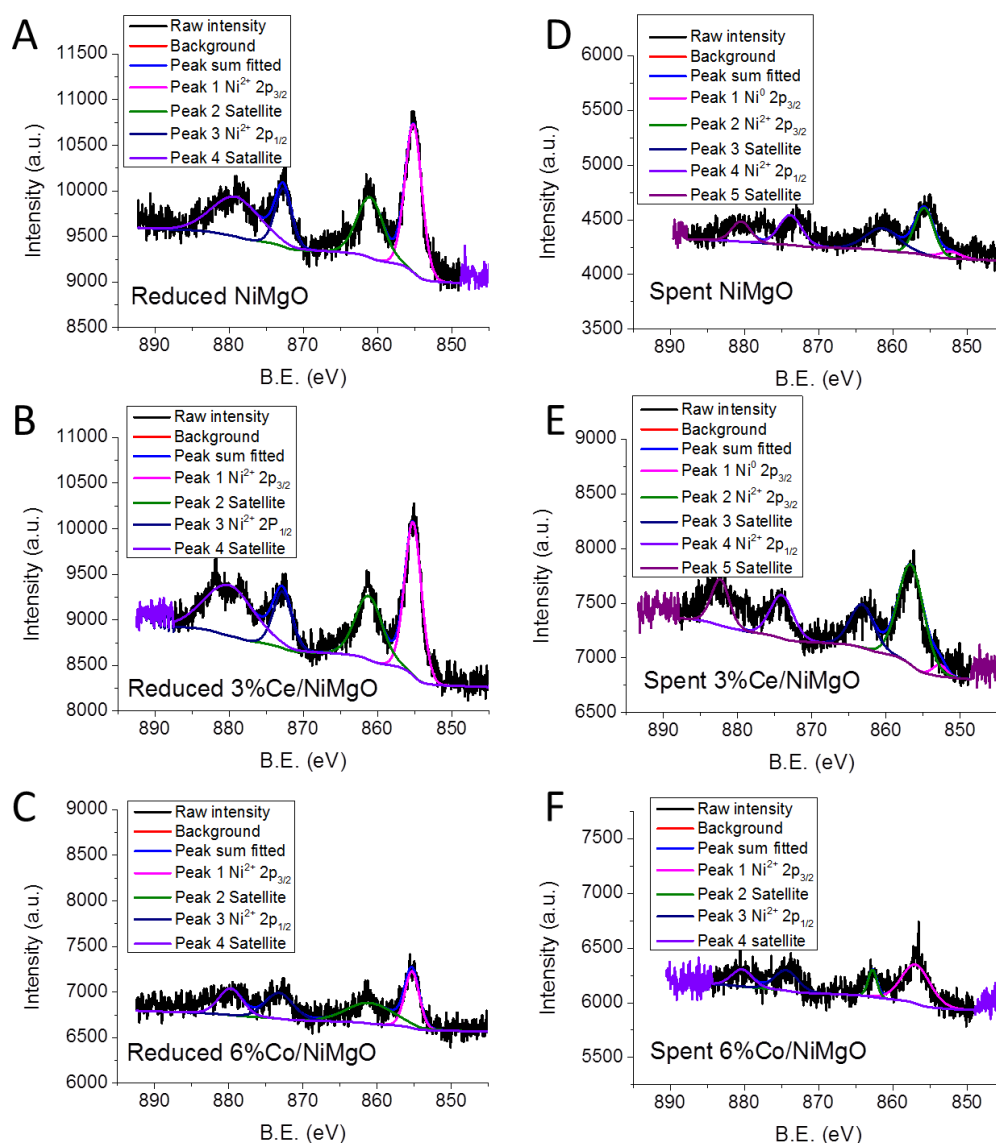
Fig. 5.11 Ni 2p spectra of both reduced and spent catalysts after 30 h reaction.

The Ni 2p envelop of the spent 6%Co/NiMgO was similar with the pristine one. The Ni^0 was not observed even after 30 h reforming test. It was due to that Co created a high affinity towards surface Ni^{2+} ions, which also had been proved by both XRD and H$_2$-TPR results. In Fig. 5.12 (C), the XPS pattern of Co 2p$_{3/2}$ was also discerned from 775 to 790 eV. The peak of spent catalyst shifted to

higher binding energy, which indicated the partially transition of oxidation state of cobalt from Co_3O_4 to low valence cobalt compounds like CoO and $Co(OH)_2$ (Tan et al., 1991, Jacobs et al., 2004). The existence of $Co(OH)_2$ might be linked to the strong affinity of Co towards $-OH$ species (Jones et al., 2008). The further reduction to Co^0 (777.3 eV) was not evident from XPS analysis. The support material MgO could act as a hindering agent for Co^{2+} reduction (Sexton et al., 1986). For the spent 6%La/NiMgO catalyst, the binding energies of La^{3+} doublet peaks shifted from 834/837.6 eV to 835.5/839.2 eV, as shown in Fig. 5.12 (B). This finding further confirmed with XRD results, which showed that the carbonate phase of $La_2O_2CO_3$ formed from the transition of La_2O_3 due to adsorption of CO_2 (Gu et al., 2015).
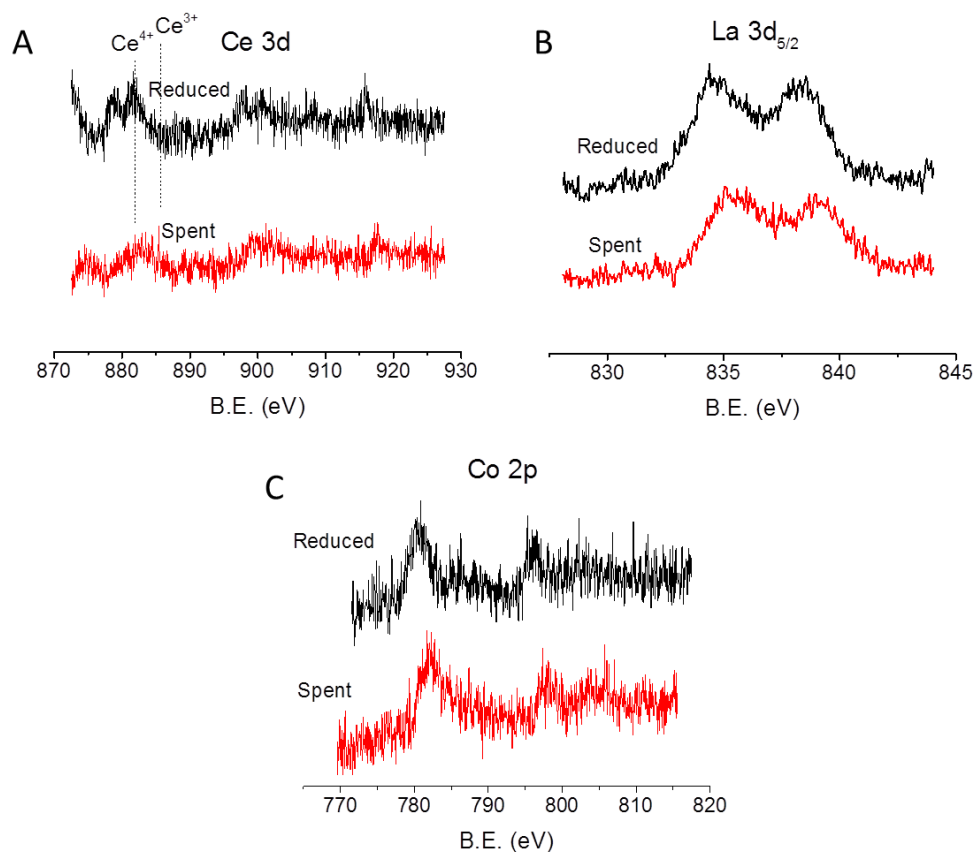
Fig. 5.12 XPS patterns of promoted elements in both reduced and spent catalysts.

5.7 Summary

In this research, it was found that all three promoter elements, i.e., Ce, La and Co, improved the performance of Ni_xMg_yO solid solution in SRE. The promotion effects include increasing of hydrogen yields, mitigation of carbon deposition issue and extension of the catalyst durability. For the hydrogen enrichment, it is believed that enhancement of WGSR played a dominant role. It is also particularly true for the La-containing catalysts where a dramatic promotion on hydrogen yield was monitored at low temperature condition (at

500 ℃). In the long-term tests with severe conditions, the 3%Ce/NiMgO and 2%Co/NiMgO catalysts showed stable hydrogen yields above 80mol%, which are already acceptable for the application of hydrogen production from SRE.

Furthermore, these modified catalysts need to be continually tested in steam reforming of other bio-oil model compounds, i.e. acetic acid and phenol, to deliver a more comprehensive understanding of their performance in steam reforming of bio-oil.

Chapter 6. Steam reforming of model bio-oil

In this chapter, the modified Ni_xMg_yO solid solution catalysts were tested in the steam reforming of phenol and acetic acid (HAc). The catalytic performance of each catalyst was evaluated based on the results of steam reforming of ethanol, phenol and HAc. Besides the catalytic activity, the ability of carbon resistance was also evaluated as a crucial factor via TGA analysis. The catalysts 1%Ce/NiMgO, 2%La/NiMgO and 2%Co/NiMgO were concluded as the best catalysts in each modification group and subsequently tested in the steam reforming of a model bio-oil. The model bio-oil was synthesized based on the elemental composition of a bio-oil derived from rice husk (Lan et al., 2010). The durability tests were carried out at 800 ℃ for 100 h.

6.1 Steam reforming of phenol

Apart from the alcohols, aromatic compounds are also amongst the main constituents of biomass gasification products such as the phenolic species, which account for up to 5wt% (Polychronopoulou et al., 2004). Steam reforming of phenol has not been widely studied compared to that of ethanol, HAc and methanol. That being said, the mechanisms of phenol decomposition over nickel surface has already been proposed by previous studies whereby the dissociation of the O-H bond is identified as the first step of the

reaction (Russell et al., 1995).The following mechanistic routes could be illustrated in two ways (Fig. 6.1): (i) open ring with the C=C bond splitting in positions 1 and 6 to form C_xH_y species; (ii) form benzene via scission of C-O bond followed by further decomposition to form C_xH_y, H_2 and CO as main products.
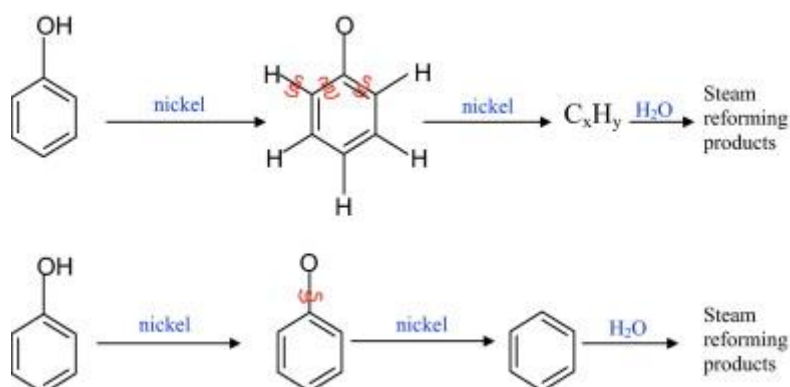
Fig. 6.1 Mechanism of phenol decomposition over nickel surface, reprint from Güell et al. (Matas Güell et al., 2011).

6.1.1 Methodology

The catalysts used in this section are identical with those used in the study of Chapter 5 (steam reforming of ethanol). There are 11 different types of catalyst, namely one unmodified NiMgO catalyst, four X%Ce/NiMgO catalysts (X = 1, 2, 3 and 4), three X%La/NiMgO catalysts (X= 2, 4 and 6) and three X%Co/NiMgO catalysts (X= 2, 4 and 6). The characterization focused on TGA test which can determine the amounts of deposited carbon on spent catalysts. The procedure of TGA experiment has been described previously in Section 3.3.7.

The only difference in this experiment was the higher operating temperature ranging from 600-900 ℃ whilst the stability tests were carried out at 800 ℃ for 30 h. This was based on the fact that higher energy would be required for the dissociation of C=C bond in benzene ring as compared with the decomposition of ethanol and HAc. The steam to carbon ratio applied was also adjusted to 12 due to the low solubility of phenol in water at room temperature. Consequently, the inflow rate of phenol was relatively low (ca. 0.060 ml/min) if the total mixture inflow rate was fixed at 1 ml/min. Therefore, the catalyst loading weight was reduced from 1 g to 0.5 g to keep a high GHSV of 143,000 ml/g$_{cat}$·h. The effluent gas components were measured via the GC monitoring. The yield of hydrogen gas was calculated according to the stoichiometric reaction of phenol steam reforming i.e. $C_6H_5OH + 11H_2O \rightarrow 6CO_2 + 14H_2$:

$$H_2 \text{ yield (mol\%)} = \frac{\text{moles of } H_2 \text{ produced}}{\text{moles of inlet phenol} \times 14} \cdot 100\% \qquad \text{(eq 6.1)}$$

Phenol conversion (X_{phenol}) was defined based on carbon balance:

$$X_{phenol} \text{ (mol\%)} = \frac{\text{a sum of moles of converted carbon in outflow}}{\text{moles of input phenol} \times 6} \cdot 100\%$$

(eq 6.2)

The yields of carbonaceous gases, such as CO_2, CO and CH_4, were calculated as:

$$\text{Carbonaceous gas yield (mol\%)} = \frac{\text{moles of gas produced}}{\text{moles of input phenol} \times 6} \cdot 100\%$$

(eq 6.3)

6.1.2 Results and discussion

Table 6-1 shows the performance of the catalysts in steam reforming of phenol. For the initial hydrogen yield at 800 ℃, the unmodified NiMgO showed the highest productivity of 89.1mol% compared with all the Ce- and La-modified catalysts. This is due to the fact that the NiMgO catalyst had more active sites on its surface than the modified catalysts. The addition of Ce and La could partially cover the surface nickel particles. On the other hand, the Co-modified catalysts, 4%Co/NiMgO and 6%Co/NiMgO, showed hydrogen yields of 93.5mol% and 92.0mol%, respectively. Such high production of hydrogen could be attributed to the difference of chemical nature between Co and rare earth elements where the surface Co could also act as an active site like Ni.

On the aspect of catalyst durability, the hydrogen yield when using the NiMgO catalyst decreased from 89.1mol% to 73.7mol% after 30 h at 800 ℃ while the overall conversion of phenol did not show any significant changes. The only distinct variation was the selectivity of carbonaceous gases where the yield of CO_2 decreased by 33.8mol% whilst the yield of CO increased by 32.0mol%. These two values suggest that a part of CO did not transform into CO_2. It also suggests that the WGSR was inhibited during the reforming process.

According to the mechanism of WGSR, dissociated H_2O adsorbs onto the active metal and becomes H_2 and metal oxide, meanwhile, CO acts as a deoxidizer to reduce the active metal oxide and produce CO_2 (Rhodes et al., 1995). Therefore, it can be deduced that the adsorption ability for CO and H_2O over the surface Ni active sites decreased as the reforming proceeded. This could be caused by the blockage effects of carbon deposition or other adsorbed molecules such as CO_2, CH_x species or ethylene. As for the Ce- and La-modified catalysts, the hydrogen yields were still high after 30 h reactions. This can be ascribed to the outstanding oxygen storage and release capability of Ce and La (Mattos et al., 2012, Cai et al., 2008a). The earlier paper also proposed a mechanism that ceria could instead of active metal to oxidize adsorbed CO and capture oxygen from water (Bunluesin et al., 1998). For the Co-modified catalysts, 2%Co/NiMgO and 4%Co/NiMgO showed the highest hydrogen yields of 87.7mol% and 86.0mol%, respectively. One reasonable explanation was their high conversions of phenol, both of which were approaching to 100mol%. Furthermore, the WGSR was still enhanced by these two catalysts.

Table 6-1 Phenol steam reforming results.

Catalyst	T(℃)	H$_2$ yield (mol%)	X$_{phenol}$ (mol%)	CO$_2$ yield (mol%)	CH$_4$ yield (mol%)	CO yield (mol%)
NiMgO	*600 (2 h)*	6.4	5.9	4.0	0.0	1.9
	700 (2 h)	39.0	45.1	25.2	0.2	19.7
	800 (2 h)	89.1	96.0	79.5	0.2	16.3
	900 (2 h)	86.4	95.5	75.2	0.2	20.0
	800(30 h)	73.7	94.1	45.7	0.1	48.3
1%Ce/NiMgO	*600 (2 h)*	45.5	48.5	37.6	0.1	10.9
	700 (2 h)	89.0	95.1	83.2	0.0	11.9
	800 (2 h)	84.3	91.1	76.1	0.1	14.9
	900 (2 h)	84.5	92.3	73.1	0.1	19.1
	800(30 h)	85.3	94.2	75.7	0.1	18.4
2%Ce/NiMgO	*600 (2 h)*	25.6	28.8	17.0	0.1	11.8
	700 (2 h)	77.1	92.4	55.5	0.0	36.8
	800 (2 h)	85.4	92.1	76.5	0.0	15.6
	900 (2 h)	85.3	94.1	75.4	0.0	18.7
	800(30 h)	83.0	93.3	71.8	0.1	21.4
3%Ce/NiMgO	*600 (2 h)*	28.3	30.4	21.5	0.0	8.9
	700 (2 h)	82.6	90.5	74.8	0.0	15.7
	800 (2 h)	76.4	82.0	68.6	0.0	13.4
	900 (2 h)	83.0	91.2	72.4	0.0	18.8

Table 6-1 continue

Catalyst	T(℃)	H_2 yield (mol%)	X_{phenol} (mol%)	CO_2 yield (mol%)	CH_4 yield (mol%)	CO yield (mol%)
	800(30 h)	80.0	95.0	62.5	0.1	32.4
4%Ce/NiMgO	*600 (2 h)*	25.0	26.8	18.1	0.0	8.7
	700 (2 h)	79.3	90.3	62.7	0.0	27.5
	800 (2 h)	83.3	89.1	74.8	0.0	14.3
	900 (2 h)	86.4	95.1	75.9	0.0	19.2
	800(30 h)	81.5	90.1	72.7	0.1	17.2
2%La/NiMgO	*600 (2 h)*	25.8	29.3	17.9	0.0	11.5
	700 (2 h)	77.3	91.7	57.3	0.0	34.4
	800 (2 h)	84.2	91.9	73.8	0.1	18
	900 (2 h)	83.3	92.6	73.8	0.0	18.7
	800(30 h)	85.2	94.0	77.2	0.1	16.7
4%La/NiMgO	*600 (2 h)*	44.0	51.1	30.9	0.0	20.2
	700 (2 h)	78.6	87.9	64.8	0.0	23.1
	800 (2 h)	82.9	90.2	74.7	0.1	15.5
	900 (2 h)	83.3	92.5	73.8	0.1	18.6
	800(30 h)	84.8	92.7	75.5	0.1	17.2
6%La/NiMgO	*600 (2 h)*	25.6	29.2	16.9	0.0	12.3
	700 (2 h)	82.5	91.4	73.4	0.0	18.0
	800 (2 h)	81.8	89.2	74.2	0.1	14.9
	900 (2 h)	82.5	90.8	72.2	0.0	18.7

Table 6-1 continue

Catalyst	T(℃)	H_2 yield (mol%)	X_{phenol} (mol%)	CO_2 yield (mol%)	CH_4 yield (mol%)	CO yield (mol%)
	800(30 h)	84.3	93.9	72.5	0.3	21.1
2%Co/NiMgO	*600 (2 h)*	6.0	7.7	2.4	0.0	5.3
	700 (2 h)	29.0	43.7	7.3	0.0	36.4
	800 (2 h)	74.8	99.5	41.4	0.2	58.0
	900 (2 h)	90.9	100.0	80.7	0.1	19.2
	800(30 h)	87.7	98.6	74.5	0.1	24.0
4%Co/NiMgO	*600 (2 h)*	14.2	16.6	8.6	0.0	7.9
	700 (2 h)	74.1	94.8	47.8	0.1	47.0
	800 (2 h)	93.5	100.0	84.5	0.0	15.5
	900 (2 h)	92.6	100.0	80.3	0.3	19.4
	800(30 h)	86.0	99.7	68.1	0.1	31.6
6%Co/NiMgO	*600 (2 h)*	11.1	11.8	7.8	0.0	4.0
	700 (2 h)	63.6	75.8	45.3	0.0	30.5
	800 (2 h)	92.0	99.6	82.4	0.1	17.1
	900 (2 h)	91.0	100.0	79.7	0.1	20.2
	800(30 h)	73.8	100.0	38.1	0.1	61.8

Fig. 6.2 shows the TG residual mass of the spent catalysts after 30 h in steam reforming of phenol. This result is not similar with the previous data collected from steam reforming of ethanol and HAc where most of the modified catalysts encountered serious carbon

deposition with residual mass below 70wt%. The 4%Ce/NiMgO, 2%La/NiMgO and 4%La/NiMgO catalysts were the only three catalysts which retained their strong anti-carbon resistance. It has been observed that large quantity of carbon was deposited which could be due to the low O/C ratio or H/C ratio of phenol molecule. However, based on the catalyst activities in Table 6-1, it can also be concluded that the performance of catalysts on hydrogen production and phenol conversion was not influenced by the carbon deposition.
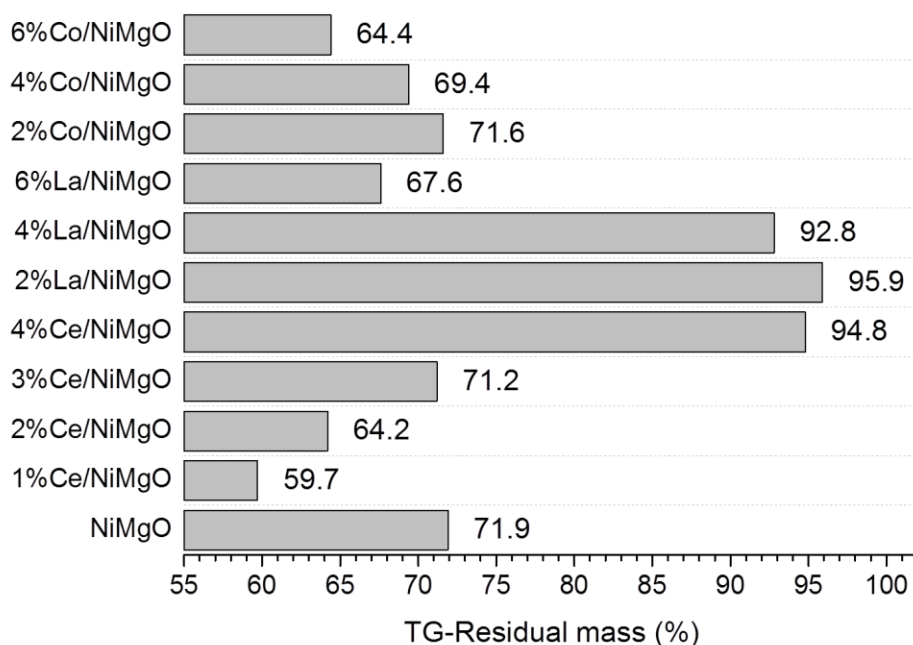
Fig. 6.2 TG-residual mass of the spent catalysts after 30 h steam reforming of phenol.

6.2 Steam reforming of acetic acid

Acetic acid is one of the major carboxylic acid compounds in bio-oil with a concentration up to 10-12wt% (Oasmaa and Meier, 2005, Branca et al., 2003, Vagia and Lemonidou, 2007, Rioche et al., 2005). The hydrogen production from catalytic steam reforming of HAc has been demonstrated with hydrogen yields between 70-80mol% by a considerable number of publications (Wang et al., 1996, Takanabe et al., 2006, Li et al., 2012, Nabgan et al., 2016, Takanabe et al., 2004). The overall stoichiometry reaction is the combination of steam reforming of HAc and water-gas shift reaction (WGSR):

$$CH_3COOH + 2H_2O \rightarrow 2CO_2 + 4H_2 \quad (R\ 6.1)$$
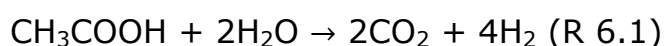
The mechanism of steam reforming of HAc has already been published elsewhere (Trane et al., 2012). The dissociative adsorption of HAc over catalyst surface was identified as the first step which involves with the decomposition of HAc into acetate or acyl species:

$$CH_3COOH + 2* \rightarrow CH_3COO* + H* \quad (R\ 6.2)$$

$$CH_3COOH + 2* \rightarrow CH_3CO* + OH* \quad (R\ 6.3)$$
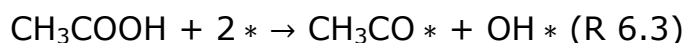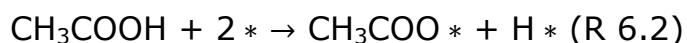
The species of acetate and acyl would further decompose into CH_x-species ($X \leq 4$), CO_2 and CO. Earlier thermodynamic studies indicated that both the operating temperature and the ratio of

steam to HAc are two principle factors which could significantly affect hydrogen production and coke formation (Vagia and Lemonidou, 2007). The rate of hydrogen production increases gradually with temperature in the region of 400-900 K before dropping slightly with further increase of temperature to 1300 K. This reversed effect at high temperature region is attributed to the equilibrium of WGSR. The equilibrium study also demonstrated the significant impact of steam to HAc ratio as determinant over the solid carbon selectivity. However, higher rates of steam input will lower the overall efficiency of the reforming process. Therefore, in this study, the steam to carbon ratio of 6 was used as the common ratio applied in steam reforming of HAc. The Ni_xMg_yO solid solutions modified with Ce, La and Co were employed and tested under a temperature range near 900 K.

6.2.1 Methodology

In this study, the catalysts used and the operating procedures were the same as those employed in steam reforming of HAc. The initial performance of catalysts at each temperature was measured at 2 h after the start of the experiment.

In each test, approximately 1.0 g of catalyst was mixed with 15 g of quartz sand and then loaded into a fixed bed reactor. The initial catalytic performance of catalysts was measured 2 h after the start of the experiment at four different temperatures, i.e., 500 ℃, 600 ℃,

700 ℃ and 800 ℃. The subsequent durability tests (30 h) were operated at 700 ℃. The operating temperature was chosen based on the results of initial catalytic performance at different temperatures. The feeding rate of liquid mixture was fixed at 1 ml/min with a steam to carbon ratio of 6 (GHSV = 64,000 ml/g$_{cat}$·h). The gas components were measured with the same off-line GC used in all previous experiments.

In this study, the yield of hydrogen gas was defined according to the stoichiometric reaction described previously in R 6.1 and used the following equations:

$$\text{H}_2 \text{ yield (mol\%)} = \frac{\text{moles of H}_2 \text{ produced}}{\text{moles of inlet acetic acid} \times 4} \cdot 100\% \qquad \text{(eq 6.4)}$$

The conversion of acetic acid ($X_{acetic\ acid}$) was defined based on carbon balance:

$$X_{acetic\ acid} \text{ (mol\%)} = \frac{\text{a sum of moles of converted carbon in outflow}}{\text{moles of input acetic acid} \times 2} \cdot 100\%$$

(eq 6.5)

The yield of carbonaceous gases, such as CO_2, CO and CH_4, was calculated as:

$$\text{Carbonaceous gas yield (mol\%)} = \frac{\text{moles of gas produced}}{\text{moles of input acetic acid} \times 2} \cdot 100\%$$

(eq 6.6)

6.2.2 Results and discussion

The conversion of HAc and the yield of hydrogen and carbonaceous gases are summarized in Table 6-2. Apparent from the table, almost all of the catalysts demonstrated higher hydrogen yield at 700 ℃ rather than the expected 800 ℃. The reason for this phenomenon is because that WGSR would be restrained at high temperature, as previously discussed. After 30 h of reaction, all of the modified catalysts exhibited higher hydrogen productivities than the unmodified NiMgO catalyst, except for 4%Co/NiMgO and 6%Co/NiMgO. However, several catalysts, such as 1%Ce/NiMgO, 4%Ce/NiMgO and 2%La/NiMgO, showed an increment after the 30 h reaction due to the slow reduction of nickel particles during reforming process. Such observation has been previously verified in Chapter 5. The unmodified NiMgO catalyst, however, showed a deactivation of hydrogen yield from 80.4mol% to 61.9mol% after 30 h. Consistent with the unmodified NiMgO, both the 4%Co/NiMgO and 6%Co/NiMgO catalysts suffered even more serious deactivation, especially the 6%Co/NiMgO catalyst, which only resulted in a hydrogen yield of 10.6mol% after 30 h. Hence, Co could promote the NiMgO catalyst, however, high doping weight of Co (> 2%) would result in fast deactivation during the steam reforming of HAc. It is also worth mentioning that the addition of La could dramatically boost hydrogen yield under low temperature conditions. The initial hydrogen yield when using 2%La/NiMgO was a staggering 79.7mol%

at 500 ℃, while the hydrogen yield of the unmodified NiMgO was only 13.3mol%. This finding was also consistent with the result obtained in the study of ethanol steam reforming. The HAc conversion data showed similar trend with the hydrogen yield data. Apparent from the combination of HAc conversion and carbonaceous gases yields analysis, the enhancement of hydrogen production over modified catalysts suggests that the improvement of WGSR led to higher CO_2 yield and lower CO yield.

Table 6-2 Acetic acid steam reforming results.

Catalyst	T(℃)	H_2 yield (mol%)	$X_{acetic\ acid}$ (mol%)	CO_2 yield (mol%)	CH_4 yield (mol%)	CO yield (mol%)
NiMgO	500 (2 h)	13.3	15.6	13.4	0.5	1.7
	600 (2 h)	55.5	67.8	51.9	1.8	14.1
	700 (2 h)	80.4	94.5	71.1	2.0	21.4
	800 (2 h)	60.0	99.9	63.0	15.1	21.8
	700(30 h)	61.9	81.7	44.3	2.2	35.2
1%Ce/NiMgO	500 (2 h)	29.9	35.3	32.7	0.7	2.0
	600 (2 h)	73.7	81.4	71.0	0.7	9.7
	700 (2 h)	79.1	86.4	71.1	0.2	15.1
	800 (2 h)	76.3	86.9	66.6	1.1	19.2
	700(30 h)	86.2	99.5	75.6	1.0	22.9
2%Ce/NiMgO	500 (2 h)	39.1	48.3	43.9	1.5	2.9

Table 6-2 continue

Catalyst	T(℃)	H_2 yield (mol%)	$X_{acetic\ acid}$ (mol%)	CO_2 yield (mol%)	CH_4 yield (mol%)	CO yield (mol%)
	600 (2 h)	79.4	86.2	75.3	0.5	10.5
	700 (2 h)	89.3	98.0	80.8	0.1	17.2
	800 (2 h)	78.9	89.3	68.8	0.5	20.0
	700(30 h)	74.7	84.0	66.5	0.5	17.0
3%Ce/NiMgO	*500 (2 h)*	36.6	47.2	42.6	1.5	3.1
	600 (2 h)	79.6	85.9	75.3	0.5	10.1
	700 (2 h)	76.5	84.0	69.2	0.1	14.7
	800 (2 h)	75.5	84.8	65.5	0.2	19.2
	700(30 h)	76.1	84.9	68.8	0.4	15.7
4%Ce/NiMgO	*500 (2 h)*	31.7	39.7	36.8	0.8	2.0
	600 (2 h)	71.5	78.0	68.6	0.6	8.8
	700 (2 h)	84.0	93.5	77.1	0.3	16.2
	800 (2 h)	78.8	90.6	69.6	1.5	19.4
	700(30 h)	85.2	97.1	76.0	1.0	20.1
2%La/NiMgO	*500 (2 h)*	79.7	91.0	75.0	1.6	14.4
	600 (2 h)	82.1	89.5	77.3	0.6	11.6
	700 (2 h)	85.5	95.5	78.5	0.6	16.3
	800 (2 h)	82.3	92.8	71.7	0.1	21.1
	700(30 h)	86.5	96.5	79.4	0.3	16.8
4%La/NiMgO	*500 (2 h)*	62.9	70.4	58.3	0.5	11.6

Table 6-2 continue

Catalyst	T(℃)	H$_2$ yield (mol%)	X$_{acetic\ acid}$ (mol%)	CO$_2$ yield (mol%)	CH$_4$ yield (mol%)	CO yield (mol%)
	600 (2 h)	77.1	87.3	73.5	1.0	12.8
	700 (2 h)	74.9	88.2	70.6	2.7	14.9
	800 (2 h)	75.5	100.0	73.9	7.5	18.6
	700(30 h)	82.3	96.0	75.1	1.7	19.2
6%La/NiMgO	*500 (2 h)*	65.6	74.2	60.1	0.7	13.4
	600 (2 h)	67.4	68.2	56.8	0.8	10.6
	700 (2 h)	81.9	94.0	75.0	2.1	16.9
	800 (2 h)	71.3	93.3	69.4	7.1	16.8
	700(30 h)	82.9	95.7	74.8	1.6	19.4
2%Co/NiMgO	*500 (2 h)*	21.5	22.7	21.0	0.4	1.3
	600 (2 h)	65.5	70.9	62.7	0.6	7.6
	700 (2 h)	87.8	98.4	80.3	0.4	17.8
	800 (2 h)	84.4	96.1	74.2	0.4	21.5
	700(30 h)	86.9	99.1	79.0	1.1	19.0
4%Co/NiMgO	*500 (2 h)*	12.8	14.8	13.4	0.2	1.1
	600 (2 h)	71.0	79.4	69.4	1.0	9.0
	700 (2 h)	87.3	97.4	80.4	0.4	16.5
	800 (2 h)	84.1	100.0	77.4	2.3	20.3
	700(30 h)	49.8	61.7	41.3	1.9	18.5
6%Co/NiMgO	*500 (2 h)*	5.0	5.8	5.0	0.1	0.7

Table 6-2 continue

Catalyst	T(℃)	H$_2$ yield (mol%)	X$_{acetic acid}$ (mol%)	CO$_2$ yield (mol%)	CH$_4$ yield (mol%)	CO yield (mol%)
	600 (2 h)	31.3	35.4	30.0	0.6	4.8
	700 (2 h)	76.8	94.2	68.0	2.0	24.1
	800 (2 h)	60.9	92.3	56.7	9.6	26.0
	700(30 h)	10.6	19.4	9.7	3.3	6.5

Fig. 6.3 shows the TG-residual mass of spent catalysts after 30 h of HAc steam reforming whilst the TG profiles are shown in Fig. A6. Apparent from the residual mass of spent catalysts, the unmodified catalyst had a residual mass of 84.4wt%, while most of the modified catalysts had residual masses above 95wt% (except for the Co-modified catalysts). The residual masses of the spent 4%Co/NiMgO and 6%Co/NiMgO catalysts were surprisingly low, i.e. 66.9wt% and 54.9wt%, respectively. Both of them were even lower than the unmodified catalysts. However, the results indicated that the addition of Ce and La could improve the anti-coking ability of the catalysts in steam reforming of HAc. The results of TG analysis are also consistent with the catalytic performance of catalysts in the steam reforming of HAc. The catalyst retained more than 95wt% of their mass whilst exhibiting stable activities during the durability tests. It was also established that small amounts of Co could decrease the carbon deposition but Co loading exceeding 2wt%

would lead to a severe issue of carbon fouling. This conclusion was reflected in the sharp deactivation of both 4%Co/NiMgO and 6%Co/NiMgO during the durability tests.

In summary, the Ce- and La-modified catalysts have shown desirable performance in steam reforming of HAc. It is worth mentioning that 1%Ce/NiMgO, 4%Ce/NiMgO and 2%La/NiMgO catalysts have all exhibited extremely high yields of hydrogen, i.e. above 85mol%, at 700 ℃ after 30 h. Their outstanding resistance to carbon deposition was confirmed by TG analysis. The low Co loading catalyst, 2%Co/NiMgO, also showed remarkable hydrogen yield of 86.9mol%, as opposed to higher loadings. It can be concluded that the Ni-Co system has great promotional effects on hydrogen production under a premise of low amounts of deposited carbon on catalyst surface.
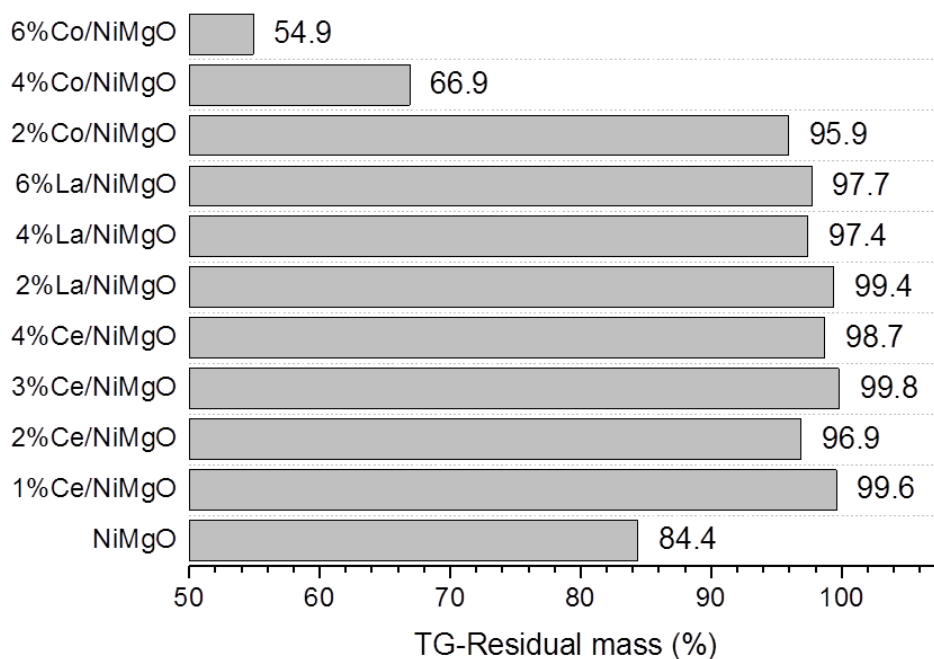
Fig. 6.3 TG-residual mass of the spent catalysts after 30 h steam reforming of acetic acid.

6.3 Steam reforming of model bio-oil

6.3.1 Preparation of model bio-oil and experiment procedure

The components of actual bio-oil derived from fast pyrolysis of biomass vary with the types of biomass and the condition of pyrolysis carried out. In order to compare between different groups of catalysts, a model bio-oil was synthesized according to the elemental contents of actual bio-oil. The referenced bio-oil was obtained via pyrolysis of rice husk. Its water-free compound was determined to be $C_{4.72}H_{7.98}O_{2.07}N_{0.12}S_{0.02}$ (Lan et al., 2010). In this

experiment, ethanol, HAc and phenol were used to simulate the actual bio-oil which consisted of alcohols, acids and aromatic species. The synthesized mixture of ethanol, HAc and phenol with a specific mixing ratio resulted in a compound of $C_{4.74}H_{8.00}O_{2.07}$. Such a compound is very similar to the actual referenced bio-oil in terms of elemental contents. N and S were excluded due to their low content, i.e. within experimental error.

As for the preparation of model bio-oil and water mixture, 50 ml of ethanol, 50 ml of HAc, 60 ml of phenol and 800 ml of water were mixed at room temperature. The synthesized mixture had a steam to carbon ratio of 5.9 (rounded up to 6). 0.5 g catalyst diluted with 8 g of silica sand was loaded in the reformer. The inflow rate of mixture was fixed at 1 ml/min and thus leading to a carbon inlet rate of 0.945 mol/g_{cat}·h. The reforming tests were carried out at 800 ℃ for 100 h. In terms of the selection of catalysts, catalysts with the best performance in steam reforming of ethanol, HAc and phenol were chosen. The ranking of catalysts in terms of performance are shown in Table 6-3. The ranking were based on hydrogen yield after 30 h of reaction, i.e. the catalyst leading to highest production scores 3, the second highest scores 2, and so on. The final score showed that 1%Ce/NiMgO, 2%La/NiMgO and 2%Co/NiMgO were the top performing catalysts and hence selected

for the subsequent steam reforming of model bio-oil. In addition, the unmodified NiMgO catalyst was also tested as reference.

Table 6-3 Evaluation of catalysts according to their performance in steam reforming of ethanol, acetic acid and phenol.

Catalysts	Ethanol	Acetic acid	Phenol	Total score
1%Ce/NiMgO	1	3	3	7
2%Ce/NiMgO	2	0	2	4
3%Ce/NiMgO	3	1	0	4
4%Ce/NiMgO	0	2	1	3
2%La/NiMgO	3	3	3	9
4%La/NiMgO	1	1	2	4
6%La/NiMgO	2	2	1	5
2%Co/NiMgO	3	3	3	9
4%Co/NiMgO	2	2	2	6
6%Co/NiMgO	1	1	1	3

6.3.2 Performance of the catalysts

Fig. 6.4 shows the performance of four catalysts in terms of bio-oil conversion and hydrogen yields for extended periods. As for the conversion of bio-oil shown in Fig. 6.4(A), the NiMgO catalyst appeared to boost the conversion rate from 85mol% to 95mol% during the first 5 h and remained above 90mol% for another 40 h. In the next 30 h, the conversion rate started to decline rapidly to 76.6mol%. This result is also consistent with the findings from the durability tests of bio-oil model compounds where the conversion rates in the presence of NiMgO catalyst did not decrease during the 30 hour test. A similar situation was found in the hydrogen yield

over the NiMgO catalysts (Fig. 6.4(B)) where the hydrogen yield climbed to 78.0mol% during the first 6 h, followed by a continuous decrease. Therefore, the results verified that the NiMgO catalyst could not maintain a stable performance in the steam reforming of bio-oil. On the other hand, the rest of the modified catalysts, i.e. all three catalysts, exhibited stable performance in bio-oil conversion within the region of 90-95mol% and hydrogen yield of above 70mol%.

The results of TG analysis are shown in Fig. 6.5. All three modified catalysts recorded very similar weight of deposited carbon within the region of 16-17wt%. Similarly, the amount of carbon deposited over the unmodified NiMgO was only slightly higher at ca. 20wt%. Therefore, the rapid decline of hydrogen yield and bio-oil conversion over the unmodified NiMgO was not entirely due to the quantity of the accumulated carbon on its surface. It has been widely accepted that the type and the location of the deposited carbon are more vital factors for catalytic deactivation rather than the quantity (San-José-Alonso et al., 2009). Previous work in Chapter 5 has observed that modified elements could alter the types of carbon species which can be verified via techniques including Raman spectra, XRD and XPS. In addition, the NiMgO catalysts may also encounter issues like metal sintering and surface restructuring at high

temperatures. However, further works are required to confirm such phenomenon.
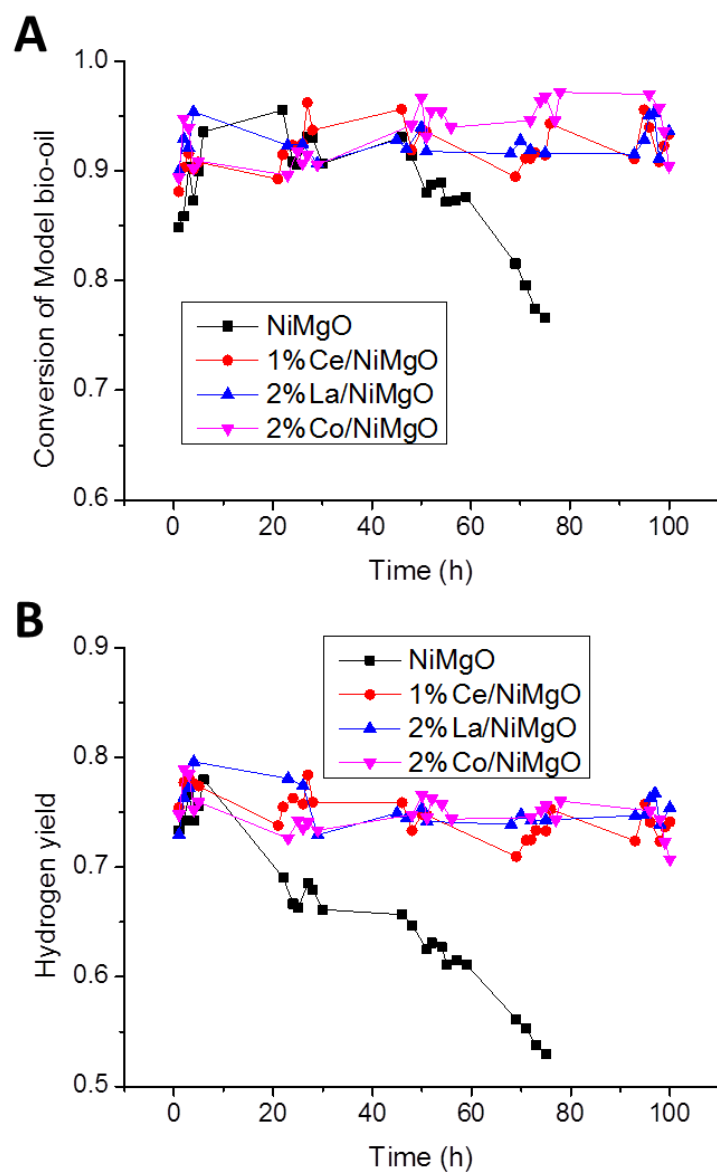
Fig. 6.4 Results of model bio-oil steam reforming, A) conversion of model bio-oil, B) hydrogen yield.
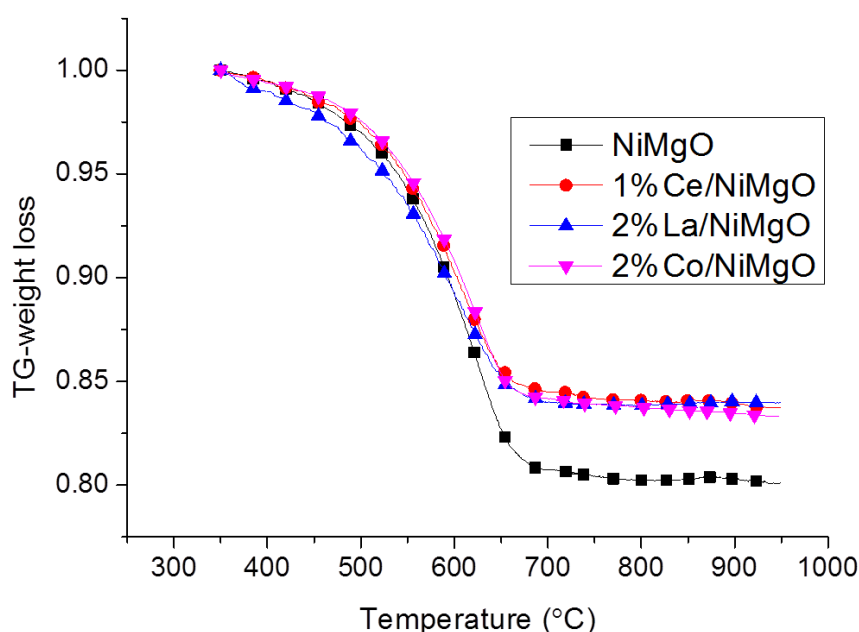
Fig. 6.5 TGA profiles for the spent catalysts after 100 h tests in steam reforming of model bio-oil (Steam/Carbon=6).

6.4 Conclusions

This chapter has continued the evaluation of modified catalysts in the reforming of two other representative compounds commonly found in bio-oil, i.e. phenol and HAc. A series of tests has been carried out at various temperature regions. The performance of catalysts in steam reforming of HAc appeared to be very similar to that of ethanol. The promotional effects of Ce, La and Co on hydrogen production due to the enhancement of WGSR were further confirmed in this chapter. In addition, it has also been verified that carbon accumulation over the catalyst surface is inhibited by promoters, except when using Co-modified catalysts that have been

loaded with Co exceeding 2wt%. In the steam reforming of phenol, most of the modified catalysts showed outstanding performance with hydrogen yield greater than 80mol% in long-term testing. The carbon resistance of the catalysts appeared to be poor as many modified catalysts had more deposited carbon compared to the unmodified NiMgO catalyst. However, this kind of deposited carbon did not have impact on the activity of reactions signally.

For the steam reforming of model bio-oil, the three selected catalysts, i.e., 1%Ce/NiMgO, 2%La/NiMgO and 2%Co/NiMgO, retained high performance during the 100 h tests and thus making them good potential catalysts. Nevertheless, longer testing, i.e. 2000 h, needs to be carried out and a more complex bio-oil compounds should be considered in the future.

Chapter 7. Conclusions and recommendations for future work

7.1 Conclusions

In this research, three catalysts, i.e., 1%Ce/NiMgO, 2%La/NiMgO and 2%Co/NiMgO, were developed for steam reforming of bio-oil in order to achieve high yield of hydrogen with enhanced stability. Initial work included research and development of Ni_xMg_yO solid solution. Various synthesis methodologies and materials were investigated to establish the optimum species of Ni_xMg_yO solid solution. It has been observed that the hydrothermally treated Ni_xMg_yO solid solution showed the highest catalytic activities regardless of steam to carbon ratio. The hydrothermal treatment also appeared to promote the removal rate of surface carbon by providing free oxygen from the dissociated CO_2 on MgO surface. This mechanism was confirmed by CO_2-TPD that the Ni_xMg_yO-hydro catalyst had more weak basic sites, which could desorb CO_2 below 400 ℃. Although the performance of hydrothermally treated NiMgO in steam reforming of methanol has been proven to be attractive, however, its quick deactivation, high CO production and serious carbon deposition during the ethanol steam reforming suggested that a further modification of the NiMgO catalyst was necessary.

Based on the experience with hydrothermal treatment, the previous catalyst was doped with promoting elements, i.e., Ce, La or Co. Each promoting element was applied at various doping ratios. All of the modified catalysts were then investigated in the steam reforming of ethanol, acetic acid (HAc) and phenol, operated at a temperature region of 500-900 ℃. The results showed the modified catalysts normally showed higher hydrogen yields after 30 h reaction. Compared the gas yields of CO_2, CO and CH_4 between the NiMgO catalyst and the modified catalysts, it showed that the modified catalysts had higher CO_2 yields but lower CO yields. This result indicated that all of the promoters had the ability to improve hydrogen production by enhancing the water-gas shift reaction (WGSR). On the other hand, the CH_4 yields of the modified catalysts were also reduced compared with that of the NiMgO catalyst. It indicated that the methanation reaction was suppressed.

There was also a valuable finding that the La-modified catalysts exhibited dramatic increases in hydrogen yield even at low temperatures (500 ℃). According to the chemical nature of La_2O_3, it would cover the suitable acid sites on catalytic surface, which would convert HAc into ethylene. Thus, the La-modified catalysts preferred to produce acetaldehyde rather than ethylene. As mentioned previously, acetaldehyde could be decomposed at much lower temperature than ethylene.

Furthermore, the carbon deposition was also restrained in the presence of promoters. The higher capability of oxygen capture and release for CeO_2 could accelerate the gasification of surface carbon deposition. The La-modified catalysts could also promote the carbon deposition removal by forming a $La_2O_2CO_3$ layer and providing CO_2.

Steam reforming of a model bio-oil was carried out for 100 h. Three catalysts were selected based on the results of steam reforming of ethanol, HAc and phenol. All three catalysts showed highly stable performance with bio-oil conversions above 90mol% and hydrogen yields in excess of 70mol%. Therefore, the modified catalysts have high potential in the area of bio-oil steam reforming. Investigations over longer tests (in excess of 100 h), poisoning effects and optimal operating conditions should be further explored.

7.2 Future work

- The promotional effects of La in Ni_xMg_yO solid solution are of great potential and thus should be investigated in the near future. As compared with other catalysts, the La-modified Ni_xMg_yO solid solution exhibits an excellent catalytic performance in steam reforming of bio-oil model compounds even at low temperature condition (at 500 ℃). The in situ FTIR analysis should be employed for the mechanism study.

- The development of novel catalysts is an ongoing work and new progress is anticipated. MgO has been proven to be a

promising material as catalyst support in this thesis. In addition, Al_2O_3 also possess favourable characteristics and should also be investigated in the near future. Its acidic surface is favourable for the adsorption of hydrocarbon. Also, its deactivation due to carbon deposition could be mitigated via the addition of alkaline elements such as K, Ca and Mg. As for the active metal, noble metals are attractive but their loading weight should be controlled at a very low level.

- The NiMgO solid solution exhibited a good durability performance with low carbon deposition in this thesis. In the future study, more types of solid solutions, such as NiCoMgO, NiCeLaMgO and NiLaCoMgO, should be developed and tested with steam reforming of bio-oil model compounds. In order to confirm the formation of solid solution, EDX analysis coupled with SEM could be applied to investigate the components of the catalysts in crystal structure. In addition, these results from EDX should also be compared with others from XRD and XPS.

- A novel integrated system combining the continuous fast pyrolysis reactor and the catalytic steam reforming reactor will be designed and built to explore the commercialization potential of hydrogen producd from biomass. A wide range of biomass materials could be tested.

Bibliography

AGUAYO, A. T., CASTAÑO, P., MIER, D., GAYUBO, A. G., OLAZAR, M. & BILBAO, J. 2011. Effect of Cofeeding Butane with Methanol on the Deactivation by Coke of a HZSM-5 Zeolite Catalyst. *Industrial & Engineering Chemistry Research,* 50**,** 9980-9988.

AL-UBAID, A. & WOLF, E. E. 1988. Steam reforming of methane on reduced non-stoichiometric nickel aluminate catalysts. *Applied Catalysis,* 40**,** 73-85.

ALDERS, D., VOOGT, F. C., HIBMA, T. & SAWATZKY, G. A. 1996. Nonlocal screening effects in 2p x-ray photoemission spectroscopy of NiO (100). *Physical Review B,* 54**,** 7716-7719.

AMPHLETT, J. C., EVANS, M. J., MANN, R. F. & WEIR, R. D. 1985. Hydrogen production by the catalytic steam reforming of methanol: Part 2: Kinetics of methanol decomposition using girdler G66B catalyst. *The Canadian Journal of Chemical Engineering,* 63**,** 605-611.

ARMOR, J. N. 1999. The multiple roles for catalysis in the production of H2. *Applied Catalysis A: General,* 176**,** 159-176.

AUPRÊTRE, F., DESCORME, C. & DUPREZ, D. 2002. Bio-ethanol catalytic steam reforming over supported metal catalysts. *Catalysis Communications,* 3**,** 263-267.

AVCı, A. K., TRIMM, D. L., AKSOYLU, A. E. & ÖNSAN, Z. İ. 2004. Hydrogen production by steam reforming of n-butane over supported Ni and Pt-Ni catalysts. *Applied Catalysis A: General,* 258**,** 235-240.

AZAD, A.-M. & DURAN, M. J. 2007. Development of ceria-supported sulfur tolerant nanocatalysts: Rh-based formulations. *Applied Catalysis A: General,* 330**,** 77-88.

BABU., N. S., SREE., R., PRASAD., P. S. S. & LINGAIAH., N. 2008. Room-Temperature Transesterification of Edible and Nonedible Oils Using a Heterogeneous Strong Basic Mg/La Catalyst. *energy & fuels,* 22**,** 1965-1971.

BALAT, M. 2008. Potential importance of hydrogen as a future solution to environmental and transportation problems. *International Journal of Hydrogen Energy,* 33**,** 4013-4029.

BALL, M. & WIETSCHEL, M. 2009. The future of hydrogen – opportunities and challenges. *International Journal of Hydrogen Energy,* 34**,** 615-627.

BARTHOLOMEW, C. H. 1982. Carbon Deposition in Steam Reforming and Methanation. *Catalysis Reviews,* 24**,** 67-112.

BARTHOLOMEW, C. H. 2001. Mechanisms of catalyst deactivation. *Applied Catalysis A: General,* 212**,** 17-60.

BARTHOLOMEW, C. H., AGRAWAL, P. K. & KATZER, J. R. 1982. Sulfur Poisoning of Metals. *In:* D.D. ELEY, H. P. & PAUL, B. W. (eds.) *Advances in Catalysis.* Academic Press.

BASAGIANNIS, A. C., PANAGIOTOPOULOU, P. & VERYKIOS, X. E. 2008. Low Temperature Steam Reforming of Ethanol Over Supported Noble Metal Catalysts. *Topics in Catalysis,* 51**,** 2-12.

BECERRA, A., DIMITRIJEWITS, M., ARCIPRETE, C. & CASTRO LUNA, A. 2001. Stable Ni/Al2O3 catalysts for methane dry reforming. *Granular Matter,* 3**,** 79-81.

BERGADÀ, O., SALAGRE, P., CESTEROS, Y., MEDINA, F. & SUEIRAS, J. 2008. Control of the Basicity in Ni–MgO Systems: Influence in the Hydrogenation of Styrene Oxide. *Catalysis Letters,* 122**,** 259-266.

BERNAL, S., BLANCO, G., CIFREDO, G., PÉREZ-OMIL, J. A., PINTADO, J. M. & RODRíGUEZ-IZQUIERDO, J. M. 1997. Reducibility of ceria–lanthana mixed oxides under temperature programmed hydrogen and inert gas flow conditions. *Journal of Alloys and Compounds,* 250**,** 449-454.

BERNARDO, C. L. & TRIMM, D. L. 1979. The kinetics of gasification of carbon deposited on nickel catalysts. *Carbon,* 17**,** 115-120.

BITTER, J. H., SESHAN, K. & LERCHER, J. A. 1999. Deactivation and Coke Accumulation during CO2/CH4Reforming over Pt Catalysts. *Journal of Catalysis,* 183**,** 336-343.

BRANCA, C., GIUDICIANNI, P. & DI BLASI, C. 2003. GC/MS Characterization of Liquids Generated from Low-Temperature Pyrolysis of Wood. *Industrial & Engineering Chemistry Research,* 42**,** 3190-3202.

BREEN, J. P. & ROSS, J. R. H. 1999. Methanol reforming for fuel-cell applications: development of zirconia-containing Cu–Zn–Al catalysts. *Catalysis Today,* 51**,** 521-533.

BRIDGWATER, A. V. 1996. Production of high grade fuels and chemicals from catalytic pyrolysis of biomass. *Catalysis Today,* 29**,** 285-295.

BRIDGWATER, A. V., MEIER, D. & RADLEIN, D. 1999. An overview of fast pyrolysis of biomass. *Organic Geochemistry,* 30**,** 1479-1493.

BRIDGWATER, A. V. & PEACOCKE, G. V. C. 2000. Fast pyrolysis processes for biomass. *Renewable and Sustainable Energy Reviews,* 4**,** 1-73.

BUNLUESIN, T., GORTE, R. J. & GRAHAM, G. W. 1998. Studies of the water-gas-shift reaction on ceria-supported Pt, Pd, and Rh: Implications for oxygen-storage properties. *Applied Catalysis B: Environmental,* 15**,** 107-114.

BUSSI, J., BESPALKO, N., VEIGA, S., AMAYA, A., FACCIO, R. & ABELLO, M. C. 2008. The preparation and properties of Ni–La–Zr catalysts for the steam reforming of ethanol. *Catalysis Communications,* 10**,** 33-38.

CAI, W., DE LA PISCINA, P. R. & HOMS, N. 2014. Oxidative steam reforming of bio-butanol for hydrogen production: effects of noble metals on bimetallic CoM/ZnO catalysts (M = Ru, Rh, Ir, Pd). *Applied Catalysis B: Environmental,* 145**,** 56-62.

CAI, W., PISCINA, P. R. D. L., GABROWSKA, K. & HOMS, N. 2013. Hydrogen production from oxidative steam reforming of bio-butanol over CoIr-based catalysts: Effect of the support. *Bioresource Technology,* 128**,** 467-471.

CAI, W., PISCINA, P. R. D. L. & HOMS, N. 2012a. Hydrogen production from the steam reforming of bio-butanol over novel supported Co-based bimetallic catalysts. *Bioresource Technology,* 107**,** 482-486.

CAI, W., WANG, F., DANIEL, C., VAN VEEN, A. C., SCHUURMAN, Y., DESCORME, C., PROVENDIER, H., SHEN, W. & MIRODATOS, C. 2012b. Oxidative steam reforming of ethanol over Ir/CeO2 catalysts: A structure sensitivity analysis. *Journal of Catalysis,* 286**,** 137-152.

CAI, W., WANG, F., VAN VEEN, A. C., PROVENDIER, H., MIRODATOS, C. & SHEN, W. 2008a. Autothermal reforming of ethanol for hydrogen production over an Rh/CeO2 catalyst. *Catalysis Today,* 138**,** 152-156.

CAI, W., WANG, F., ZHAN, E., VAN VEEN, A. C., MIRODATOS, C. & SHEN, W. 2008b. Hydrogen production from ethanol over Ir/CeO2 catalysts: A comparative study of steam reforming, partial oxidation and oxidative steam reforming. *Journal of Catalysis,* 257**,** 96-107.

CARBAJAL-RAMOS, I. A., GOMEZ, M. F., CONDÓ, A. M., BENGIÓ, S., ANDRADE-GAMBOA, J. J., ABELLO, M. C. & GENNARI, F. C. 2016. Catalytic behavior of Ru supported on Ce0.8Zr0.2O2 for hydrogen production. *Applied Catalysis B: Environmental,* 181**,** 58-70.

CARLSON, T. R., TOMPSETT, G. A., CONNER, W. C. & HUBER, G. W. 2009. Aromatic Production from Catalytic Fast Pyrolysis of Biomass-Derived Feedstocks. *Topics in Catalysis,* 52**,** 241-252.

CARRERO, A., CALLES, J. A. & VIZCAÍNO, A. J. 2010. Effect of Mg and Ca addition on coke deposition over Cu–Ni/SiO2 catalysts for ethanol steam reforming. *Chemical Engineering Journal,* 163**,** 395-402.

CHAUDHURI, S. K. & LOVLEY, D. R. 2003. Electricity generation by direct oxidation of glucose in mediatorless microbial fuel cells. *Nat Biotech,* 21**,** 1229-1232.

CHEN, F., WU, C., DONG, L., JIN, F., WILLIAMS, P. T. & HUANG, J. 2015. Catalytic steam reforming of volatiles released via pyrolysis of wood sawdust for hydrogen-rich gas production on Fe–Zn/Al2O3 nanocatalysts. *Fuel,* 158**,** 999-1005.

CHEN, F., WU, C., DONG, L., VASSALLO, A., WILLIAMS, P. T. & HUANG, J. 2016. Characteristics and catalytic properties of Ni/CaAlOx catalyst for hydrogen-enriched syngas production from pyrolysis-steam reforming of biomass sawdust. *Applied Catalysis B: Environmental,* 183**,** 168-175.

CHEN, L., CHOONG, C. K. S., ZHONG, Z., HUANG, L., ANG, T. P., HONG, L. & LIN, J. 2010. Carbon monoxide-free hydrogen production via low-temperature steam reforming of ethanol over iron-promoted Rh catalyst. *Journal of Catalysis,* 276**,** 197-200.

CHEN, P., ZHANG, H.-B., LIN, G.-D. & TSAI, K.-R. 1998. Development of coking-resistant Ni-based catalyst for partial oxidation and CO2-reforming of methane to syngas. *Applied Catalysis A: General,* 166**,** 343-350.

CHIOU, J. Y. Z., SIANG, J.-Y., YANG, S.-Y., HO, K.-F., LEE, C.-L., YEH, C.-T. & WANG, C.-B. 2012. Pathways of ethanol steam reforming over ceria-supported catalysts. *International Journal of Hydrogen Energy,* 37**,** 13667-13673.

CHOUDHARY, V. R., MONDAL, K. C. & MAMMAN, A. S. 2005. High-temperature stable and highly active/selective supported NiCoMgCeOx catalyst suitable for autothermal reforming of methane to syngas. *Journal of Catalysis,* 233**,** 36-40.

CIPRIANI, G., DI DIO, V., GENDUSO, F., LA CASCIA, D., LIGA, R., MICELI, R. & RICCO GALLUZZO, G. 2014. Perspective on hydrogen energy carrier and its automotive applications. *International Journal of Hydrogen Energy,* 39**,** 8482-8494.

CONSTANTINOU, D. A., ÁLVAREZ-GALVÁN, M. C., FIERRO, J. L. G. & EFSTATHIOU, A. M. 2012. Low-temperature conversion of phenol into CO, CO2 and H2 by steam reforming over La-containing supported Rh catalysts. *Applied Catalysis B: Environmental,* 117–118**,** 81-95.

CORTRIGHT, R. D., DAVDA, R. R. & DUMESIC, J. A. 2002. Hydrogen from catalytic reforming of biomass-derived hydrocarbons in liquid water. *Nature,* 418**,** 964-967.

CZERNIK, S. & BRIDGWATER, A. V. 2004. Overview of Applications of Biomass Fast Pyrolysis Oil. *Energy & Fuels,* 18**,** 590-598.

CZERNIK, S., FRENCH, R., FEIK, C. & CHORNET, E. 2002. Hydrogen by Catalytic Steam Reforming of Liquid Byproducts from Biomass Thermoconversion Processes. *Industrial & Engineering Chemistry Research,* 41**,** 4209-4215.

DAVDA, R. R., SHABAKER, J. W., HUBER, G. W., CORTRIGHT, R. D. & DUMESIC, J. A. 2005. A review of catalytic issues and process conditions for renewable hydrogen and alkanes by aqueous-phase reforming of oxygenated hydrocarbons over supported metal catalysts. *Applied Catalysis B: Environmental,* 56**,** 171-186.

DE LIMA, S. M., DA CRUZ, I. O., JACOBS, G., DAVIS, B. H., MATTOS, L. V. & NORONHA, F. B. 2008. Steam reforming, partial oxidation, and oxidative steam reforming of ethanol over Pt/CeZrO2 catalyst. *Journal of Catalysis,* 257**,** 356-368.

DEMIRBAS, A. 2004. Combustion characteristics of different biomass fuels. *Progress in Energy and Combustion Science,* 30**,** 219-230.

DEMIRBAŞ, A. 2001. Biomass resource facilities and biomass conversion processing for fuels and chemicals. *Energy Conversion and Management,* 42**,** 1357-1378.

DESHMANE, V. G., ABROKWAH, R. Y. & KUILA, D. 2015. Synthesis of stable Cu-MCM-41 nanocatalysts for H2 production with high selectivity via steam reforming of methanol. *International Journal of Hydrogen Energy,* 40**,** 10439-10452.

ELAM, C. C., PADRÓ, C. E. G., SANDROCK, G., LUZZI, A., LINDBLAD, P. & HAGEN, E. F. 2003. Realizing the hydrogen future: the International Energy Agency's efforts to advance

hydrogen energy technologies. *International Journal of Hydrogen Energy,* 28**,** 601-607.

ESTRADE-SZWARCKOPF, H. 2004. XPS photoemission in carbonaceous materials: A "defect" peak beside the graphitic asymmetric peak. *Carbon,* 42**,** 1713-1721.

FAAIJ, A. 2006. Modern Biomass Conversion Technologies. *Mitigation and Adaptation Strategies for Global Change,* 11**,** 335-367.

FALLOT, A., SAINT-ANDRÉ, L., LE MAIRE, G., LACLAU, J.-P., NOUVELLON, Y., MARSDEN, C., BOUILLET, J.-P., SILVA, T., PIKETTY, M.-G. & HAMEL, O. 2009. Biomass sustainability, availability and productivity. *Rev. Met. Paris,* 106**,** 410-418.

FAN, M.-S., ABDULLAH, A. Z. & BHATIA, S. 2010. Utilization of greenhouse gases through carbon dioxide reforming of methane over Ni–Co/MgO–ZrO2: Preparation, characterization and activity studies. *Applied Catalysis B: Environmental,* 100**,** 365-377.

FAN, S., ZHAO, N., LI, J., XIAO, F., WEI, W. & SUN, Y. 2008. Effective and Green Synthesis of Methyl Pyrrole-1-carboxylate with Dimethyl Carbonate Over Solid Base. *Catalysis Letters,* 120**,** 299-302.

FANG, W., PAUL, S., CAPRON, M., BIRADAR, A. V., UMBARKAR, S. B., DONGARE, M. K., DUMEIGNIL, F. & JALOWIECKI-DUHAMEL, L. 2015. Highly loaded well dispersed stable Ni species in NiXMg2AlOY nanocomposites: Application to hydrogen production from bioethanol. *Applied Catalysis B: Environmental,* 166–167**,** 485-496.

FATSIKOSTAS, A. N., KONDARIDES, D. I. & VERYKIOS, X. E. 2002. Production of hydrogen for fuel cells by reformation of biomass-derived ethanol. *Catalysis Today,* 75**,** 145-155.

FATSIKOSTAS, A. N. & VERYKIOS, X. E. 2004. Reaction network of steam reforming of ethanol over Ni-based catalysts. *Journal of Catalysis,* 225**,** 439-452.

FERREIRA-APARICIO, P., GUERRERO-RUIZ, A. & RODRíGUEZ-RAMOS, I. 1998. Comparative study at low and medium reaction temperatures of syngas production by methane reforming with carbon dioxide over silica and alumina supported catalysts. *Applied Catalysis A: General,* 170**,** 177-187.

FIDALGO, B., ARENILLAS, A. & MENÉNDEZ, J. Á. 2010. Synergetic effect of a mixture of activated carbon + Ni/Al2O3 used as catalysts for the CO2 reforming of CH4. *Applied Catalysis A: General,* 390**,** 78-83.

FIELD, C. B., BEHRENFELD, M. J., RANDERSON, J. T. & FALKOWSKI, P. 1998. Primary Production of the Biosphere: Integrating Terrestrial and Oceanic Components. *Science,* 281**,** 237-240.

FORZATTI, P. & LIETTI, L. 1999. Catalyst deactivation. *Catalysis Today,* 52**,** 165-181.

FRANK, B., JENTOFT, F. C., SOERIJANTO, H., KRÖHNERT, J., SCHLÖGL, R. & SCHOMÄCKER, R. 2007. Steam reforming of methanol over copper-containing catalysts: Influence of support material on microkinetics. *Journal of Catalysis,* 246**,** 177-192.

FRUSTERI, F., FRENI, S., SPADARO, L., CHIODO, V., BONURA, G., DONATO, S. & CAVALLARO, S. 2004. H2 production for MC fuel cell by steam reforming of ethanol over MgO supported Pd, Rh, Ni and Co catalysts. *Catalysis Communications,* 5**,** 611-615.

FUENTES, S., BOGDANCHIKOVA, N. E., DIAZ, G., PERAAZA, M. & SANDOVAL, G. C. 1997. Desorption and catalytic properties of palladium, supported on Al2O3-La2O3, prepared by the sol-gel method. *Catalysis Letters,* 47**,** 27-34.

FURUSAWA, T. & TSUTSUMI, A. 2005. Comparison of Co/MgO and Ni/MgO catalysts for the steam reforming of naphthalene as a model compound of tar derived from biomass gasification. *Applied Catalysis A: General,* 278**,** 207-212.

FUSHIMI, C., ARAKI, K., YAMAGUCHI, Y. & TSUTSUMI, A. 2003. Effect of Heating Rate on Steam Gasification of Biomass. 2. Thermogravimetric-Mass Spectrometric (TG-MS) Analysis of Gas Evolution. *Industrial & Engineering Chemistry Research,* 42**,** 3929-3936.

GALETTI, A. E., GOMEZ, M. F., ARRUA, L. A., MARCHI, A. J. & ABELLO, M. C. 2008. Study of CuCoZnAl oxide as catalyst for the hydrogen production from ethanol reforming. *Catalysis Communications,* 9**,** 1201-1208.

GAN, M., FAN, X., CHEN, X., JI, Z., LV, W., WANG, Y., YU, Z. & JIANG, T. 2012. Reduction of Pollutant Emission in Iron Ore Sintering Process by Applying Biomass Fuels. *ISIJ International,* 52**,** 1574-1578.

GAO, L., SUN, G. & KAWI, S. 2008. A study on methanol steam reforming to CO2 and H2 over the La2CuO4 nanofiber catalyst. *Journal of Solid State Chemistry,* 181**,** 7-13.

GAUDERNACK, B. 1998. Hydrogen Production from Fossil Fuels. *In:* SAETRE, T. O. (ed.) *Hydrogen Power: Theoretical and Engineering Solutions: Proceedings of the Hypothesis II Symposium held in Grimstad, Norway, 18–22 August 1997.* Dordrecht: Springer Netherlands.

GU, W., LIU, J., HU, M., WANG, F. & SONG, Y. 2015. La2O2CO3 Encapsulated La2O3 Nanoparticles Supported on Carbon as Superior Electrocatalysts for Oxygen Reduction Reaction. *ACS Applied Materials & Interfaces,* 7**,** 26914-26922.

HARYANTO, A., FERNANDO, S., MURALI, N. & ADHIKARI, S. 2005. Current Status of Hydrogen Production Techniques by Steam Reforming of Ethanol: A Review. *Energy & Fuels,* 19**,** 2098-2106.

HE, C., ZHENG, J., WANG, K., LIN, H., WANG, J.-Y. & YANG, Y. 2015. Sorption enhanced aqueous phase reforming of glycerol for hydrogen production over Pt-Ni supported on multi-walled carbon nanotubes. *Applied Catalysis B: Environmental,* 162**,** 401-411.

HIGGINBOTHAM, C. P., BROWNER, R. F., JENKINS, J. D. & RICE, J. K. 2003. Dependence of drying technique on surface area and pore size for polyethylene glycol/tetramethoxysilicate hybrid gels. *Materials Letters,* 57**,** 3970-3975.

HIROSHI ONISHI, C. E., TETSUYA ARUGA, YASUHIRO IWASAWA 1987. Adsorption of Na atoms and oxygen-containing molecules on MgO(100) and (111) surfaces. *Surface Science,* 191**,** 479-491.

HOU, T., ZHANG, S., CHEN, Y., WANG, D. & CAI, W. 2015. Hydrogen production from ethanol reforming: Catalysts and reaction mechanism. *Renewable and Sustainable Energy Reviews,* 44**,** 132-148.

HU, X. & LU, G. 2010. Acetic acid steam reforming to hydrogen over Co–Ce/Al2O3 and Co–La/Al2O3 catalysts—The promotion effect of Ce and La addition. *Catalysis Communications,* 12**,** 50-53.

HU, Y. H. 2009. Solid-solution catalysts for CO2 reforming of methane. *Catalysis Today,* 148**,** 206-211.

HU, Y. H. & RUCKENSTEIN, E. 1996. Temperature-Programmed Desorption of CO Adsorbed on NiO/MgO. *Journal of Catalysis,* 163**,** 306-311.

HU, Y. H. & RUCKENSTEIN, E. 1997. The characterization of a highly effective NiO/MgO solid solution catalyst in the CO2 reforming of CH4. *Catalysis Letters,* 43**,** 71-77.

HUANG, G., LIAW, B.-J., JHANG, C.-J. & CHEN, Y.-Z. 2009. Steam reforming of methanol over CuO/ZnO/CeO2/ZrO2/Al2O3 catalysts. *Applied Catalysis A: General,* 358**,** 7-12.

HUBER, G. W., IBORRA, S. & CORMA, A. 2006. Synthesis of Transportation Fuels from Biomass: Chemistry, Catalysts, and Engineering. *Chemical Reviews,* 106**,** 4044-4098.

JACOBS, G., CHANEY, J. A., PATTERSON, P. M., DAS, T. K. & DAVIS, B. H. 2004. Fischer–Tropsch synthesis: study of the promotion of Re on the reduction property of Co/Al2O3 catalysts by in situ EXAFS/XANES of Co K and Re LIII edges and XPS. *Applied Catalysis A: General,* 264**,** 203-212.

JI, S.-F., XIAO, T.-C., WANG, H.-T., FLAHAUT, E., COLEMAN, K. S. & GREEN, M. L. H. 2001. Catalytic Combustion of Methane over Cobalt–Magnesium Oxide Solid Solution Catalysts. *Catalysis Letters,* 75**,** 65-71.

JIANG, C. J., TRIMM, D. L., WAINWRIGHT, M. S. & CANT, N. W. 1993a. Kinetic mechanism for the reaction between methanol and water over a Cu-ZnO-Al2O3 catalyst. *Applied Catalysis A: General,* 97**,** 145-158.

JIANG, C. J., TRIMM, D. L., WAINWRIGHT, M. S. & CANT, N. W. 1993b. Kinetic study of steam reforming of methanol over copper-based catalysts. *Applied Catalysis A: General,* 93**,** 245-255.

JONES, G., JAKOBSEN, J. G., SHIM, S. S., KLEIS, J., ANDERSSON, M. P., ROSSMEISL, J., ABILD-PEDERSEN, F., BLIGAARD, T., HELVEG, S., HINNEMANN, B., ROSTRUP-NIELSEN, J. R., CHORKENDORFF, I., SEHESTED, J. & NØRSKOV, J. K. 2008. First principles calculations and experimental insight into methane steam reforming over transition metal catalysts. *Journal of Catalysis,* 259**,** 147-160.

JONES, S. D. & HAGELIN-WEAVER, H. E. 2009. Steam reforming of methanol over CeO2- and ZrO2-promoted Cu-ZnO catalysts supported on nanoparticle Al2O3. *Applied Catalysis B: Environmental,* 90**,** 195-204.

KANG, S., SUB KWAK, B. & KANG, M. 2014. Synthesis of Ni-alkaline earth metals particles encapsulated by porous SiO2 (NiMO@SiO2) and their catalytic performances on ethanol steam reforming. *Ceramics International,* 40**,** 14197-14206.

KARIM, A. M., CONANT, T. & DATYE, A. K. 2008. Controlling ZnO morphology for improved methanol steam reforming reactivity. *Physical Chemistry Chemical Physics,* 10**,** 5584-5590.

KIM, S. S., LEE, S. M., WON, J. M., YANG, H. J. & HONG, S. C. 2015. Effect of Ce/Ti ratio on the catalytic activity and stability of Ni/CeO2–TiO2 catalyst for dry reforming of methane. *Chemical Engineering Journal,* 280**,** 433-440.

KOO, K. Y., ROH, H.-S., SEO, Y. T., SEO, D. J., YOON, W. L. & PARK, S. B. 2008. Coke study on MgO-promoted Ni/Al2O3 catalyst in combined H2O and CO2 reforming of methane for gas to liquid (GTL) process. *Applied Catalysis A: General,* 340**,** 183-190.

KUGAI, J., SUBRAMANI, V., SONG, C., ENGELHARD, M. H. & CHIN, Y.-H. 2006. Effects of nanocrystalline CeO2 supports on the properties and performance of Ni–Rh bimetallic catalyst for oxidative steam reforming of ethanol. *Journal of Catalysis,* 238**,** 430-440.

LAN, P. 2011. *Investigation of Hydrogen Production from Steam Reforming of Bio-oil and Catalytic Deactivation by Carbon Deposition.* PhD, East China University of Science and Technology.

LAN, P., XU, Q., ZHOU, M., LAN, L., ZHANG, S. & YAN, Y. 2010. Catalytic Steam Reforming of Fast Pyrolysis Bio-Oil in Fixed Bed and Fluidized Bed Reactors. *Chemical Engineering & Technology,* 33**,** 2021-2028.

LAOSIRIPOJANA, N. & ASSABUMRUNGRAT, S. 2007. Catalytic steam reforming of methane, methanol, and ethanol over Ni/YSZ: The possible use of these fuels in internal reforming SOFC. *Journal of Power Sources,* 163**,** 943-951.

LEVIN, D. B. & CHAHINE, R. 2010. Challenges for renewable hydrogen production from biomass. *International Journal of Hydrogen Energy,* 35**,** 4962-4969.

LI, C. & STAIR, P. C. 1997. Ultraviolet Raman spectroscopy characterization of coke formation in zeolites. *Catalysis Today,* 33**,** 353-360.

LI, D., ZENG, L., LI, X., WANG, X., MA, H., ASSABUMRUNGRAT, S. & GONG, J. 2015. Ceria-promoted Ni/SBA-15 catalysts for ethanol steam reforming with enhanced activity and resistance to deactivation. *Applied Catalysis B: Environmental,* 176–177**,** 532-541.

LI, Z., HU, X., ZHANG, L., LIU, S. & LU, G. 2012. Steam reforming of acetic acid over Ni/ZrO2 catalysts: Effects of nickel loading and particle size on product distribution and coke formation. *Applied Catalysis A: General,* 417–418**,** 281-289.

LIGURAS, D. K., KONDARIDES, D. I. & VERYKIOS, X. E. 2003. Production of hydrogen for fuel cells by steam reforming of ethanol over supported noble metal catalysts. *Applied Catalysis B: Environmental,* 43**,** 345-354.

LIM, Z.-Y., WU, C., WANG, W. G., CHOY, K.-L. & YIN, H. 2016. Porosity effect on ZrO2 hollow shells and hydrothermal stability for catalytic steam reforming of methane. *Journal of Materials Chemistry A*.

LIMA DA SILVA, A., MALFATTI, C. D. F. & MÜLLER, I. L. 2009. Thermodynamic analysis of ethanol steam reforming using Gibbs energy minimization method: A detailed study of the conditions of carbon deposition. *International Journal of Hydrogen Energy,* 34**,** 4321-4330.

LIN, R., LUO, M.-F., ZHONG, Y.-J., YAN, Z.-L., LIU, G.-Y. & LIU, W.-P. 2003. Comparative study of CuO/Ce0.7Sn0.3O2, CuO/CeO2 and CuO/SnO2 catalysts for low-temperature CO oxidation. *Applied Catalysis A: General,* 255**,** 331-336.

LIN, Y. & TANAKA, S. 2006. Ethanol fermentation from biomass resources: current state and prospects. *Applied Microbiology and Biotechnology,* 69**,** 627-642.

LINDSAY, I., LOWE, C., REDDY, S., BHAKTA, M. & BALKENENDE, S. 2009. Designing a climate friendly hydrogen plant. *Energy Procedia,* 1**,** 4095-4102.

LIU, C.-J., YE, J., JIANG, J. & PAN, Y. 2011. Progresses in the Preparation of Coke Resistant Ni-based Catalyst for Steam and CO2 Reforming of Methane. *ChemCatChem,* 3**,** 529-541.

LIU, X., ZHOU, K., WANG, L., WANG, B. & LI, Y. 2009. Oxygen Vacancy Clusters Promoting Reducibility and Activity of Ceria Nanorods. *Journal of the American Chemical Society,* 131**,** 3140-3141.

LIU, Y., XU, Z., CHENG, T., ZHOU, G., WANG, J., LI, W., BI, Y. & ZHEN, K. 2002. Studies on Carbon Deposition on Hexaaluminate LaNiAl11O19 Catalysts during CO2 Reforming of Methane. *Kinetics and Catalysis,* 43**,** 522-527.

LIU, Z., CHE, R., ELZATAHRY, A. A. & ZHAO, D. 2014. Direct Imaging Au Nanoparticle Migration Inside Mesoporous Silica Channels. *ACS Nano,* 8**,** 10455-10460.

LLORCA, J., HOMS, N. S., SALES, J. & DE LA PISCINA, P. R. R. 2002. Efficient Production of Hydrogen over Supported Cobalt Catalysts from Ethanol Steam Reforming. *Journal of Catalysis,* 209**,** 306-317.

LLORCA, J., HOMS, N. S., SALES, J., FIERRO, J.-L. G. & RAMíREZ DE LA PISCINA, P. 2004. Effect of sodium addition on the performance of Co–ZnO-based catalysts for hydrogen production from bioethanol. *Journal of Catalysis,* 222**,** 470-480.

LRZ 1993. Downdraft Gasifiers under 200 kWe. B/M3/00388/04/Rep: ETSU.

LUO, X., HONG, Y., WANG, F., HAO, S., PANG, C., LESTER, E. & WU, T. 2016. Development of nano NixMgyO solid solutions with outstanding anti-carbon deposition capability for the steam reforming of methanol. *Applied Catalysis B: Environmental,* 194**,** 84-97.

MA, H., ZENG, L., TIAN, H., LI, D., WANG, X., LI, X. & GONG, J. 2016. Efficient hydrogen production from ethanol steam reforming over La-modified ordered mesoporous Ni-based catalysts. *Applied Catalysis B: Environmental,* 181**,** 321-331.

MANN, M., CHORNET, E. & CZERNIK, S. 1994. *Biomass to hydrogen via pyrolysis and reforming*.

MASCHIO, G., KOUFOPANOS, C. & LUCCHESI, A. 1992. Pyrolysis, a promising route for biomass utilization. *Bioresource Technology,* 42**,** 219-231.

MATAS GÜELL, B., BABICH, I. V., LEFFERTS, L. & SESHAN, K. 2011. Steam reforming of phenol over Ni-based catalysts – A comparative study. *Applied Catalysis B: Environmental,* 106**,** 280-286.

MATTHEWS, M. J., PIMENTA, M. A., DRESSELHAUS, G., DRESSELHAUS, M. S. & ENDO, M. 1999. Origin of dispersive effects of the Raman \textbf{ \textit{D} } band in carbon materials. *Physical Review B,* 59**,** R6585-R6588.

MATTOS, L. V., JACOBS, G., DAVIS, B. H. & NORONHA, F. B. 2012. Production of Hydrogen from Ethanol: Review of Reaction Mechanism and Catalyst Deactivation. *Chemical Reviews,* 112**,** 4094-4123.

MCKENDRY, P. 2002a. Energy production from biomass (part 1): overview of biomass. *Bioresource Technology,* 83**,** 37-46.

MCKENDRY, P. 2002b. Energy production from biomass (part 2): conversion technologies. *Bioresource Technology,* 83**,** 47-54.

MD ZIN, R., ROSS, A. B., JONES, J. M. & DUPONT, V. 2015. Hydrogen from ethanol reforming with aqueous fraction of pine pyrolysis oil with and without chemical looping. *Bioresource Technology,* 176**,** 257-266.

MEN, Y., GNASER, H., ZAPF, R., HESSEL, V., ZIEGLER, C. & KOLB, G. 2004. Steam reforming of methanol over Cu/CeO2/γ-Al2O3 catalysts in a microchannel reactor. *Applied Catalysis A: General,* 277**,** 83-90.

MENON, P. G. 1990. Coke on catalysts-harmful, harmless, invisible and beneficial types. *Journal of Molecular Catalysis,* 59**,** 207-220.

MOHAN, D., PITTMAN, C. U. & STEELE, P. H. 2006. Pyrolysis of Wood/Biomass for Bio-oil: A Critical Review. *Energy & Fuels,* 20**,** 848-889.

MONTEIRO, R. S., NORONHA, F. B., DIEGUEZ, L. C. & SCHMAL, M. 1995. Characterization of Pd-CeO2 interaction on alumina support and hydrogenation of 1,3-butadiene. *Applied Catalysis A: General,* 131**,** 89-106.

MONTERO, C., OCHOA, A., CASTAÑO, P., BILBAO, J. & GAYUBO, A. G. 2015. Monitoring Ni0 and coke evolution during the deactivation of a Ni/La2O3–αAl2O3 catalyst in ethanol steam reforming in a fluidized bed. *Journal of Catalysis,* 331**,** 181-192.

MORTENSEN, P. M., GRUNWALDT, J. D., JENSEN, P. A., KNUDSEN, K. G. & JENSEN, A. D. 2011. A review of catalytic upgrading of bio-oil to engine fuels. *Applied Catalysis A: General,* 407**,** 1-19.

NABGAN, W., ABDULLAH, T. A. T., MAT, R., NABGAN, B., JALIL, A. A., FIRMANSYAH, L. & TRIWAHYONO, S. 2016. Production of hydrogen via steam reforming of acetic acid over Ni and Co supported on La2O3 catalyst. *International Journal of Hydrogen Energy*.

NATESAKHAWAT, S., WATSON, R. B., WANG, X. & OZKAN, U. S. 2005. Deactivation characteristics of lanthanide-promoted sol–gel Ni/Al2O3 catalysts in propane steam reforming. *Journal of Catalysis,* 234**,** 496-508.

NAVARRO, R. M., PEÑA, M. A. & FIERRO, J. L. G. 2007. Hydrogen Production Reactions from Carbon Feedstocks: Fossil Fuels and Biomass. *Chemical Reviews,* 107**,** 3952-3991.

NI, J., CHEN, L., LIN, J. & KAWI, S. 2012. Carbon deposition on borated alumina supported nano-sized Ni catalysts for dry reforming of CH4. *Nano Energy,* 1**,** 674-686.

NI, M., LEUNG, D. Y. C. & LEUNG, M. K. H. 2007. A review on reforming bio-ethanol for hydrogen production. *International Journal of Hydrogen Energy,* 32**,** 3238-3247.

NICHELE, V., SIGNORETTO, M., MENEGAZZO, F., GALLO, A., DAL SANTO, V., CRUCIANI, G. & CERRATO, G. 2012. Glycerol steam reforming for hydrogen production: Design of Ni supported catalysts. *Applied Catalysis B: Environmental,* 111–112**,** 225-232.

OASMAA, A. & CZERNIK, S. 1999. Fuel Oil Quality of Biomass Pyrolysis OilsState of the Art for the End Users. *Energy & Fuels,* 13**,** 914-921.

OASMAA, A. & MEIER, D. 2005. Norms and standards for fast pyrolysis liquids: 1. Round robin test. *Journal of Analytical and Applied Pyrolysis,* 73**,** 323-334.

OKU, M. & HIROKAWA, K. 1977. The effect of the next nearest neighbor ion on the X-ray photoelectron spectra of 2p levels for Co2+, Ni2+ and Cu2+ in MgO. *Journal of Electron Spectroscopy and Related Phenomena,* 10**,** 103-110.

PALMA, V., CASTALDO, F., CIAMBELLI, P. & IAQUANIELLO, G. 2014. CeO2-supported Pt/Ni catalyst for the renewable and clean H2 production via ethanol steam reforming. *Applied Catalysis B: Environmental,* 145**,** 73-84.

PALO, D. R., DAGLE, R. A. & HOLLADAY, J. D. 2007. Methanol Steam Reforming for Hydrogen Production. *Chemical Reviews,* 107**,** 3992-4021.

PARIZOTTO, N. V., ZANCHET, D., ROCHA, K. O., MARQUES, C. M. P. & BUENO, J. M. C. 2009. The effects of Pt promotion on the oxi-reduction properties of alumina supported nickel catalysts for oxidative steam-reforming of methane: Temperature-resolved XAFS analysis. *Applied Catalysis A: General,* 366**,** 122-129.

PARK, S., BANG, Y., HAN, S. J., YOO, J., SONG, J. H., SONG, J. C., LEE, J. & SONG, I. K. 2015. Hydrogen production by steam reforming of liquefied natural gas (LNG) over mesoporous nickel–iron–alumina catalyst. *International Journal of Hydrogen Energy,* 40**,** 5869-5877.

PARMALIANA, A., ARENA, F., FRUSTERI, F. & GIORDANO, N. 1990. Temperature-programmed reduction study of NiO-MgO interactions in magnesia-supported Ni catalysts and NiO-MgO physical mixture. *Journal of the Chemical Society, Faraday Transactions,* 86**,** 2663-2669.

PATEL, S. & PANT, K. K. 2006. Activity and stability enhancement of copper–alumina catalysts using cerium and zinc promoters for the selective production of hydrogen via steam reforming of methanol. *Journal of Power Sources,* 159**,** 139-143.

PEPPLEY, B. A., AMPHLETT, J. C., KEARNS, L. M. & MANN, R. F. 1999. Methanol–steam reforming on Cu/ZnO/Al2O3. Part 1: the reaction network. *Applied Catalysis A: General,* 179**,** 21-29.

PEREZ-HERNANDEZ, R., MONDRAGON-GALICIA, G., ALLENDE MARAVILLA, A. & PALACIOS, J. 2013. Nano-dimensional CeO2 nanorods for high Ni loading catalysts: H2 production by autothermal steam reforming of methanol reaction. *Physical Chemistry Chemical Physics,* 15**,** 12702-12708.

PEREZ-LOPEZ, O. W., SENGER, A., MARCILIO, N. R. & LANSARIN, M. A. 2006. Effect of composition and thermal pretreatment on properties of Ni–Mg–Al catalysts for CO2 reforming of methane. *Applied Catalysis A: General,* 303**,** 234-244.

PILLAI, U. R. & DEEVI, S. 2006. Copper-zinc oxide and ceria promoted copper-zinc oxide as highly active catalysts for low temperature oxidation of carbon monoxide. *Applied Catalysis B: Environmental,* 65**,** 110-117.

POLYCHRONOPOULOU, K., FIERRO, J. L. G. & EFSTATHIOU, A. M. 2004. The phenol steam reforming reaction over MgO-based supported Rh catalysts. *Journal of Catalysis,* 228**,** 417-432.

QUEK, X.-Y., LIU, D., CHEO, W. N. E., WANG, H., CHEN, Y. & YANG, Y. 2010. Nickel-grafted TUD-1 mesoporous catalysts for carbon dioxide reforming of methane. *Applied Catalysis B: Environmental,* 95**,** 374-382.

RADLEIN, D., PISKORZ, J. & SCOTT, D. S. 1991. Proceedings of the 9th International Conference on Fundamentals Aspects, Analytical Techniques, Processes and Applications of PyrolysisFast pyrolysis of natural polysaccharides as a potential industrial process. *Journal of Analytical and Applied Pyrolysis,* 19**,** 41-63.

RAFFELT, K., HENRICH, E., KOEGEL, A., STAHL, R., STEINHARDT, J. & WEIRICH, F. 2006. The BTL2 process of biomass utilization entrained-flow gasification of pyrolyzed biomass slurries. *Applied Biochemistry and Biotechnology,* 129**,** 153-164.

RAMOS, M. C., NAVASCUÉS, A. I., GARCÍA, L. & BILBAO, R. 2007. Hydrogen Production by Catalytic Steam Reforming of Acetol, a Model Compound of Bio-Oil. *Industrial & Engineering Chemistry Research,* 46**,** 2399-2406.

RAVEENDRAN, K., GANESH, A. & KHILAR, K. C. 1996. Pyrolysis characteristics of biomass and biomass components. *Fuel,* 75**,** 987-998.

REZAEI, M., ALAVI, S. M., SAHEBDELFAR, S. & YAN, Z.-F. 2006. Syngas Production by Methane Reforming with Carbon Dioxide on Noble Metal Catalysts. *Journal of Natural Gas Chemistry,* 15**,** 327-334.

RHODES, C., HUTCHINGS, G. J. & WARD, A. M. 1995. Recent Advances in C1 ChemistryWater-gas shift reaction: finding the mechanistic boundary. *Catalysis Today,* 23**,** 43-58.

RIOCHE, C., KULKARNI, S., MEUNIER, F. C., BREEN, J. P. & BURCH, R. 2005. Steam reforming of model compounds and fast pyrolysis bio-oil on supported noble metal catalysts. *Applied Catalysis B: Environmental,* 61**,** 130-139.

ROBERTSON, J. 2002. Diamond-like amorphous carbon. *Materials Science and Engineering: R: Reports,* 37**,** 129-281.

ROH, H.-S., PLATON, A., WANG, Y. & KING, D. L. 2006. Catalyst deactivation and regeneration in low temperature ethanol steam reforming with Rh/CeO2–ZrO2 catalysts. *Catalysis Letters,* 110**,** 1-6.

ROSEN, M. A. & KOOHI-FAYEGH, S. 2016. The prospects for hydrogen as an energy carrier: an overview of hydrogen energy and hydrogen energy systems. *Energy, Ecology and Environment,* 1**,** 10-29.

ROSTRUP-NIELSEN, J. & TRIMM, D. L. 1977. Mechanisms of carbon formation on nickel-containing catalysts. *Journal of Catalysis,* 48**,** 155-165.

ROSTRUP-NIELSEN, J. R. 1974. Coking on nickel catalysts for steam reforming of hydrocarbons. *Journal of Catalysis,* 33**,** 184-201.

ROSTRUP-NIELSEN, J. R. 1984a. Catalytic Steam Reforming. *In:* ANDERSON, J. R. & BOUDART, M. (eds.) *Catalysis: Science and Technology.* Berlin, Heidelberg: Springer Berlin Heidelberg.

ROSTRUP-NIELSEN, J. R. 1984b. Sulfur-passivated nickel catalysts for carbon-free steam reforming of methane. *journal of Catalysis,* 85**,** 31-43.

ROSTRUP-NIELSEN, J. R., SEHESTED, J. & NØRSKOV, J. K. 2002. Hydrogen and synthesis gas by steam- and C02 reforming. *Advances in Catalysis.* Academic Press.

RUSSELL, J. N., SARVIS, S. S. & MORRIS, R. E. 1995. Adsorption and thermal decomposition of phenol on Ni(110). *Surface Science,* 338**,** 189-203.

SÁ, S., SILVA, H., BRANDÃO, L., SOUSA, J. M. & MENDES, A. 2010. Catalysts for methanol steam reforming—A review. *Applied Catalysis B: Environmental,* 99**,** 43-57.

SAN-JOSÉ-ALONSO, D., JUAN-JUAN, J., ILLÁN-GÓMEZ, M. J. & ROMÁN-MARTÍNEZ, M. C. 2009. Ni, Co and bimetallic Ni–Co catalysts for the dry reforming of methane. *Applied Catalysis A: General,* 371**,** 54-59.

SÁNCHEZ, E. A., D'ANGELO, M. A. & COMELLI, R. A. 2010. Hydrogen production from glycerol on Ni/Al2O3 catalyst. *International Journal of Hydrogen Energy,* 35**,** 5902-5907.

SANTACESARIA, E. & CARRÁ, S. 1983. Kinetics of catalytic steam reforming of methanol in a cstr reactor. *Applied Catalysis,* 5**,** 345-358.

SATO, K. & FUJIMOTO, K. 2007. Development of new nickel based catalyst for tar reforming with superior resistance to sulfur poisoning and coking in biomass gasification. *Catalysis Communications,* 8**,** 1697-1701.

SENANAYAKE, S., EVANS, J., AGNOLI, S., BARRIO, L., CHEN, T.-L., HRBEK, J. & RODRIGUEZ, J. 2011. Water–Gas Shift and CO Methanation Reactions over Ni–CeO2(111) Catalysts. *Topics in Catalysis,* 54**,** 34-41.

SEXTON, B. A., HUGHES, A. E. & TURNEY, T. W. 1986. An XPS and TPR study of the reduction of promoted cobalt-kieselguhr Fischer-Tropsch catalysts. *Journal of Catalysis,* 97**,** 390-406.

SHARMA, S. & GHOSHAL, S. K. 2015. Hydrogen the future transportation fuel: From production to applications. *Renewable and Sustainable Energy Reviews,* 43**,** 1151-1158.

SHI, K., YAN, J., LESTER, E. & WU, T. 2014. Catalyst-Free Synthesis of Multiwalled Carbon Nanotubes via Microwave-Induced Processing of Biomass. *Industrial & Engineering Chemistry Research,* 53**,** 15012-15019.

SHI, Q., PENG, Z., CHEN, W. & ZHANG, N. 2011. La2O2CO3 supported Ni-Fe catalysts for hydrogen production from steam reforming of ethanol. *Journal of Rare Earths,* 29**,** 861-865.

SHISHIDO, T., YAMAMOTO, Y., MORIOKA, H., TAKAKI, K. & TAKEHIRA, K. 2004. Active Cu/ZnO and Cu/ZnO/Al2O3 catalysts prepared by homogeneous precipitation method in steam reforming of methanol. *Applied Catalysis A: General,* 263**,** 249-253.

SIANG, J.-Y., LEE, C.-C., WANG, C.-H., WANG, W.-T., DENG, C.-Y., YEH, C.-T. & WANG, C.-B. 2010. Hydrogen production from steam reforming of ethanol using a ceria-supported iridium catalyst: Effect of different ceria supports. *International Journal of Hydrogen Energy,* 35**,** 3456-3462.

SING, K. W. 1995. Physisorption of nitrogen by porous materials. *Journal of Porous Materials,* 2**,** 5-8.

SING., K. S. W., EVERETT., D. H., HAUL., R. A. W., MOSCOU., L., PIEROTTI., R. A., ROUQUEROL., J. & SIEMIENIEWSKA, T. 1985. Reporting physisorption data for gas/solid systems with special reference to the determination of surface area and porosity. *Pure and Applied Chemistry,* 57**,** 603-619.

STURZENEGGER, M., D'SOUZA, L., STRUIS, R. P. W. J. & STUCKI, S. 2006. Oxygen transfer and catalytic properties of nickel iron oxides for steam reforming of methane. *Fuel,* 85**,** 1599-1602.

SUN, N., WEN, X., WANG, F., WEI, W. & SUN, Y. 2010. Effect of pore structure on Ni catalyst for CO2 reforming of CH4. *Energy & Environmental Science,* 3**,** 366-369.

SUTTHIUMPORN, K. & KAWI, S. 2011. Promotional effect of alkaline earth over Ni–La2O3 catalyst for CO2 reforming of CH4: Role of surface oxygen species on H2 production and carbon suppression. *International Journal of Hydrogen Energy,* 36**,** 14435-14446.

TAKAHASHI, K., TAKEZAWA, N. & KOBAYASHI, H. 1982. The mechanism of steam reforming of methanol over a copper-silica catalyst. *Applied Catalysis,* 2**,** 363-366.

TAKANABE, K., AIKA, K.-I., INAZU, K., BABA, T., SESHAN, K. & LEFFERTS, L. 2006. Steam reforming of acetic acid as a biomass derived oxygenate: Bifunctional pathway for hydrogen formation over Pt/ZrO2 catalysts. *Journal of Catalysis,* 243**,** 263-269.

TAKANABE, K., AIKA, K.-I., SESHAN, K. & LEFFERTS, L. 2004. Sustainable hydrogen from bio-oil—Steam reforming of acetic acid as a model oxygenate. *Journal of Catalysis,* 227**,** 101-108.

TAKEZAWA, N. & IWASA, N. 1997. Steam reforming and dehydrogenation of methanol: Difference in the catalytic functions of copper and group VIII metals. *Catalysis Today,* 36**,** 45-56.

TAN, B. J., KLABUNDE, K. J. & SHERWOOD, P. M. A. 1991. XPS studies of solvated metal atom dispersed (SMAD) catalysts. Evidence for layered cobalt-manganese particles on alumina and silica. *Journal of the American Chemical Society,* 113**,** 855-861.

TANG, S., LIN, J. & TAN, K. L. 1998. Partial oxidation of methane to syngas over Ni/MgO, Ni/CaO and Ni/CeO2. *Catalysis Letters,* 51**,** 169-175.

TIPPAWAN, P. & ARPORNWICHANOP, A. 2014. Energy and exergy analysis of an ethanol reforming process for solid oxide fuel cell applications. *Bioresource Technology,* 157**,** 231-239.

TORRES, D. & LIU, P. 2012. Vacancy-Driven Surface Segregation in Ni x Mg1–x O(100) Solid Solutions from First Principles Calculations. *Catalysis Letters,* 142**,** 1211-1217.

TRANE, R., DAHL, S., SKJØTH-RASMUSSEN, M. S. & JENSEN, A. D. 2012. Catalytic steam reforming of bio-oil. *International Journal of Hydrogen Energy,* 37**,** 6447-6472.

TRIMM, D. L. 1991. Thermal Stability of Catalyst Supports. *In:* CALVIN, H. B. & JOHN, B. B. (eds.) *Studies in Surface Science and Catalysis.* Elsevier.

TRIMM, D. L. 1997. Coke formation and minimisation during steam reforming reactions. *Catalysis Today,* 37**,** 233-238.

TRIMM, D. L. 1999. Catalysts for the control of coking during steam reforming. *Catalysis Today,* 49**,** 3-10.

TRIMM, D. L. & ÖNSAN, Z. I. 2001. ONBOARD FUEL CONVERSION FOR HYDROGEN-FUEL-CELL-DRIVEN VEHICLES. *Catalysis Reviews,* 43**,** 31-84.

TROVARELLI, A., DOLCETTI, G., DE LEITENBURG, C., KASPAR, J., FINETTI, P. & SANTONI, A. 1992. Rh-CeO2 interaction induced by high-temperature reduction. Characterization and catalytic behaviour in transient and continuous conditions. *Journal of the Chemical Society, Faraday Transactions,* 88**,** 1311-1319.

TSANEVA, V. N., KWAPINSKI, W., TENG, X. & GLOWACKI, B. A. 2014. Assessment of the structural evolution of carbons from microwave plasma natural gas reforming and biomass pyrolysis using Raman spectroscopy. *Carbon,* 80**,** 617-628.

TSYGANOK, A. I., TSUNODA, T., HAMAKAWA, S., SUZUKI, K., TAKEHIRA, K. & HAYAKAWA, T. 2003. Dry reforming of methane over catalysts derived from nickel-containing Mg–Al layered double hydroxides. *Journal of Catalysis,* 213**,** 191-203.

TURCO, M., BAGNASCO, G., COSTANTINO, U., MARMOTTINI, F., MONTANARI, T., RAMIS, G. & BUSCA, G. 2004. Production of hydrogen from oxidative steam reforming of methanol: I. Preparation and characterization of Cu/ZnO/Al2O3 catalysts from a hydrotalcite-like LDH precursor. *Journal of Catalysis,* 228**,** 43-55.

VAGIA, E. C. & LEMONIDOU, A. A. 2007. Thermodynamic analysis of hydrogen production via steam reforming of selected components of aqueous bio-oil fraction. *International Journal of Hydrogen Energy,* 32**,** 212-223.

VAGIA, E. C. & LEMONIDOU, A. A. 2008. Hydrogen production via steam reforming of bio-oil components over calcium aluminate supported nickel and noble metal catalysts. *Applied Catalysis A: General,* 351**,** 111-121.

VAIDYA, P. D. & RODRIGUES, A. E. 2006. Insight into steam reforming of ethanol to produce hydrogen for fuel cells. *Chemical Engineering Journal,* 117**,** 39-49.

VAN DEN BROEK, R., FAAIJ, A. & VAN WIJK, A. 1996. Biomass combustion for power generation. *Biomass and Bioenergy,* 11**,** 271-281.

VIZCAÍNO, A. J., ARENA, P., BARONETTI, G., CARRERO, A., CALLES, J. A., LABORDE, M. A. & AMADEO, N. 2008. Ethanol steam reforming on Ni/Al2O3 catalysts: Effect of Mg addition. *International Journal of Hydrogen Energy,* 33**,** 3489-3492.

VIZCAÍNO, A. J., CARRERO, A. & CALLES, J. A. 2009. Ethanol steam reforming on Mg- and Ca-modified Cu–Ni/SBA-15 catalysts. *Catalysis Today,* 146**,** 63-70.

VOGELAAR, B. M., VAN LANGEVELD, A. D., EIJSBOUTS, S. & MOULIJN, J. A. 2007. Analysis of coke deposition profiles in commercial spent hydroprocessing catalysts using Raman spectroscopy. *Fuel,* 86**,** 1122-1129.

WACKE, S., GÓRECKI, T., GÓRECKI, C. & KSIĄŻEK, K. 2011. Relations between the cohesive energy, atomic volume, bulk modulus and sound velocity in metals. *Journal of Physics: Conference Series,* 289**,** 012020.

WALLACE, J. S. & WARD, C. A. 1983. Hydrogen as a fuel. *International Journal of Hydrogen Energy,* 8**,** 255-268.

WANG, D., MONTANÉ, D. & CHORNET, E. 1996. Catalytic steam reforming of biomass-derived oxygenates: acetic acid and hydroxyacetaldehyde. *Applied Catalysis A: General,* 143**,** 245-270.

WANG, L.-C., LIU, Y.-M., CHEN, M., CAO, Y., HE, H.-Y., WU, G.-S., DAI, W.-L. & FAN, K.-N. 2007. Production of hydrogen by steam reforming of methanol over Cu/ZnO catalysts

prepared via a practical soft reactive grinding route based on dry oxalate-precursor synthesis. *Journal of Catalysis,* 246**,** 193-204.

WANG, N., SHEN, K., HUANG, L., YU, X., QIAN, W. & CHU, W. 2013. Facile Route for Synthesizing Ordered Mesoporous Ni–Ce–Al Oxide Materials and Their Catalytic Performance for Methane Dry Reforming to Hydrogen and Syngas. *ACS Catalysis,* 3**,** 1638-1651.

WANG, S. & LU, G. Q. 1998a. Role of CeO_2 in Ni/CeO_2–Al_2O_3 catalysts for carbon dioxide reforming of methane. *Applied Catalysis B: Environmental,* 19**,** 267-277.

WANG, S. & LU, G. Q. M. 1998b. CO_2 reforming of methane on Ni catalysts: Effects of the support phase and preparation technique. *Applied Catalysis B: Environmental,* 16**,** 269-277.

WANG, Y.-H., LIU, H.-M. & XU, B.-Q. 2009. Durable Ni/MgO catalysts for CO_2 reforming of methane: Activity and metal–support interaction. *Journal of Molecular Catalysis A: Chemical,* 299**,** 44-52.

WU, C. & WILLIAMS, P. T. 2010. A Novel Nano-Ni/SiO_2 Catalyst for Hydrogen Production from Steam Reforming of Ethanol. *Environmental Science & Technology,* 44**,** 5993-5998.

WU, G., ZHANG, C., LI, S., HAN, Z., WANG, T., MA, X. & GONG, J. 2013. Hydrogen Production via Glycerol Steam Reforming over Ni/Al_2O_3: Influence of Nickel Precursors. *ACS Sustainable Chemistry & Engineering,* 1**,** 1052-1062.

WU, G., ZHANG, C., LI, S., HUANG, Z., YAN, S., WANG, S., MA, X. & GONG, J. 2012. Sorption enhanced steam reforming of ethanol on Ni-CaO-Al_2O_3 multifunctional catalysts derived from hydrotalcite-like compounds. *Energy & Environmental Science,* 5**,** 8942-8949.

XING, T., LI, L. H., HOU, L., HU, X., ZHOU, S., PETER, R., PETRAVIC, M. & CHEN, Y. 2013. Disorder in ball-milled graphite revealed by Raman spectroscopy. *Carbon,* 57**,** 515-519.

XU, J. & FROMENT, G. F. 1989. Methane steam reforming, methanation and water-gas shift: I. Intrinsic kinetics. *AIChE Journal,* 35**,** 88-96.

YAN, C.-F., CHENG, F.-F. & HU, R.-R. 2010. Hydrogen production from catalytic steam reforming of bio-oil aqueous fraction over Ni/CeO_2–ZrO_2 catalysts. *International Journal of Hydrogen Energy,* 35**,** 11693-11699.

YANG, G., YU, H., HUANG, X., PENG, F. & WANG, H. 2012. Effect of calcium dopant on catalysis of Ir/La_2O_3 for hydrogen production by oxidative steam reforming of glycerol. *Applied Catalysis B: Environmental,* 127**,** 89-98.

YAO, C.-Z., WANG, L.-C., LIU, Y.-M., WU, G.-S., CAO, Y., DAI, W.-L., HE, H.-Y. & FAN, K.-N. 2006. Effect of preparation method on the hydrogen production from methanol steam reforming over binary Cu/ZrO_2 catalysts. *Applied Catalysis A: General,* 297**,** 151-158.

YU, M., ZHU, K., LIU, Z., XIAO, H., DENG, W. & ZHOU, X. 2014. Carbon dioxide reforming of methane over promoted $Ni_xMg_{1-x}O$ (1 1 1) platelet catalyst derived from solvothermal synthesis. *Applied Catalysis B: Environmental,* 148–149**,** 177-190.

YUAN, Z., WU, P., GAO, J., LU, X., HOU, Z. & ZHENG, X. 2009. Pt/Solid-Base: A Predominant Catalyst for Glycerol Hydrogenolysis in a Base-Free Aqueous Solution. *Catalysis Letters,* 130**,** 261-265.

ZHAN, Y., LI, D., NISHIDA, K., SHISHIDO, T., OUMI, Y., SANO, T. & TAKEHIRA, K. 2009. Preparation of "intelligent" Pt/Ni/Mg(Al)O catalysts starting from commercial Mg–Al LDHs for daily start-up and shut-down steam reforming of methane. *Applied Clay Science,* 45**,** 147-154.

ZHANG, B., TANG, X., LI, Y., CAI, W., XU, Y. & SHEN, W. 2006. Steam reforming of bio-ethanol for the production of hydrogen over ceria-supported Co, Ir and Ni catalysts. *Catalysis Communications,* 7**,** 367-372.

ZHANG, J., WANG, H. & DALAI, A. K. 2007a. Development of stable bimetallic catalysts for carbon dioxide reforming of methane. *Journal of Catalysis,* 249**,** 300-310.

ZHANG, J., WANG, H. & DALAI, A. K. 2008. Effects of metal content on activity and stability of Ni-Co bimetallic catalysts for CO2 reforming of CH4. *Applied Catalysis A: General,* 339**,** 121-129.

ZHANG, Q., CHANG, J., WANG, T. & XU, Y. 2007b. Review of biomass pyrolysis oil properties and upgrading research. *Energy Conversion and Management,* 48**,** 87-92.

ZHAO, C., KOU, Y., LEMONIDOU, A. A., LI, X. & LERCHER, J. A. 2009. Highly Selective Catalytic Conversion of Phenolic Bio-Oil to Alkanes. *Angewandte Chemie,* 121**,** 4047-4050.

ZHAO, H., LUO, X., HE, J., PENG, C. & WU, T. 2015. Recovery of elemental sulphur via selective catalytic reduction of SO2 over sulphided CoMo/γ-Al2O3 catalysts. *Fuel,* 147**,** 67-75.

ZHOU, K., WANG, X., SUN, X., PENG, Q. & LI, Y. 2005. Enhanced catalytic activity of ceria nanorods from well-defined reactive crystal planes. *Journal of Catalysis,* 229**,** 206-212.

ZHU, H., QIN, Z., SHAN, W., SHEN, W. & WANG, J. 2004. Pd/CeO2–TiO2 catalyst for CO oxidation at low temperature: a TPR study with H2 and CO as reducing agents. *Journal of Catalysis,* 225**,** 267-277.

ZHU, K., HU, J., KÜBEL, C. & RICHARDS, R. 2006. Efficient Preparation and Catalytic Activity of MgO(111) Nanosheets. *Angewandte Chemie,* 118**,** 7435-7439.
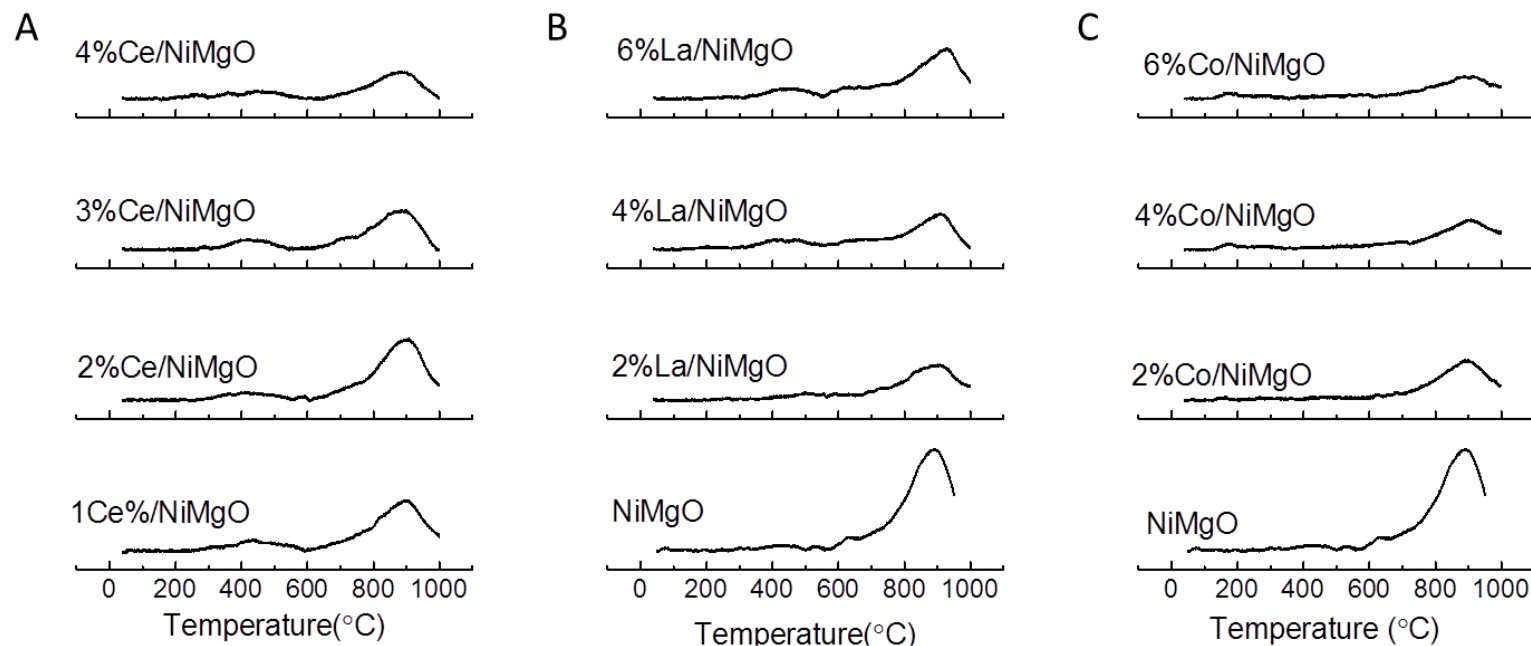
Appendix

Fig. A1 H$_2$-TPR patterns of catalysts, (A) Ce-containing catalysts, (B) La-containing catalysts, (C) Co-containing catalysts.
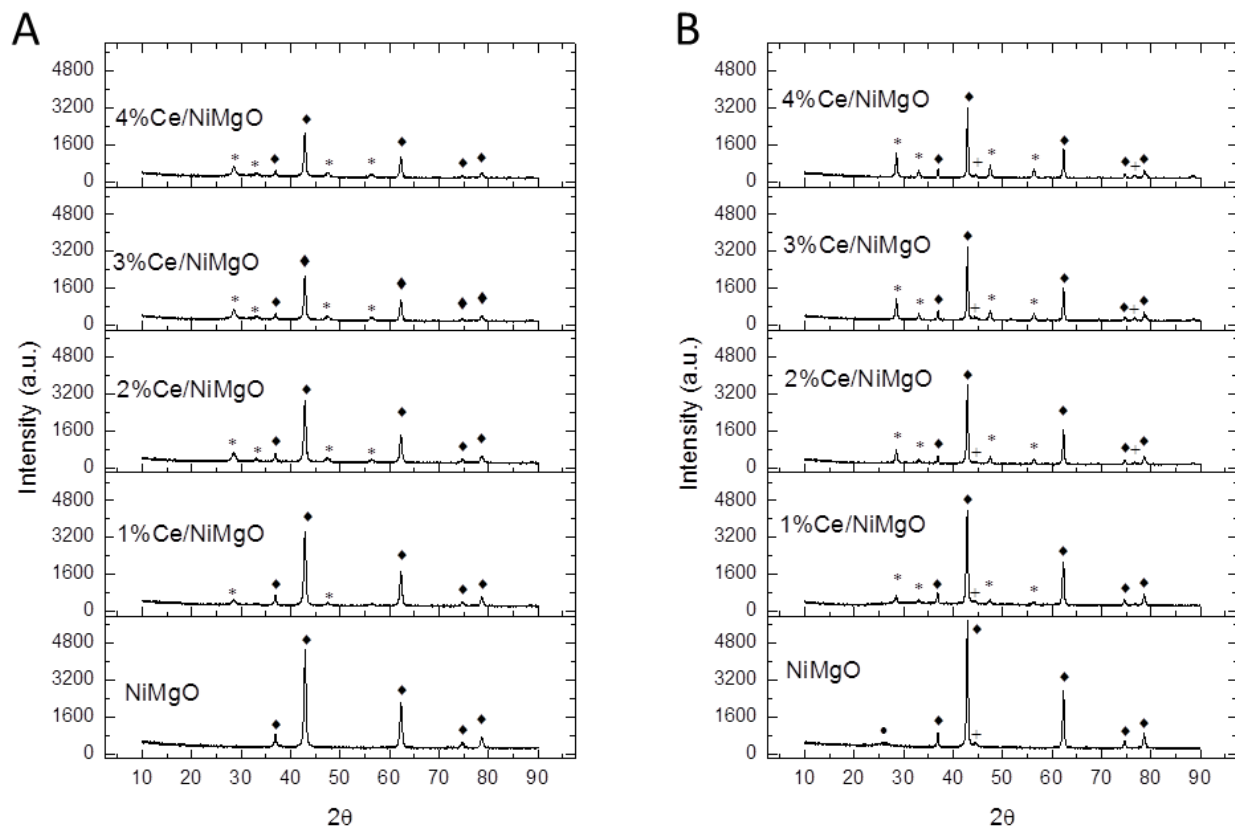
Fig. A2 XRD profiles of both fresh and spent Ce-containing catalysts, (A) fresh catalysts, (B) used catalysts, ($\diamond$): NiO or MgO, ($*$): CeO_2, (+): Ni^0, ($\bullet$): Carbon.
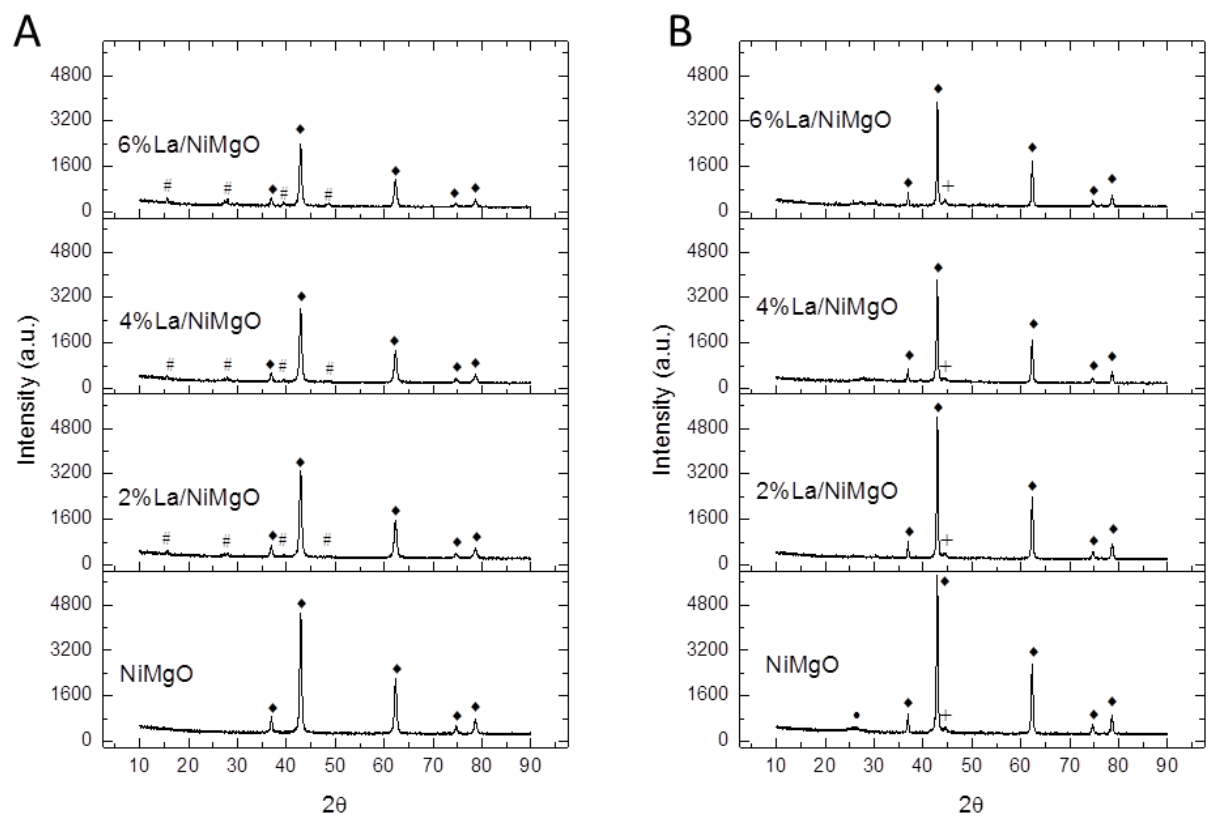
Fig. A3 XRD profiles of both fresh and spent La-containing catalysts, (A) fresh catalysts, (B) used catalysts, (♦): NiO or MgO, (#): La_2O_3, (+): Ni^0, (●): Carbon.

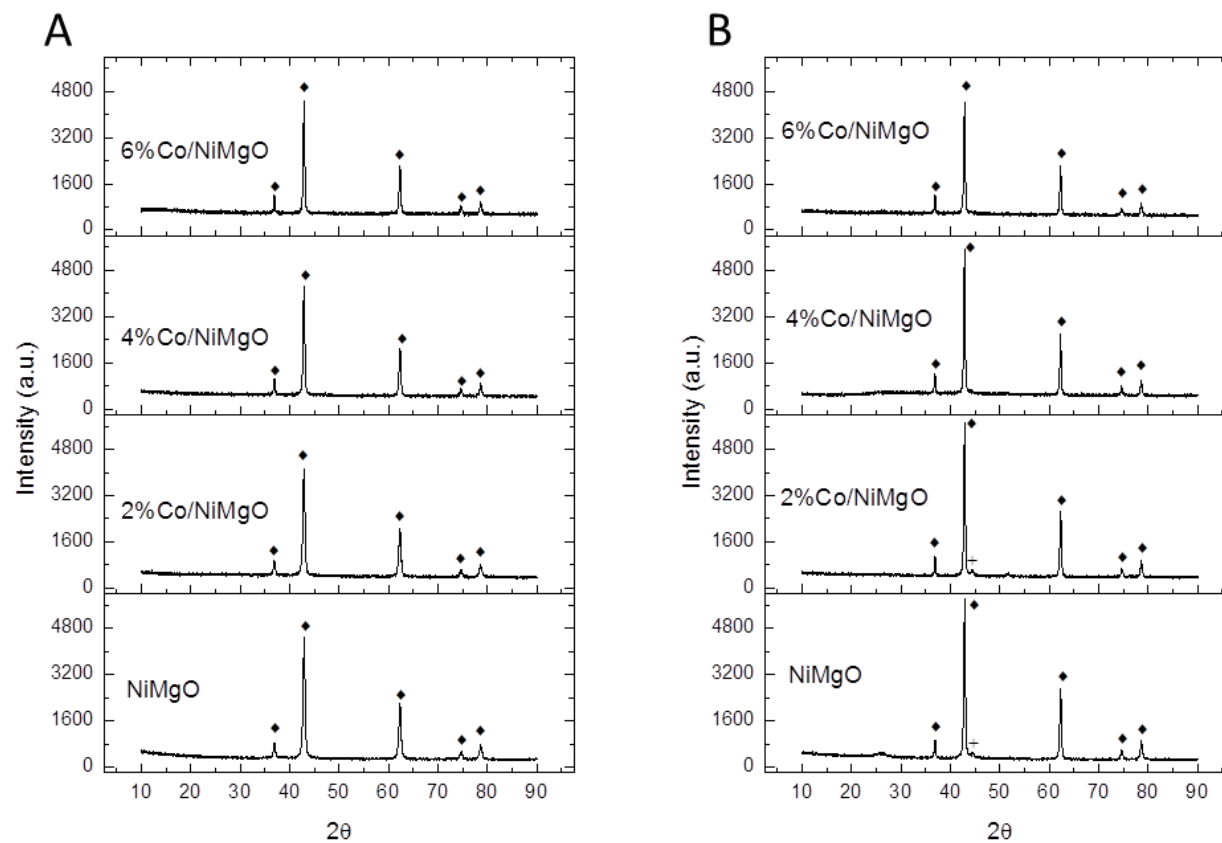**Fig. A4 XRD profiles of both fresh and spent Co-containing catalysts, (A) fresh catalysts, (B) used catalysts, (♦): NiO or MgO, (+): Ni^0, (●): Carbon.**

Fig. A5 TGA profiles of spent catalysts after 30h reforming tests at 700 ℃ of ethanol (S/C=6, GHSV: 63800 ml/g$_{cat}$/h), (A) Ce-containing catalysts, (B) La-containing catalysts, (C) Co-containing catalysts.

Fig. A6 TGA profiles of spent catalysts after 30h reforming tests at 700 ℃ of acetic acid (S/C=6, GHSV: 64000 ml/g$_{cat}$/h), (A) Ce-containing catalysts, (B) La-containing catalysts, (C) Co-containing catalysts.
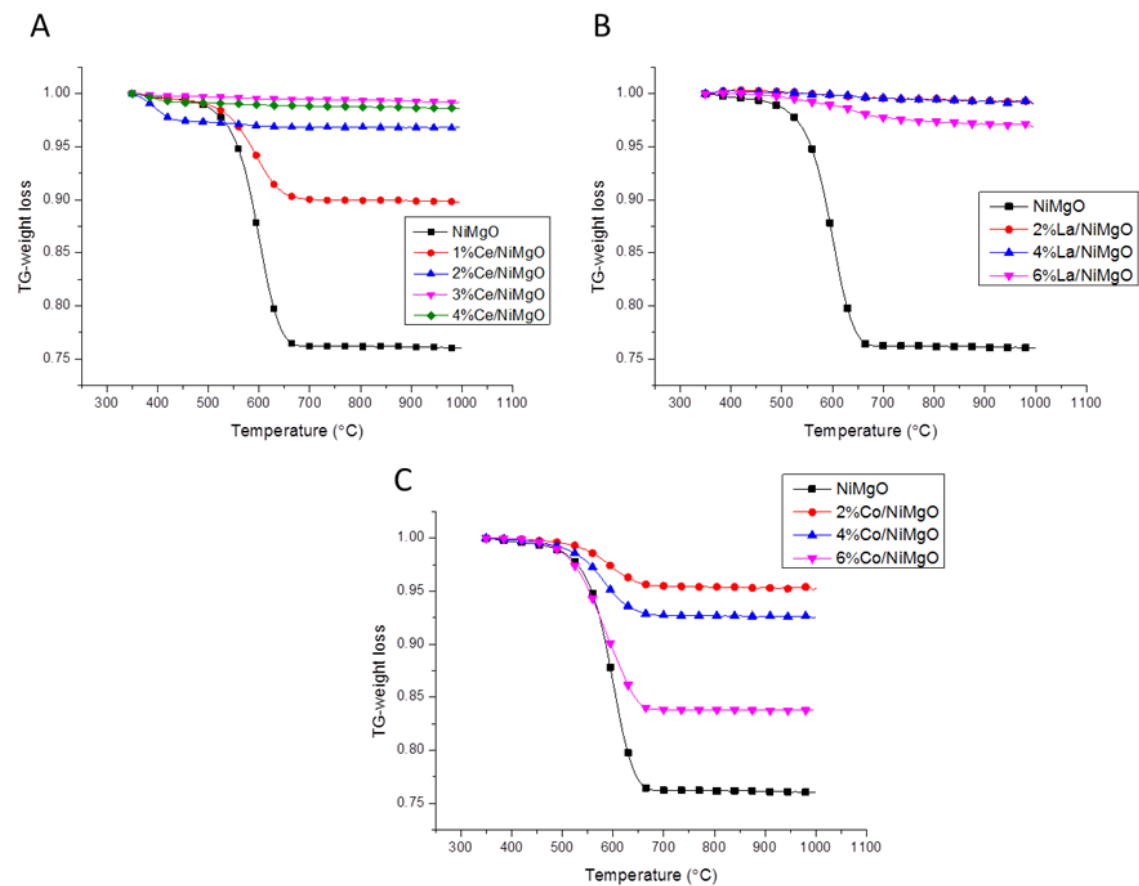
Fig. A7 TGA profiles of spent catalysts after 30h reforming tests of phenoal at 800 ℃ (S/C=12, GHSV: 143000 ml/g$_{cat}$/h), (A) Ce-containing catalysts, (B) La-containing catalysts, (C) Co-containing catalysts.
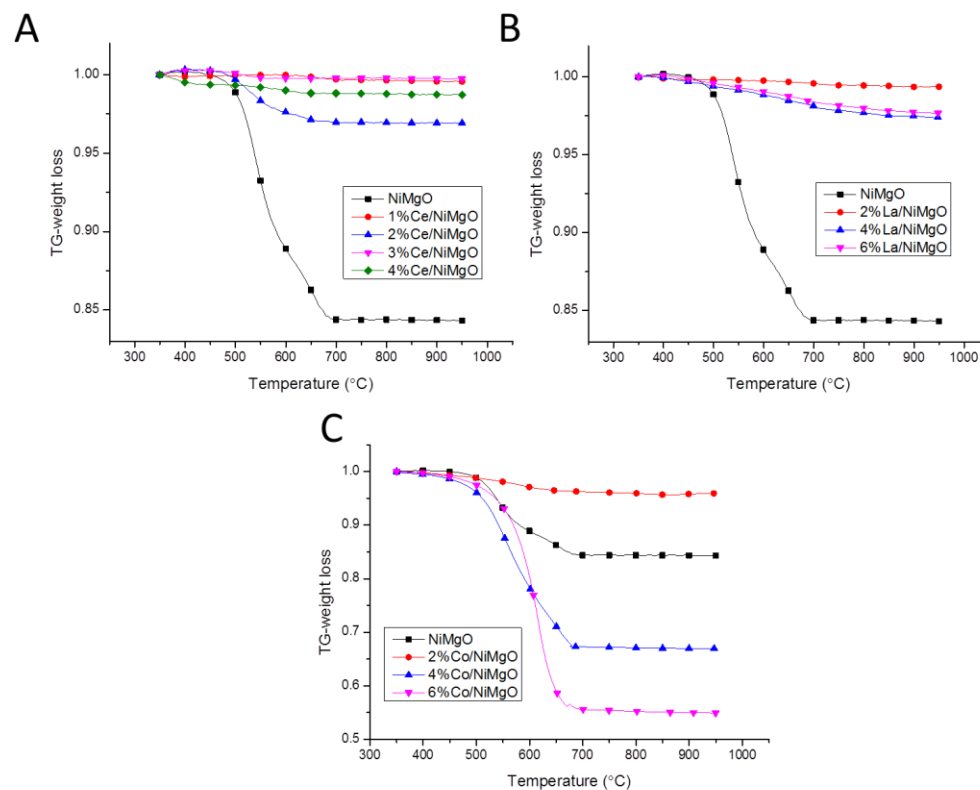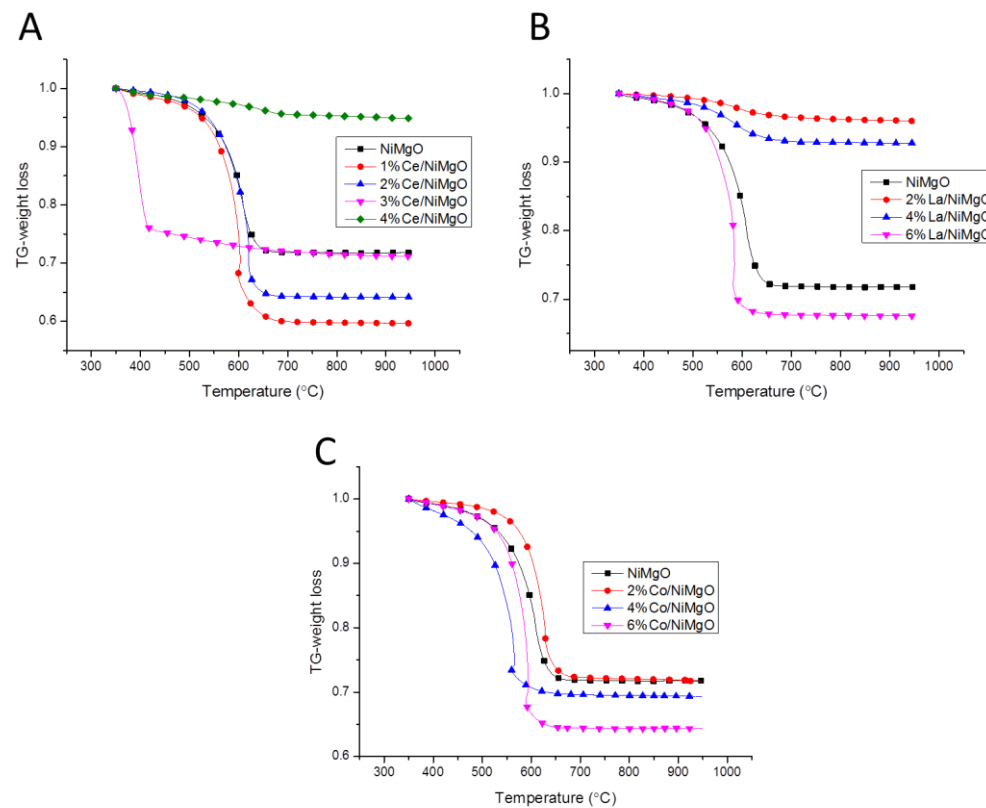
Table A-1 Performance characteristics and cost of various hydrogen production technologies, reprint from (Lindsay et al., 2009).

Hydrogen production process	Energy required (kWh/Nm^3 of H$_2$)		Status of Technology	Efficiency (%)	Costs relative to SMR	% of total production	Need for CO$_2$ sequestration
	Ideal	Practical					
Steam methane reforming	0.78	2-2.5	Mature	70-80	1	48	Y
Methane/NG pyrolysis			R&D to mature	72-54	0.9		N
H$_2$S methane reforming	1.5		R&D	50	< 1		N
Landfill gas dry reforming			R&D	47-58	~ 1		Y
Partial oxidation of heavy oil	0.94	4.9	Mature	70	1.8	30	Y
Naphtha reforming			Mature				
Steam reforming of waste oil			R&D	75	< 1		Y
Coal gasification (TEXACO)	1.01	8.6	Mature	60	1.4-2.6		Y
Partial oxidation of coal			Mature	55		18	Y
Steam-iron process			R&D	46	1.9		Y

Table A-1 continue

Hydrogen production process	Energy required (kWh/Nm^3 of H$_2$)		Status of Technology	Efficiency (%)	Costs relative to SMR	% of total production	Need for CO$_2$ sequestration
	Ideal	Practical					
Chloralkali electrolysis			Mature		By-product	4	N
Grid electrolysis of water	3.54	4.9	R&D	27	3-10		Y
Solar & PV-electrolysis of water			R&D to mature	10	> 3		N
High-temperature electrolysis of water			R&D	48	2.2		N
Thermochemical water splitting cycles			Early R&D	35-45	6		N
Biomass gasification			R&D	45-50	2.0-2.4		N
Photobiological			Early R&D	<1			N

Table A-2 Assignments of the fitting components and binding energies (eV) for Ni 2p and C 1s in XPS spectra of spent catalysts.

Catalysts	C 1s	Assignment	Content %	Ni 2p$_{3/2}$	Assignment	Content %	Ni 2p$_{1/2}$	Assignment
Spent NiMgO	285.2	Graphite	37.9	852.3	Ni^0	19.1	ND^a	Ni^0
	285.6	Defect	49.1	855.8	Ni^{2+}	80.9	873.8	Ni^{2+}
	289.9	CO$_3^{2-}$	13.0	861.4	Satellite		880.5	Satellite
Spent 3%Ce/NiMgO	284.8	Graphite	13.8	852.8	Ni^0	12.4	ND	Ni^0
	285.7	Defect	70.8	856.6	Ni^{2+}	85.6	874.0	Ni^{2+}
	289.8	CO$_3^{2-}$	15.4	863.2	Satellite		882.4	Satellite

Table A-2 continue

Catalysts	C 1s	Assignment	Content %	Ni 2p$_{3/2}$	Assignment	Content %	Ni 2p$_{1/2}$	Assignment
Spent 6%La/NiMgO	284.8	Graphite	27.7	N/A[b]	Ni^0		N/A	Ni^0
	285.8	Defect	44.3	N/A	Ni^{2+}		N/A	Ni^{2+}
	288.3	CO$_3^{2-}$	28.0	N/A	Satellite		N/A	Satellite
Spent 6%Co/NiMgO	284.9	Graphite	34.9	ND	Ni^0	0	ND	Ni^0
	286.0	Defect	55.7	856.9	Ni^{2+}	100	874.4	Ni^{2+}
	290.7	CO$_3^{2-}$	9.4	862.8	Satellite		880.3	Satellite

[a] ND means non-detectable, the deconvolution of Ni^0 2p$_{1/2}$ was hardly applied due to its low content.
[b] The Ni 2p of the spent 6%La/NiMgO cannot be derived due to the overlapping of the Ni 2p and La 3d profiles.

Table A-3 Assignments of the fitting components and binding energies (eV) for Ni 2p in XPS spectra of fresh catalysts.

Catalysts	Ni 2p$_{3/2}$	Assignment	Ni 2p$_{1/2}$	Assignment	Peak area
Reduce NiMgO	855.2	Ni^{2+}	872.7	Ni^{2+}	49.9%
	861.0	Satellite	879.1	Satellite	50.1%
Reduced 3Ce%/NiMgO	855.2	Ni^{2+}	872.8	Ni^{2+}	46.4%
	861.2	Satellite	880.0	Satellite	53.6%
Reduced 6%Co/NiMgO	855.3	Ni^{2+}	873.2	Ni^{2+}	49.1%
	860.9	Satellite	879.8	Satellite	50.9%